NETWORKED SENSING TECHNIQUE FOR 6G INTEGRATED SENSING AND COMMUNICATION

SHI QIN

PhD

The Hong Kong Polytechnic University

2025

The Hong Kong Polytechnic University
Department of Electrical and Electronic Engineering

Networked Sensing Technique for 6G Integrated Sensing and Communication

Shi Qin

A thesis submitted in partial fulfilment of the requirements
for the degree of
Doctor of Philosophy

December 2024

CERTIFICATE OF ORIGINALITY

I hereby declare that this thesis is my own work and that, to the best of my knowledge and belief, it reproduces no material previously published or written, nor material that has been accepted for the award of any other degree or diploma, except where due acknowledgement has been made in the text.

_____ (Signed)

SHI Qin (Name of student)

Abstract

Recently, integrated sensing and communication (ISAC) has been listed as one of the six key usage scenarios in the sixth-generation (6G) network by International Telecommunication Union (ITU). Specifically, base stations (BSs) in 6G network will emit orthogonal frequency division multiplexing (OFDM) signals not only to convey information to communication users, but also to sense the environment with ultra-high range/angle resolutions. The key challenge of 6G ISAC lies in how to achieve high-resolution sensing in a communication network. In this thesis, we aim to leverage the technique of networked sensing to tackle the above challenge. Specifically, in practice, the BSs can fuse their observations to reap the joint estimation gain. We will propose various signal processing techniques to enable network sensing for 6G ISAC.

The first work considers an OFDM-based multi-cell localization system, where multiple BSs emit downlink OFDM signals simultaneously to localize the targets. A novel two-phase sensing framework is proposed, under which we design a model-free range estimation approach by leveraging the OFDM channel estimation technique for determining the delay values of all the two-way BS-target-BS paths in Phase I and localize each target based on its distances to various BSs in Phase II. Especially, we build new theory about data association in Phase II, which is a long-standing issue for multi-anchor multi-target localization.

Our second work extends the networked sensing results from a pure line-of-sight (LOS) environment to a complicated multipath environment. We propose efficient methods that can mitigate the effect arising from non-line-of-sight (NLOS) paths on 6G multi-cell localization.

In our third work, we extend our study from localization to target three-dimension (3D) reconstruction. We consider a multi-view approach, under which a mobile transceiver equipped with multiple transmit and receive antennas moves to different known sites to image an extended target from different angles, and fuse all the single-view images into a multi-view image at last. It is shown that the multi-view technique can significantly improve the reconstruction quality.

Last, we build a millimeter wave (mmWave) ISAC platform that works at 27-29 GHz. We implement our proposed methods on this platform and achieve very high localization accuracy.

In summary, in this thesis, we propose advanced signal processing technique to enable point target localization and extended target reconstruction via the networked sensing technique in 6G ISAC systems. Platform is also built to verify our results. These works can provide new insight into investigation of the 6G ISAC technique.

Publications Arising from the Thesis

[1] **Q. Shi**, L. Liu, S. Zhang, and S. Cui, "Device-free sensing in OFDM cellular network," *IEEE J. Sel. Areas Commun.*, vol. 40, no. 6, pp. 1838-1853, Jun. 2022.

[2] **Q. Shi**, L. Liu, and S. Zhang, "Joint data association, NLOS mitigation, and clutter suppression for networked device-free sensing in 6G cellular network," in *Proc. IEEE International Conference on Acoustics, Speech, and Signal Processing (ICASSP)*, 2023.

[3] **Q. Shi** and L. Liu, "Joint LOS identification and data association for 6G-enabled networked device-free sensing," *IEEE Trans. Commun.*, vol. 72, no. 8, pp. 5117-5129, Aug. 2024.

[4] **Q. Shi**, S. Zhang, and L. Liu, "A 6G-based Multi-View Reconstruction Approach," to appear in *Proc. IEEE Wireless Communications and Networking Conference (WCNC)* 2024.

Acknowledgements

The four years of PhD study at The Hong Kong Polytechnic University is very impressive and fulfilling, and I want to give thanks to some people for their support in this journey.

First and most importantly, I would like to give my deepest and most sincere thanks and gratitude to my supervisor Prof. Liang LIU, who provided me with a lot of guidance in my PhD study. He gives me an opportunity to pursue my academic career again and tries his best to guide me on how to be a good researcher. In these four years, I really enjoyed working with him and learned a lot from him. His outstanding academic insight, wisdom, and enthusiasm encouraged me to fight with each challenge in these years. More importantly, his patient guidance and encouragement push me beyond my boundaries of ability, which makes me a better researcher. It is a great honor to be a PhD student under the supervision of Prof. Liang Liu.

I would like to express thanks to my Thesis Committee Members, Prof. Lin DAI and Prof. Kaibin Huang for spending time reviewing my thesis and attending my oral defense. Besides, I appreciate the help from Prof. Changyuan YU and Prof. Shuowen ZHANG in Hong Kong and Prof. Wei YU during the visit to University of Toronto, who provided great support for my research. I am also grateful to Prof. Francis LAU, Prof. Wen CHEN, Prof. Angela ZHANG, and Prof. Daniel PALOMAR for their impressive and enlightening courses.

It is lucky to have many good friends in Hong Kong and Toronto, and I have many thanks to my research groupmates: Zipei YAN, Yinan ZOU, Yiming LIU, Yinghan LI, Han HAN, Zhichao WANZHONG, Yinghan LI, Tao JIANG, Binyu LU, Zhe LI, Dr. Xinyu BIAN, Dr. Zhaorui WANG, Dr. Xiangming CAI, Dr. Weifeng ZHU, Xianzhen GUO, Rui WANG, Ziyi ZHAO, Lin ZHU, Jishan YAN, Tongkai LI, Yiyang ZHANG, Jingchuan WANG, Haowen PAN.

Last, but the most, I will never forget the love and support from my parents during the whole study journey. They always accompany me and give me the courage to be faced with every challenge in my life.

Contents

List of Figures

List of Tables

Abbreviations

Symbol	Description
M	The number of BSs or time slots
K	The number of targets of point targets
N	The number of sub-carriers
B	The bandwidth
L	The maximum number of channel taps
Δf	The sub-carrier spacing
$h_{u,m,l}$	The channel coefficient for the l-th path from BS u to BS m
$s_{m,n}$	The n-th transmitted frequency-domain OFDM sample at BS m
$\chi x_{m,n}$	The n-th transmitted time-domain OFDM sample at BS m
$z_{m,n}$	The nosie in the n-th OFDM sample period at BS m
$y_{m,n}$	The received time-domain signal in the n-th OFDM sample period at BS m
$\boldsymbol{W}$	The discrete fourier transform matrix
(a_m, b_m, c_m)	The location BS m
(x_k, y_k, z_k)	The location target k
$d_{m,k}$	The range between BS m and target k
$d_{u,m,k}$	The range of the path from BS u to target k to BS m
$\mathcal{D}_m$	The estimated measurement set at BS m
$\tau_{u,m}$	The sampling timing offset between BS m and BS u
$N_T(N_R)$	The number of transmit (receive) antennas
$s_{n_T,n}^{(m)}$	The n-th frequency-domain OFDM sample for transmit antenna n_T at time slot m
$\chi_{n_T,n}^{(m)}$	The n-th time-domain OFDM sample for transmit antenna n_T at time slot m
$h_{n_R,n_T,l}^{(m)}$	The channel for the l-th path from transmit antenna n_T to receive antenna n_T at time slot m
$y_{n_R,n}^{(m)}$	The n-th received time-domain OFDM sample for receive antenna n_R at time slot m
$\theta_{m,k}(\phi_{m,k})$	The elevation (azimuth) angle for point target k at time slot m

Chapter 1

Introduction

1.1 Background

In the past several decades, there have been great developments in communication and radar technologies. In radar, the pre-designed radios are leveraged for target detection and target localization, including but not limited to estimating the range, the direction, and the velocity of target, while the communication waveform is utilized for accurately sending the message from the source to the destination. There are a number of applications for radar systems in both military and civilian, such as unmanned aerial vehicle (UAV), aircraft detection and tracking, and robot navigation. The communication systems go through several generations to the current 5G network with lower latency, higher data transmission and enhanced bandwidth, which are more compatible with the nowadays needs of information exchange, especially for mobile phones.

1.1.1 Radar Technology

A typical radar system consists of three parts, transmitter, receiver, and switch. The switch is connected to the transmitter and the receiver to determine whether to emit the electrical waves or receive the echoes. The main process of the radar system detecting the targets and/or estimating the parameters of targets is: (i) the transmitter produces the pre-designed waveforms and emits the signals into the environment towards the direction of interest; (ii) if there are targets in the region of interest, the sent electrical waves will be reflected by the target or scatted into the environment; (iii) if the signal echoes can be received by the radar

system, the received signals will be processed and analyzed, from which the information about targets can be extracted.

To avoid self-interference from the transmitter located in the same radar system, e.g., mono-static radar, the switch is used to make sure that the transmitter and receiver will not work at the same time. However, if the transmitter is far away from the receiver, e.g., bi-static radar, the switch is not needed. At the receiver, the received signals are first downconverted into the intermediate frequency (IF) band. After that, an IF amplifier is used to convert the passband signals to the baseband signals. Then, the detector will extract information from the processed signals, which is normally followed by analog-to-digital converter (ADC) and signal processor in order to obtain more results. Note that in the radar system with only the aim of detecting the targets, the ADC and the signal processor are not required.

1.1.2 Communication Technology

A typical communication system comprises two parts, transmitter and receiver. The transmitter is used to process the input message, where redundant information in the source will be removed (source coding) and additional information will be added to mitigate the effect caused by the channel (channel coding). When propagating through the channel, the signals will experience the distortion and the noise. The goal of the receiver is to recover the original message from the encoded and polluted signals. The main process of the communication sending message is: (i) the input message will be first processed by the source encoder to compress the message or remove the redundant information. Following the source encoding, the channel encoder is applied, where additional information is added to the message but can be used to correct the error or combat the distortion caused by the channel. Then, the encoded baseband signals will be modulated into the passband, i.e., multiplying signals by higher frequency carriers for transmission. (ii) the pre-processed signals are transmitted and then go through the environment or the channel, where there will be noise and distortion in the propagation. (iii) if the power of the received signals exceeds the threshold, the receiver will demodulate the signals into baseband. After that, the channel decoder will make use of the additional information to correct the error and remove it. Then, the source decoder leverages the corrected data to decompress and get the original information. Note that there is also ADC to convert the continuous signal into a discrete signal at the receiver, i.e. sampling. Besides, to eliminate

the inter-symbol interference (ISI), the matched filter and the equalization will be both implemented. Moreover, there will be beamforming or precoding at the transmitter to achieve the spatial gain.

1.1.3 Motivation for joint radar and communication

Joint radar and communication (JRC) has been proposed recently. The reasons are threefold: (i) the demanded high-speed data transmission of the increasing number of devices and services results in frequency congestion, which requires JRC to enhance spectral efficiency. (ii) sensing and communication functions are expected to be provided simultaneously in many emerging scenarios, such as vehicle navigation in intelligent transportation systems and object detection in smart home. (iii) sensing and communication functions can benefit each other such that the performance of the whole system can be improved. For example, the real-time sensory information can be fused with the map downloaded from the cloud in the intelligent transportation system, which can help navigate the vehicle accurately and avoid collision.

1.2 Literature Review

To enable the communication and the radar functions simultaneously, there are two main research directions, one is Radar and Communication Coexistence (RCC) and the other one is Integrated Sensing and Communication (ISAC). In RCC, only the spectrum is reused, while the communication and radar systems are independent. Therefore, the main issue of RCC is interference management. The latter enables JRC via the same waveforms, i.e., both the spectrum and the hardware are shared. As a result, the spectral and energy efficiency of the system can be improved. Compared to RCC, the key of ISAC lies in the joint waveform design and signal processing techniques such that the two functions can be realized simultaneously via the same waveform at the same platform. The comparison between RCC and ISAC is shown in Table 1.1. Appealed by the fancy benefits of JRC, there are many interesting and important explorations made for this emerging direction, as discussed in the following.

Table 1.1: The comparison between RCC and ISAC.

	RCC	ISAC
Spectrum	reused	reused
Waveforms	distinct	same
Hardware Platforms	different	same
Main Challenge	interference management	waveform design

1.2.1 Radar and Communication Coexistence

For RCC, there are different degrees of cooperation between the communication and sensing systems. On one side, the cooperation between the two sub-systems is limited, since the attention is only paid to the performance of either the communication system or the radar system. Moreover, from the view of the signal processing, there are two main research directions in interference management, one is to cancel the interference from the radar system at the communication system, i.e., communication-centric RCC, and the other one is the interference cancellation from the communication system at the radar system, i.e., sensing-centric RCC. For example, the characteristics of MIMO in radar systems are exploited to deal with communication interference, and the performance of the radar system is considered in priority[1]. The interference at the radar system from the sub-bandwidths allocated for the communication users is limited in [2] and [3]. Similarly, the communication-centric strategy is adopted in [4], where the sparsity of a proper representation of the interference is exploited to perform adaptive radar interference removal at the communication receiver. The prior information about the radar interference is directly utilized at the communication transmitter for radar interference mitigation in [5], [6].

On the other side, the information between the two sub-systems is exchanged, where the transmit policies are negotiated to guarantee the performance of both communication and sensing. In [7], the objective is to minimize the effective interference power (EIP) at the radar in RCC systems, while maintaining the communication capacity over the predefined value under the constraint of transmit power. The radar sampling and communication precoding matrix are jointly optimized using alternating optimization (AO). Furthermore, [8] takes account into the interference from both radar return and clutter, where the local optimum is obtained based on AO and then the global optimum can be inferred. The millimeter wave (mmWave) RCC is investigated in [9], where the cross-interference between radar and communication is eliminated by designing the beamformer assuming the known perfect CSI. The summary of the

Table 1.2: The classification of RCC techniques.

RCC techniques	Characteristics
non-cooperation RCC	cancel the radar (communication) interference at the communication (radar) receiver
cooperation RCC	predesign the signals at the communication and radar transmitters

above RCC techniques is shown in Table 1.2.

1.2.2 Integrated Sensing and Communication

Compared with RCC, it is much more complicated to achieve ISAC, since there is no dedicated hardware for the two functions, respectively. Besides, the integration of communication and radar will give rise to the trade-off between the performance of the two systems, as their objectives are different. Generally, ISAC also needs expert knowledge in the two fields as well, which makes it more intractable to be implemented in practice. However, the main trend in JRC is ISAC, because there will be gains brought by such integration. Specifically, ISAC captures two advantages over the independent communication and radar systems: 1) integration gain to improve spectral and energy efficiency, 2) coordination gain to perform mutual assistance in communication and sensing functions. To achieve ISAC, there are two popular ways, one is radar-based ISAC, where the radar is the primary function and the communication is the secondary function; the other one is communication-based ISAC, where the communication is dominant over the radar. For the former direction, the key challenge lies in how to embed information into the radar signals; while for the latter direction, the key challenge lies in how to sense the targets using the communication signals.

1.2.2.1 Radar-centric ISAC

A major advantage of radar-centric ISAC is that long-range communication can be achieved, but the communication rate in radar-centric is inherently limited. There are two main radar waveforms for information embedding, one is pulsed radar signal and the other one is continuous-wave radar signal. For example, the interval between radar pulses is utilized for realizing communication functions [10]. On the other hand, FMCW is also investigated to convey the communication data, one simple method is adjusting the frequency chirp rate, i.e., transmit bit “0" if the sign of chirp rate is positive, and bit “1" otherwise. Furthermore, FMCW is

Table 1.3: The techniques of radar-centric ISAC.

Methods	Examples
Pulsed radar	the pulse interval of the signals to embed information
FMCW	the sign or the value of the chirp rate to convey message
IM	the index over space, time, frequency and code domains

combined with OFDM and minimum shift keying (MSK) for improving the spectrum efficiency in [11, 12], since the chirp radar waveform occupies a large range of frequencies that leads to low spectral efficiency. However, the previous works cannot achieve high data rate transmission, as the modulated phase is discontinuous. To address this issue, [13] proposes continuous phase modulation (CPM) by mapping the bit sequence into bipolar amplitude modulated sequence, which is then converted into the phase.

Instead of applying conventional modulations, incorporating communication information into radar waveforms via index modulation (IM) is studied in MIMO-OFDM radar [14]. Here, IM means different combinations and/or permutations of signal parameters over space, time, frequency and code domains for integrating communication functions into radar systems[15–17]. For instance, the indexes of subcarriers and antennas can be leveraged for conveying communication information. Another example is frequency-hopping technique, where the signal frequency is rapidly changed among a large number of different frequencies. Note that the radar waveform and signal structure are not modified in index modulation such that there is little impact on the radar systems. The summarization of the above radar-centric ISAC techniques is shown in Table 1.3.

1.2.2.2 Communication-centric ISAC

The communication system can inherently provide high data rate transmission, since the standardized communication waveforms, protocols, and architectures can be utilized in communication-centric ISAC. The communication data are normally random to embed as many messages as possible, while the radar waveform is deterministic for extracting the information from the channel. To tackle this issue, there are some works proposing excellent methods in this direction. Particularly, pilot signals and frame preambles are utilized for sensing in[18, 19], since they have a good auto-correlation property and can be predesigned according to the sensing condition. In [20], the spread spectrum in communication system is utilized for radar probing. However, the imperfect orthogonality of the spread sequence limits the radar

Table 1.4: The techniques of communication-centric ISAC.

Methods	Pros	Cons
Preamble	orthogonal	limited sequences
Spread Spectrum	good auto-correlation property	low spectral efficiency
OFDM	multi-carrier and robust to multipath	PAPR
OTFS	handle both multipath and high Doppler frequency	high complexity

dynamic range. Besides, it is quite complicated to estimate the velocity of the target from radar echoes due to its high complexity.

Apart from the spread spectrum technique, there is increasing attention paid to OFDM based communication-centric ISAC [21, 22], because the OFDM technique is compatible with the current 5G and the future 6G standards [20]. OFDM waveform is widely applied in communication system for its high spectral efficiency and good ability to handle inter-symbol interference. As discussed above, OFDM is also implemented in radar, i.e., OFDM-radar. Hence, OFDM is a promising technology for ISAC. The sub-carrier spacing is optimized to maximize the unambiguous range and the velocity in [23]. Besides, [24] studies the allocation of sub-carriers to maximize the sum of the mutual information of the communication and radar systems. The disadvantage of OFDM signal is its peak-to-average-power ratio (PAPR), which introduces a serious degradation in performance when the signal passes through the amplifier. To address this issue, a weighted OFDM waveform is considered to prevent the high PAPR in [25].

Another communication signal waveform is OTFS, which can be regarded as a combination of the OFDM and the CDMA. Compared with OFDM signal which is aimed at handling the frequency selective channel, the OTFS signal is developed to deal with both time and frequency selective channels, i.e., the channel with multipath and Doppler frequency. Similar to OFDM, [26] explores the possibility of utilizing the OTFS signal for target sensing. Besides, it is shown in [27] that the OTFS can achieve a similar performance of target sensing as the conventional radar waveform, which verifies the effectiveness of the OTFS communication signal based ISAC. Furthermore, the effect of the inter-symbol interference (ISI) and intercarrier interference (ICI) is considered in OTFS based ISAC system[28], which can be exploited to enhance the unambiguous range and velocity detection scope. The summarization of the above communication-centric ISAC techniques is shown in Table 1.4.

1.2.3 Network-level Sensing

Several interesting works have been done to propose practical algorithms for realizing ISAC in the 6G network. For instance, efficient algorithms have been proposed such that a BS can extract the range/angle/Doppler information of the targets based on the OFDM signals [29, 30], the orthogonal time frequency space (OTFS) signals [27], and the millimeter wave signals [31], that are reflected by these targets. Moreover, [32, 33] have devised powerful estimation schemes such that a mobile user can utilize the cellular signals for realizing simultaneous localization and mapping (SLAM). It is worth noting that the above works mainly consider the scenario where localization is performed with one transmitter and one collocated/separate receiver, as in the monostatic/bistatic radar systems, i.e., standalone-level sensing. However, it is difficult to provide high-resolution sensing in a point-to-point communication network due to the limited detection capability and range/angle resolution of each BS. Inspired by the cloud radio access network (C-RAN) where the BSs can collaborate to mitigate inter-cell interference, we aim to leverage a unique advantage of the cellular network to tackle the above challenge - networked sensing. Specifically, in practice, the BSs are connected via the fronthaul links. When a target's echo signals are heard by multiple BSs, they should fuse their observations for improving the sensing performance. This is a notable difference to radar systems, where radars usually perform sensing in an independent manner. Therefore, in this thesis, we are devoted to exploiting the power of networked sensing in performing high-resolution target sensing tasks.

1.3 Thesis Contributions and Organization

Motivated by the above discussion, we devote our endeavor to the study of advanced signal processing techniques for estimating the locations of passive targets by leveraging the communication signals sent by the base stations (BSs) in the cellular network. The ultimate goal of this line of research is to pave the way for transforming the cellular network into a huge sensor, such that the new function of networked localization can be provided to users in the future beyond-fifth-generation (B5G) and sixth-generation (6G) cellular networks. We focus on the communication-centric ISAC, where the 6G OFDM communication signal is leveraged to realize device-free sensing. Specifically, we consider point target localization and extended

target reconstruction in networked device-free sensing, where the multi-view information of the target via communication signals is fused. The rest of the thesis is organized as follows.

Chapter 2 is the foundation of the thesis. This chapter considers an OFDM-based multi-cell localization system, where multiple BSs emit downlink OFDM signals simultaneously to localize the targets. A novel two-phase sensing framework is proposed to localize the passive targets that cannot transmit/receive reference signals to/from the base stations (BSs), under which we design a model-free range estimation approach by leveraging the OFDM channel estimation technique for determining the delay values of all the two-way BS-target-BS paths in Phase I and localize each target based on its distances to various BSs in Phase II. Particularly, we face the data association issue in Phase II, because each BS does not know how to match its estimated distance values to the targets. Theoretically speaking, a wrong data association solution may lead to the detection of ghost targets that do not exist. Interestingly, we show that under the ideal case of perfect range estimation in Phase I, ghost targets will not be detected almost surely in Phase II. This builds a theoretical foundation to 6G networked sensing - its performance is not fundamentally limited by data association. Moreover, under the practical case of imperfect range estimation in Phase I, we propose an efficient algorithm for joint data association and target localization in Phase II.

To extend our results to the scenario where non-line-of-sight (NLOS) paths exist, we explores networked device-free sensing in an OFDM cellular system with a multipath environment in Chapter 3. Similar to the first work, a two-phase protocol is considered, where target range information is estimated in Phase I, and target locations are estimated in Phase II. However, there are two main differences over the first work. First, in Phase I, besides the path from a BS to the target to the same BS, we also estimate the range of any path from a BS to some target to another BS. Because the BSs are not synchronized, we propose a novel method to estimate the time offsets among BSs such that range estimation in Phase I is accurate. Second, in Phase II, besides data association, we also need to find out the range information corresponding to the LOS paths. To achieve this goal, we propose an efficient algorithm for joint data association, NLOS mitigation, LOS identification, and localization. The first two works then complete our study of the networked sensing technique for localization.

In Chapter 4, we consider the networked sensing technique for multi-view target three-dimension (3D) reconstruction, which is an important application due to its ability to provide

accurate and detailed digital models of objects or scenes. Under our considered setup, a radio frequency (RF) transceiver equipped with multiple transmit and receive antennas moves to different known sites at several time slots. At each time slot, the transceiver emits OFDM communication signals to image an extended target that is modeled as multiple adjacent scatter points. We propose a novel scheme that is able to construct a single-view image of the target that can be observed by the RF transceiver at each time slot via the OFDM signals, and fuse these single-view images into a multi-view image, which is more accurate and complete compared to all the single-view images.

Chapter 5 describes the built ISAC platform that works at 27-29 GHz. Under this platform, there is a 64-element transmitter that is able to generate a narrow beam, and a 4-antenna receiver. We implement our range and angle estimation algorithms, and our platform can achieve the range estimation error and the angle estimation error are less than 0.15 meter and 4°, respectively. Building on these exciting results, our future work will collect sensing data from multiple sites and perform data fusion techniques as in our theoretical works to implement the networked sensing technique via our platform.

Chapter 6 summarizes this thesis, list the future research directions and present an outlook on the future development of networked device-free sensing in the future 6G network.

Chapter 2

Device-free sensing in OFDM cellular network

2.1 Introduction

2.1.1 Motivation

Radar and wireless communication are probably the two most successful applications of radio technology over the past decades. Recently, there has been growing interests in achieving integrated sensing and communication (ISAC) under a common system via reusing the same radio frequency (RF) signals due to its significant benefits brought to many use cases [20, 34–40]. For example, the intelligent transportation system can take advantage of the ISAC techniques for sensing the environment and disseminating the sensed data among vehicles to improve the traffic efficiency and safety. Moreover, ISAC techniques can play a crucial role in future communication systems as well. For instance, sensing information in millimeter wave (mmWave) systems can be leveraged to design efficient beam selection and alignment [41].

Despite the appealing future promised by ISAC techniques, how to realize the functions of sensing and communication simultaneously in a practical system is still an open problem. Motivated by this, in this paper, we devote our endeavor to the study of advanced signal processing techniques for estimating the locations of targets by leveraging the communication signals sent by the base stations (BSs) in the cellular network. The ultimate goal of this line of research is to pave the way for transforming the cellular network into a huge sensor, such

that the new function of networked localization can be provided to the users in the future beyond-fifth-generation (B5G) and sixth-generation (6G) cellular networks.

2.1.2 Prior Work

The study of ISAC techniques is still in its infancy. However, there are many interesting and important explorations made recently for this emerging direction, as discussed in the following.

2.1.2.1 Radar Signal Based Versus Communication Signal Based ISAC

Intuitively, we can use either the radar signals or the communication signals to achieve ISAC. For the former direction, the key challenge lies in how to embed information into the radar signals; while for the latter direction, the key challenge lies in how to localize the targets using the communication signals. Although several interesting works have been done to modulate a small number of bits into the radar signals [42, 43], this approach cannot achieve high-rate data transmission that is necessary for many ISAC applications (e.g., autonomous cars may generate a huge amount of sensing data to be exchanged among adjacent cars in a short time), since modulating high-order random data symbols on the radar signals will significantly reduce the autocorrelation between the transmitted and reflected signals, thus deteriorating the sensing performance. Motivated by this limitation, this paper aims to exploit the use of communication signals in the cellular network for achieving target localization with an accuracy level similar to that achieved by the radar system.

2.1.2.2 Device-Based Versus Device-Free ISAC

Along the line of communication signal based ISAC, the sensing techniques can be further divided into two categories: device-based sensing for localizing registered targets with communication capabilities, and device-free sensing for localizing unregistered targets that cannot transmit/receive communication signals.

Device-based sensing estimates the target locations based on a set of wireless reference signals exchanged between the targets and the BSs [44, 45], and has been available in the cellular network since the second generation (2G), e.g., the location of a mobile phone can be

estimated when it makes an emergency call. Typical methods include time-of-arrival (ToA) based localization which estimates each target's location at the intersection of at least three circles whose radii are products of the speed of the light and the signal propagation time, and angle-of-arrival (AoA) based localization which estimates each target's location at the intersection of lines formed by measuring the arrival angles of radio signals between the target and multiple BSs.

On the other hand, for passive targets that do not have communication capabilities or are unregistered in the network, device-free sensing needs to be leveraged for their localization. For example, in low-altitude economy scenario, it is required to monitor those unregistered unmanned aerial vehicle (UAV) in the sky for security. Note that in device-free sensing, the cellular network can only estimate the locations of the targets based on their *reflected* communication signals (instead of the actively exchanged reference signals in device-based sensing), similar to the radar systems. However, the signal processing techniques used in radar systems cannot be applied because the communication signals usually do not have an ambiguity function with steep and narrow main lobes. This thus motivates our work on developing new methods for device-free sensing.

2.1.2.3 Fundamental Limits Versus Practical Solutions

For device-free sensing based on cellular communication signals, there are generally two research directions: revealing fundamental limits on the communication-sensing trade-off, and designing practical sensing solutions.

Firstly, the optimal waveform design for communication is generally different from that for sensing due to the distinct objectives (i.e., to maximize the mutual information versus to minimize the sensing error), thus leading to a fundamental trade-off between the capacity in communication and the estimation distortion in sensing. Several pioneering works have been done to characterize such an important capacity-distortion trade-off, to reveal the performance upper bound of ISAC systems (see, e.g., [46–51]). Secondly, it is also crucial to design practical signal processing solutions for approaching the above fundamental limits. Note that the BS-target-BS reflected channel is generally a function of the target location, thus making it possible to extract the location information by exploiting the reflected channel that can be estimated via channel training. To achieve this goal, several prior works have proposed advanced algorithms

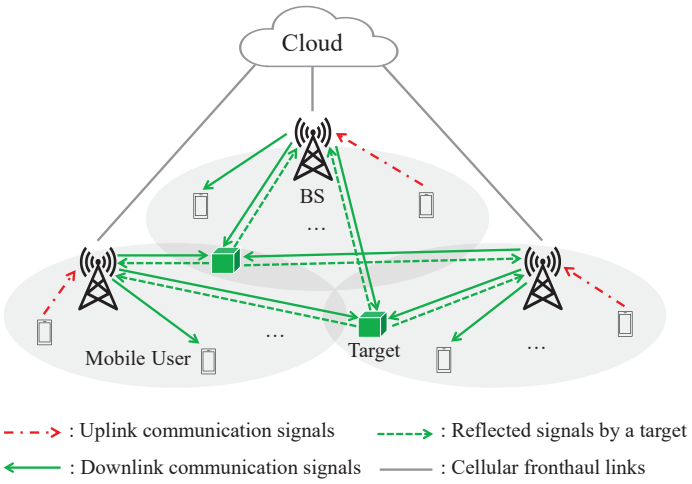

Figure 2.1: System model for an ISAC network with simultaneous downlink/uplink communication and target sensing.

based on knowledge of the reflected channel models [18, 52–55]. However, the exact BS-target-BS reflected channel models are generally difficult to obtain in practice due to the complicated and time-varying wireless environment, while inexact channel models that do not match with the actual channels will lead to erroneously estimated location even if channel estimation is perfect. This thus motivates us to propose a *model-free* scheme for localization that does not depend on knowledge of the reflected channel model, similar to device-based sensing.

2.1.3 Main Contributions

In this paper, we aim to devise practical solutions to achieve device-free sensing in a cellular network, where multiple BSs and multiple mobile users send downlink and uplink communication signals, respectively, while the BSs also collaboratively estimate the locations of multiple passive targets based on the downlink communication signals reflected by the targets, as illustrated in Fig. 2.1. In particular, we consider the *orthogonal frequency division multiplexing (OFDM)* scheme for communication signal transmission, thus our results are compatible with the 5G and beyond cellular networks. Under this setup, we propose advanced signal processing techniques for localizing the passive targets based on their reflected OFDM signals back to the BSs. The main contributions of this paper are summarized as follows.

- First, we propose a novel *two-phase framework for device-free sensing* as shown in Fig. 2.2. Specifically, in Phase I, each BS estimates the values of its distance (also termed as *range*) to the multiple targets by extracting the delay information embedded in the BS-target-BS

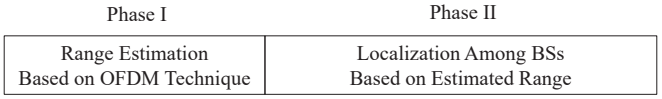

Figure 2.2: Proposed two-phase framework for device-free sensing in OFDM-based ISAC cellular networks.

channels; then, in Phase II, all the BSs share their range information through the fronthaul links in the cellular network (as illustrated in Fig. 2.1), such that the location of each target can be estimated based on the values of its distance to different BSs, similar to the ToA-based localization approach [44, 45].

- Second, for Phase I in our considered framework, we propose a new *model-free* scheme to estimate the values of the distance between the BSs and the targets. Specifically, we identify that the signal propagation from the BSs to the targets and then back to the BSs automatically forms a *multi-path channel*, where each BS-target-BS link can be viewed as a (delayed) path between the transmitter and the receiver. Such channels are similar to those in wideband communications, thus the channels at different delayed taps can be efficiently estimated using mature techniques in OFDM communications [56]. Note that if the channel tap associated with a particular delay value is non-zero, a path causing that delay exists between the transmitter and the receiver. Inspired by the above, we propose to first estimate the non-zero channel taps and their associated delay values between the BSs and the targets, and then estimate the range of each target as half of the reflection delay multiplied by the speed of the light. The range estimation accuracy is shown to increase with the channel bandwidth, thus is practically high due to the sufficiently large bandwidth in future cellular networks (e.g., up to 400 MHz in the 5G network [57]). Note that in contrast to the conventional device-free sensing approaches [18, 52–54], our proposed range estimation method does not depend on the assumption of any BS-target channel model for extracting the distance information.

- Third, note that the target localization in Phase II of the proposed framework has a key difference from the conventional ToA-based localization. Specifically, in ToA-based localization, different active targets can transmit/receive signals with different signatures such that each BS has a clear mapping between different ranges and different targets. On the contrary, in device-free sensing, all the targets reflect the same signals to the BSs, thus the BSs do not directly know how to match the ranges with the right targets. In the literature, such a matching process is referred to as data acquisition [58], and it is well-known that an incorrect matching solution may result in ghost targets that do not exist [58, 59]. To tackle this

challenge, we first consider the ideal case with perfect range estimation in Phase I, and prove that ghost targets never exist when the number of BSs is more than twice of the number of targets, and do not exist almost surely even when the number of BSs is much smaller than the number of targets. As a result, the ghost target issue is not a fundamental limitation for device-free sensing. Moreover, in the case with imperfect range estimation in Phase I, we propose a maximum-likelihood (ML) based algorithm to match each range with the right target, and then estimate the location of each target based on its matched distance values to different BSs.

2.1.4 Organization

The rest of this paper is organized as follows. Section 2.2 describes the ISAC system model. Section 2.3 introduces the proposed framework for OFDM-based device-free sensing. Section 2.4 presents the method to estimate the values of distance between the BSs and the targets. Section 2.5 studies the fundamental limits for the ghost target existence probability in the ideal case with perfect range estimation; and Section 2.6 proposes an ML algorithm to estimate the target locations with high accuracy and low ghost target detection probability in the practical case with imperfect range estimation. At last, Section 2.7 concludes this paper and points out some interesting future research directions.

2.2 System Model

2.2.1 Device-Free Sensing Network

In this paper, we consider an OFDM-based ISAC cellular system that consists of $M \geq 3$ BSs,[1] denoted by $\mathcal{M} = \{1, \ldots, M\}$; $I \geq 1$ mobile users with communication capability, denoted by $\mathcal{I} = \{1, \ldots, I\}$; and $K \geq 1$ targets without communication capability, denoted by $\mathcal{K} = \{1, \ldots, K\}$, as illustrated in Fig. 2.1. Under a two-dimensional (2D) Cartesian coordinate system, the locations of the k-th target and the m-th BS are denoted as (x_k, y_k) and (a_m, b_m) in meter (m), respectively, $\forall k \in \mathcal{K}$ and $\forall m \in \mathcal{M}$. Thus, the distance between the m-th BS and the k-th target is given by $d_{m,k} = \sqrt{(a_m - x_k)^2 + (b_m - y_k)^2}$ m, and that between the m-th BS and

[1] We consider $M \geq 3$ since at least 3 BSs are needed for localization even in device-based sensing where targets can transmit/receive reference signals.

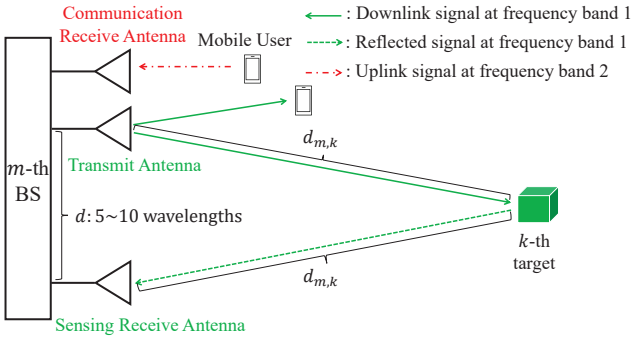

Figure 2.3: Proposed FDD architecture at the BSs for ISAC.

the u-th BS is given by $d_{m,u}^{\mathrm{BS}} = \sqrt{(a_m - a_u)^2 + (b_m - b_u)^2}$ m, $\forall k \in \mathcal{K}$ and $\forall m, u \in \mathcal{M}$.[2] In the above ISAC system, the BSs send downlink communication signals to the mobile users, while the mobile users send uplink communication signals to the BSs. Moreover, the downlink communication signals from the BSs are reflected by the targets back to the BSs, based on which the cellular network can estimate the locations of the targets as well, similar to radar systems.

To simultaneously enable downlink communication, uplink communication, as well as target sensing, this paper proposes a *frequency-division duplexing (FDD)* based ISAC framework. Specifically, as shown in Fig. 2.3, each BS is equipped with one transmit antenna working at frequency band 1 for transmitting the downlink communication signals to the mobile users, one communication receive antenna working at frequency band 2 that is non-overlapping with frequency band 1 for receiving the uplink communication signals from the mobile users, and one sensing receive antenna working at frequency band 1 to receive the downlink signals reflected by the targets. Under this FDD architecture, the communication receive antennas will not receive interference from the signals reflected by the targets, while the sensing receive antennas will not receive interference from the uplink signals sent by the mobile users. However, each sensing receive antenna will receive strong self-interference from the transmit antenna at the same BS, since each BS works in the full-duplexing mode at frequency band 1. To deal with this issue, we propose to use the techniques of RF isolation and digital-domain cancellation together to mitigate the self-interference [60]. Specifically, RF isolation works well in practice when the distance between the transmit and receive antennas is equal to $5-10$ wavelengths of

[2] Similar to [44, 45, 59], this paper focuses on 2D localization for the purpose of exposition. In practice, the height of each target is usually negligible as compared to that of a BS. Thus, with H_m denoting the height of the m-th BS, the results in this paper can be directly applied by re-expressing $d_{m,k}$ and $d_{m,u}^{\mathrm{BS}}$ as $d_{m,k} = \sqrt{(a_m - x_k)^2 + (b_m - y_k)^2 + H_m^2}$ and $d_{m,u}^{\mathrm{BS}} = \sqrt{(a_m - a_u)^2 + (b_m - b_u)^2 + (H_m - H_u)^2}$, respectively. On the other hand, when the height of each target is non-negligible and needs to be accurately estimated, our results can also be extended to three-dimensional (3D) localization by considering an additional height coordinate for each target.

the RF signals. For example, considering a typical 5G carrier frequency at 3.5 GHz, the transmit antenna and sensing receive antenna can be placed around $0.43-0.86$ m away from each other at each BS to achieve RF isolation. Then, since each BS knows its transmit signals, the self-interference can be cancelled in the the digital domain efficiently. Note that in practice, the distance between a remote target and the BS is much larger than the aforementioned RF isolation distance between antennas. As a result, we assume in this paper that the distance between target k and the transmit antenna at BS m as well as that between target k and the sensing receive antenna at BS m are both equal to $d_{m,k}$, $\forall k \in \mathcal{K}$ and $\forall m \in \mathcal{M}$, as illustrated in Fig. 2.3.

2.2.2 Sensing Signal Model

Since the OFDM cellular communication technology is quite mature, in the rest of this paper, we mainly study how to leverage the OFDM communication signals for sensing the targets in our considered ISAC cellular system. Let N and Δf (in Hz) denote the number of sub-carriers and the sub-carrier spacing of the downlink OFDM signals, respectively, thus the channel bandwidth is $B = N\Delta f$ Hz. Then, in the baseband domain, define

$$\boldsymbol{\chi}_m = [\chi_{m,1}, \ldots, \chi_{m,N}]^T = \sqrt{p}\boldsymbol{W}^H \boldsymbol{s}_m, \ \forall m, \tag{2.1}$$

as a time-domain OFDM symbol transmitted from BS m consisting of N OFDM samples, $\chi_{m,1}, \ldots, \chi_{m,N}$, where p denotes the common transmit power at the BSs; $\boldsymbol{s}_m = [s_{m,1}, \ldots, s_{m,N}]^T$ denotes the frequency-domain OFDM symbol with $s_{m,n}$ denoting the unit-power signal at the m-th BS over the n-th sub-carrier; and $\boldsymbol{W} \in \mathbb{C}^{N\times N}$ denotes the discrete Fourier transform (DFT) matrix with $\boldsymbol{W}\boldsymbol{W}^H = \boldsymbol{W}^H\boldsymbol{W} = \boldsymbol{I}$. Note that the lengths of each OFDM symbol period and each OFDM sample period are $1/\Delta f$ seconds (s) and $1/(N\Delta f)$ s, respectively.

Before the beginning of each OFDM symbol, a cyclic prefix (CP) consisting of $Q < N$ OFDM samples is inserted to eliminate the inter-symbol interference. The overall time-domain transmitted signal by the m-th BS for one OFDM symbol is thus expressed as

$$\begin{aligned}\bar{\boldsymbol{\chi}}_m =& [\underbrace{\bar{\chi}_{m,-Q}, \ldots, \bar{\chi}_{m,-1}}_{\text{CP}}, \underbrace{\bar{\chi}_{m,0}, \ldots, \bar{\chi}_{m,N-1}}_{\text{pilot or data}}]^T \\ =& [\underbrace{\chi_{m,N-Q+1}, \ldots, \chi_{m,N}}_{\text{CP}}, \underbrace{\chi_{m,1}, \ldots, \chi_{m,N}}_{\text{pilot or data}}]^T, \ \forall m.\end{aligned} \tag{2.2}$$

In this paper, we neglect the signals that are reflected by more than one target since they are generally too weak to be detected at the sensing receive antennas. The received signal at the sensing receive antenna at each BS is thus the superposition of the receiver noise and the downlink OFDM signals sent from all the M BSs, each reflected by all the K targets. Note that this automatically constitutes a *multi-path channel* between the BSs' transmit antennas and the BSs' sensing receive antennas, with each target serving as a scatter that causes a delayed path. Let L denote the maximum number of resolvable paths, with $L < Q$. The received signal at the sensing receive antenna at the m-th BS in the n-th OFDM sample period is thus expressed as

$$y_{m,n} = \sum_{u=1}^{M} \sum_{l=1}^{L} h_{u,m,l} \bar{\chi}_{u,n-l} + z_{m,n}, \quad \forall m, n, \tag{2.3}$$

where $h_{u,m,l}$ denotes the complex channel for the path from the u-th BS to the m-th BS scattered by a target that causes a delay of l OFDM sample periods, and $z_{m,n} \sim \mathcal{CN}(0, \sigma_z^2)$ denotes the circularly symmetric complex Gaussian (CSCG) noise at the sensing receive antenna of the m-th BS during the n-th OFDM sample period, with σ_z^2 denoting the average noise power.

After removing the first Q samples corrupted by the CP, the received signal at the sensing receive antenna of the m-th BS over one OFDM symbol period can be expressed as

$$\boldsymbol{y}_m = \sum_{u=1}^{M} \boldsymbol{H}_{u,m} \boldsymbol{\chi}_u + \boldsymbol{z}_m, \quad \forall m, \tag{2.4}$$

where $\boldsymbol{y}_m = [y_{m,1}, \ldots, y_{m,N}]^T$; $\boldsymbol{H}_{u,m}$ is an $N \times N$ circulant matrix with the first row defined as $[h_{u,m,1}, 0, \cdots, 0, h_{u,m,L}, \cdots, h_{u,m,2}] \in \mathbb{C}^{1\times N}$; and $\boldsymbol{z}_m = [z_{m,1}, \ldots, z_{m,N}]^T \sim \mathcal{CN}(0, \sigma_z^2 \boldsymbol{I})$. After multiplying the time-domain signal by the DFT matrix, the received signal at the sensing receive antenna of the m-th BS in the frequency domain is given by

$$\begin{aligned} \bar{\boldsymbol{y}}_m =& [\bar{y}_{m,1}, \ldots, \bar{y}_{m,N}]^T \\ =& \boldsymbol{W} \boldsymbol{y}_m = \sqrt{p} \sum_{u=1}^{M} \operatorname{diag}(\boldsymbol{s}_u) \boldsymbol{G} \boldsymbol{h}_{u,m} + \bar{\boldsymbol{z}}_m, \quad \forall m, \end{aligned} \tag{2.5}$$

where $\boldsymbol{h}_{u,m} = [h_{u,m,1}, \ldots, h_{u,m,L}]^T$; $\operatorname{diag}(\boldsymbol{s}_u)$ is a diagonal matrix with the main diagonal being $\boldsymbol{s}_u$; $\boldsymbol{G} \in \mathbb{C}^{N\times L}$ with the (n,l)-th element being $G_{n,l} = e^{\frac{-j2\pi(n-1)(l-1)}{N}}$; and $\bar{\boldsymbol{z}}_m = [\bar{z}_{m,1}, \ldots, \bar{z}_{m,N}]^T = \boldsymbol{W} \boldsymbol{z}_m \sim \mathcal{CN}(0, \sigma_z^2 \boldsymbol{I})$ since $\boldsymbol{W}\boldsymbol{W}^H = \boldsymbol{I}$.

2.3 Two-Phase Device-Free Sensing Framework

In this section, we propose a two-phase framework for device-free sensing based on the signals received by the sensing receive antennas, as illustrated in Fig. 2.2.

2.3.1 Phase I: Range Estimation

First, in Phase I, each BS m estimates the channels between its transmit antenna and its sensing receive antenna, $h_{m,m,l}$'s, $l = 1, \ldots, L$. A key observation is that if $h_{m,m,l} \neq 0$ for some l, a target indexed by $\bar{k}_{m,l} \in \mathcal{K}$ exists, where the signal propagation from BS m to target $\bar{k}_{m,l}$ and then back to BS m experiences a delay of l OFDM sample periods. Hence, by recalling that the duration of one OFDM sample period is $1/(N\Delta f)$ s, the distance (range) between target $\bar{k}_{m,l}$ and BS m (which is half of the propagated distance) lies in the following range set (in m):

$$\Theta(l) = \left\{ d \,\middle|\, \frac{(l-1)c_0}{2N\Delta f} < d \leq \frac{lc_0}{2N\Delta f} \right\}, \tag{2.6}$$

where c_0 denotes the speed of the light (in m/s). In this case, we propose to estimate the distance between the m-th BS and the $\bar{k}_{m,l}$-th target, $d_{m,\bar{k}_{m,l}}$, as the middle point in the above range set $\Theta(l)$:

$$\bar{d}_{m,\bar{k}_{m,l}} = \frac{(l-1)c_0}{2N\Delta f} + \frac{c_0}{4N\Delta f}, \text{ if } \bar{h}_{m,m,l} \geq \delta_0, \tag{2.7}$$

where $\bar{h}_{m,m,l}$ is the channel estimation for $h_{m,m,l}$, and δ_0 is a predefined constant. Note that under the above estimation rule, the worst-case range estimation error is given by

$$|\bar{d}_{m,\bar{k}_{m,l}} - d_{m,\bar{k}_{m,l}}| \leq \frac{c_0}{4N\Delta f} \triangleq \Delta d. \tag{2.8}$$

For example, in 5G OFDM systems, the channel bandwidth is $B = 100$ MHz at the sub-6G frequency band and $B = 400$ MHz at the mmWave band according to 3GPP Release 15 [57]. In this case, the worst-case range estimation errors are 0.75 m and 0.1875 m, respectively. Since Δd is practically very small, we assume in the sequel that the values of distance for any two paths reflected back to a BS by two different targets differ by more than $2\Delta d$, thus the corresponding paths are resolvable. Therefore, there are K non-zero entries in each $\boldsymbol{h}_{m,m}$.

After obtaining $\bar{d}_{m,\bar{k}_{m,l}}$'s, each BS m has a range set consisting of the values of distance (ranges) with the targets:

$$\mathcal{D}_m = \{\bar{d}_{m,\bar{k}_{m,l}} | \forall l \text{ satisfying } \bar{h}_{m,m,l} \geq \delta_0\}, \quad \forall m. \tag{2.9}$$

For convenience, we define $\mathcal{D}_m(g)$ as the g-th largest element in $\mathcal{D}_m$, $\forall m$. Moreover, define $g_{m,k}$'s as the mapping (or matching) between the element in $\mathcal{D}_m$ and the k-th target, such that $\bar{d}_{m,k}$ is the $g_{m,k}$-th largest element in $\mathcal{D}_m$, i.e.,

$$\bar{d}_{m,k} = \mathcal{D}_m(g_{m,k}), \quad \forall m,k. \tag{2.10}$$

In Section 2.4, we will introduce in details the estimation of $h_{m,m,l}$'s based on the signals at the sensing receive antennas for obtaining the range sets $\mathcal{D}_m$'s in Phase I.

2.3.2 Phase II: Localization Among BSs Based on Estimated Range

Next, in Phase II, all the BSs share their range sets $\mathcal{D}_m$'s with each other via the cellular fronthaul links, and jointly estimate the location of each target k based on the values of its distance to the M BSs, $\{\bar{d}_{1,k},\ldots,\bar{d}_{M,k}\}$, $\forall k$. Note that in conventional device-based sensing for active targets that can send/receive RF signals with different signatures, the BSs can know the exact mapping between a range and a target, i.e., each BS m knows which element in $\mathcal{D}_m$ is $\bar{d}_{m,k}$, $\forall k$. However, in our considered device-free sensing for passive targets without communication capability, all the targets will reflect the same signals to the BSs. As a result, each BS m only knows that the range of target k lies in the set $\mathcal{D}_m$, but does not know which element in $\mathcal{D}_m$ corresponds to this range, i.e., $g_{m,k}$ is unknown, $\forall k$. In this case, a wrong matching solution of $g_{m,k}$'s may lead to the detection of *ghost targets* (for which the exact definition will be given in Section 2.5) that do not exist, as illustrated in Example 2.1.

Example 2.1. *Suppose that there are $M = 3$ BSs and $K = 2$ targets. The coordinates of BSs 1, 2, and 3 are $(0,3)$, $(5,0)$, and $(0,-4)$, respectively, and the coordinates of targets 1 and 2 are $(2,-2)$ and $(-2,2)$, respectively. Suppose that the BSs can perfectly estimate the ranges of targets, i.e., $\bar{d}_{m,k} = d_{m,k}$, $\forall m,k$. Thus, we have $\mathcal{D}_1 = \{\sqrt{29},\sqrt{5}\}$, $\mathcal{D}_2 = \{\sqrt{13},\sqrt{53}\}$, and $\mathcal{D}_3 = \{2\sqrt{2},2\sqrt{10}\}$.*

The job of the BSs is to solve the set of equations $\sqrt{(a_m - x_k)^2 + (b_m - y_k)^2} = \mathcal{D}(g_{m,k})$, $m = 1,2,3$, $k = 1,2$, where x_k's, y_k's, and $g_{m,k}$'s are all unknown variables. If the BSs set $g_{1,1} = 1$,

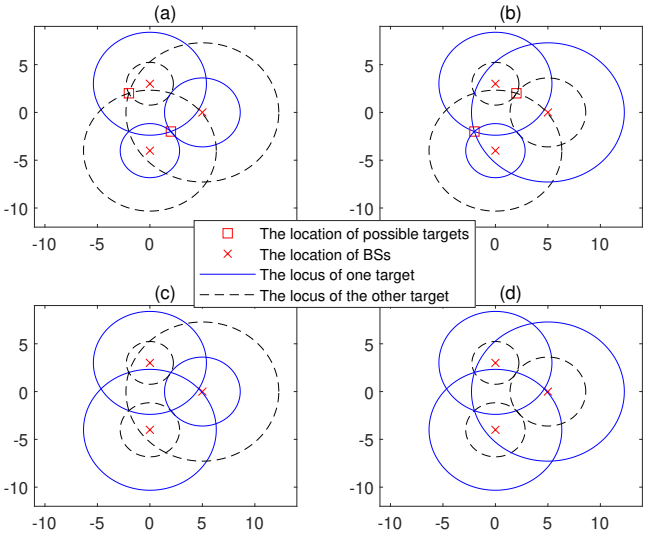

Figure 2.4: An example with ghost targets. In (a), we have $g_{1,1}=1$, $g_{2,1}=2$, $g_{3,1}=2$, $g_{1,2}=2$, $g_{2,2}=1$, $g_{3,2}=1$; in (b), we have $g_{1,1}=1$, $g_{2,1}=1$, $g_{3,1}=2$, $g_{1,2}=2$, $g_{2,2}=2$, $g_{3,2}=1$; in (c), we have $g_{1,1}=1$, $g_{2,1}=2$, $g_{3,1}=1$, $g_{1,2}=2$, $g_{2,2}=1$, $g_{3,2}=2$; in (d), we have $g_{1,1}=1$, $g_{2,1}=1$, $g_{3,1}=1$, $g_{1,2}=2$, $g_{2,2}=2$, $g_{3,2}=2$.

$g_{2,1}=2$, $g_{3,1}=2$ for sensing one target, and $g_{1,2}=2$, $g_{2,2}=1$, $g_{3,2}=1$ for sensing the other target, i.e., $d_{1,1}=\mathcal{D}_1(1)=\sqrt{29}$, $d_{2,1}=\mathcal{D}_2(2)=\sqrt{13}$, and $d_{3,1}=\mathcal{D}_3(2)=2\sqrt{2}$ are used for sensing one target, and $d_{1,2}=\mathcal{D}_1(2)=\sqrt{5}$, $d_{2,2}=\mathcal{D}_2(1)=\sqrt{53}$, and $d_{3,2}=\mathcal{D}_3(1)=2\sqrt{10}$ are used for sensing the other target, then the real targets $(2,-2)$ and $(-2,2)$ can be detected, as shown in Fig. 2.4 (a). However, if the BSs set $g_{1,1}=1$, $g_{2,1}=1$, $g_{3,1}=2$ for sensing one target and $g_{1,2}=2$, $g_{2,2}=2$, $g_{3,2}=1$ for sensing the other target, i.e., $d_{1,1}=\mathcal{D}_1(1)=\sqrt{29}$, $d_{2,1}=\mathcal{D}_2(1)=\sqrt{53}$, and $d_{3,1}=\mathcal{D}_3(2)=2\sqrt{2}$ are used for sensing one target, and $d_{1,2}=\mathcal{D}_1(2)=\sqrt{5}$, $d_{2,2}=\mathcal{D}_2(2)=\sqrt{13}$, and $d_{3,2}=\mathcal{D}_3(1)=2\sqrt{10}$ are used for sensing the other target, then two ghost targets with coordinates $(-2,-2)$ and $(2,2)$ will be detected, as shown in Fig. 2.4 (b). Note that under the other matching solutions, e.g., $g_{1,1}=1$, $g_{2,1}=2$, $g_{3,1}=1$ for sensing one target and $g_{1,2}=2$, $g_{2,2}=1$, $g_{3,2}=2$ for sensing the other target, as shown in Fig. 2.4 (c), and $g_{1,1}=1$, $g_{2,1}=1$, $g_{3,1}=1$ for one target and and $g_{1,2}=2$, $g_{2,2}=2$, $g_{3,2}=2$ for the other target, as shown in Fig. 2.4 (d), no ghost target exists.

Although Example 2.1 indicates that ghost targets may be detected under certain setups, it is worth noting that they do not always exist, as shown in the following example.

Example 2.2. *Suppose that there are $M=3$ BSs and $K=2$ targets. The coordinates of BSs 1, 2, and 3 are $(0,3)$, $(5,0)$ and $(0,-4)$, respectively, and the coordinates of targets 1 and 2 are $(-1,2)$ and $(2,-1)$, respectively. Similar to Example 2.1, suppose that the BSs can perfectly estimate the ranges of targets, i.e., $\mathcal{D}_1=\{\sqrt{2},2\sqrt{5}\}$, $\mathcal{D}_2=\{2\sqrt{10},\sqrt{10}\}$, and $\mathcal{D}_3=\{\sqrt{37},\sqrt{13}\}$. If the BSs*

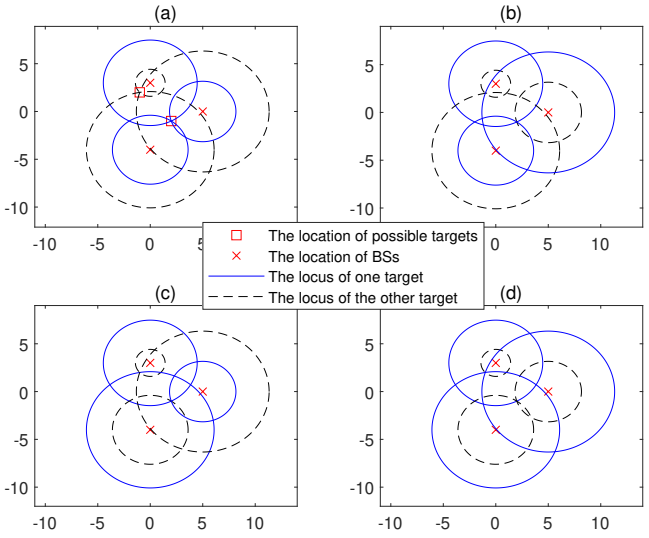

Figure 2.5: An example without ghost targets. In (a), we have $g_{1,1}=1$, $g_{2,1}=2$, $g_{3,1}=2$, $g_{1,2}=2$, $g_{2,2}=1$, $g_{3,2}=1$; in (b), we have $g_{1,1}=1$, $g_{2,1}=1$, $g_{3,1}=2$, $g_{1,2}=2$, $g_{2,2}=2$, $g_{3,2}=1$; in (c), we have $g_{1,1}=1$, $g_{2,1}=2$, $g_{3,1}=1$, $g_{1,2}=2$, $g_{2,2}=1$, $g_{3,2}=2$; in (d), we have $g_{1,1}=1$, $g_{2,1}=1$, $g_{3,1}=1$, $g_{1,2}=2$, $g_{2,2}=2$, $g_{3,2}=2$.

set $g_{1,1}=1$, $g_{2,1}=2$, $g_{3,1}=2$ *for sensing one target and* $g_{1,2}=2$, $g_{2,2}=1$, $g_{3,2}=1$ *for sensing the other target, as shown in Fig. 2.5 (a), then the location of the real targets can be correctly estimated. Otherwise, with the other matching solutions of* $g_{m,k}$*'s, no ghost targets will be detected, as shown in Fig. 2.5 (b), (c) and (d).*

In Section 2.5, we will study the fundamental limit of the ghost target detection probability arising from the range matching issue at each BS; then, we will propose an ML algorithm to solve the joint range matching and target localization problem to approach the above limit in Section 2.6.

2.4 Phase I: Range Estimation

In this section, we propose a range estimation algorithm for obtaining $\bar{d}_{m,\bar{k}_{m,l}}$'s as well as $\mathcal{D}_m$'s in Phase I, by estimating the multi-path channels $h_{m,m,l}$'s via OFDM channel estimation techniques.

2.4.1 Algorithm Design

Note that each BS m only knows its own transmitted signals, i.e., $\boldsymbol{s}_m$, but does not know the transmitted signals of the other BSs, i.e., $\boldsymbol{s}_u$, $\forall u \neq m$. As a result, the main challenge to

estimate the channels based on the frequency-domain received signal in (2.5) at each BS lies in the partial (instead of full) knowledge about the sensing matrix in (2.5). In the following, we show that the above challenge can be tackled by the fractional frequency reuse technique that is widely used in cellular networks to control the inter-cell interference. Specifically, suppose that each BS m occupies a partial of the N sub-carriers denoted by the set $\mathcal{N}_m \subset \{1,\ldots,N\}$, i.e.,

$$s_{m,n} = 0,\ \forall n \notin \mathcal{N}_m,\ \forall m. \tag{2.11}$$

For simplicity, define $\mathcal{N}_m(n)$ as the n-th smallest element in the set $\mathcal{N}_m$. Moreover, adjacent BSs will be assigned with totally different sub-carrier sets under the fractional frequency reuse scheme. Let Υ_m denote the set of BSs that are far away from BS m and thus share the same sub-carrier set with BS m, i.e., $\mathcal{N}_m = \mathcal{N}_u$ holds $\forall u \in \Upsilon_m$. Under the above scheme and according to (2.5), the received signal of BS m at its assigned sub-carriers, denoted by $\tilde{\boldsymbol{y}}_m = [\bar{y}_{m,\mathcal{N}_m(1)},\ldots,\bar{y}_{m,\mathcal{N}_m(|\mathcal{N}_m|)}]^T$, is given by

$$\tilde{\boldsymbol{y}}_m = \sqrt{p}\,\mathrm{diag}(\tilde{\boldsymbol{s}}_m)\tilde{\boldsymbol{G}}_m\boldsymbol{h}_{m,m} + \tilde{\boldsymbol{z}}_m,\ \forall m, \tag{2.12}$$

where $\tilde{\boldsymbol{s}}_u = [s_{u,\mathcal{N}_u(1)},\ldots,s_{u,\mathcal{N}_u(|\mathcal{N}_u|)}]^T, \forall u \in \mathcal{M}$, $\tilde{\boldsymbol{G}}_m = [\boldsymbol{g}_{\mathcal{N}_m(1)},\ldots,\boldsymbol{g}_{\mathcal{N}_m(|\mathcal{N}_m|)}]^T$ with $\boldsymbol{g}_n^T$ being the n-th row of $\boldsymbol{G}$, and $\tilde{\boldsymbol{z}}_m = \sqrt{p}\sum_{u\in\Upsilon_m}\mathrm{diag}(\tilde{\boldsymbol{s}}_u)\tilde{\boldsymbol{G}}_m\boldsymbol{h}_{u,m} + [\bar{z}_{m,\mathcal{N}_m(1)},\ldots,\bar{z}_{m,\mathcal{N}_m(|\mathcal{N}_m|)}]^T$ is the effective noise at BS m with weak interference caused by the distant BSs in the set Υ_m.

Note that among the L elements in each $\boldsymbol{h}_{m,m}$, only $K \ll L$ of them are non-zero since there are merely K scatters (targets) for each BS. Recovering the sparse channels $\boldsymbol{h}_{m,m}$'s based on (2.12) is thus a compressed sensing problem, which motivates us to use the least absolute shrinkage and selection operator (LASSO) [61] technique to estimate $\boldsymbol{h}_{m,m}$'s. Specifically, given a carefully designed parameter $\lambda \geq 0$,[3] the LASSO problem for estimating each $\boldsymbol{h}_{m,m}$ is formulated as

$$\underset{\boldsymbol{h}_{m,m}}{\text{minimize}}\ \frac{1}{2}\|\bar{\boldsymbol{y}}_{m,m} - \sqrt{p}\,\mathrm{diag}(\tilde{\boldsymbol{s}}_m)\tilde{\boldsymbol{G}}_m\boldsymbol{h}_{m,m}\|_2^2 + \lambda\|\boldsymbol{h}_{m,m}\|_1. \tag{2.13}$$

Note that (2.13) is a convex optimization problem, for which the optimal solution can be efficiently obtained by CVX and serve as the estimated channel $\bar{\boldsymbol{h}}_{m,m} = [\bar{h}_{m,m,1},\ldots,\bar{h}_{m,m,L}]^T$.[4]

[3] More details on LASSO can be found in [61].

[4] For the special case of $\mathrm{rank}(\mathrm{diag}(\tilde{\boldsymbol{s}}_m)\tilde{\boldsymbol{G}}_m) = L$ (e.g., $N/M \geq L$) where (2.12) describes an overdetermined linear system, we can set $\lambda = 0$ in problem (2.13), which leads to the ML channel estimators $\bar{\boldsymbol{h}}_{m,m} = (\tilde{\boldsymbol{G}}_m^H\mathrm{diag}(\tilde{\boldsymbol{s}}_m)\mathrm{diag}(\tilde{\boldsymbol{s}}_m)\tilde{\boldsymbol{G}}_m)^{-1}\tilde{\boldsymbol{G}}_m^H\mathrm{diag}(\tilde{\boldsymbol{s}}_m)\tilde{\boldsymbol{y}}_m/\sqrt{p}, \forall m$.

Then, if $\bar{h}_{m,m,l} \neq 0$ for some l, $\bar{d}_{m,\bar{k}_{m,l}}$ can be estimated via (2.7), and the range sets $\mathcal{D}_m$'s can be obtained via (2.9).

2.4.2 Numerical Examples

In the following, we provide a numerical example to evaluate the accuracy of the proposed range estimation algorithm. Specifically, we set $N = 3300$ and $\Delta f = 30$ kHz such that $B = 100$ MHz [57]. According to [62], with $\Delta f = 30$ kHz, the length of the CP is 2.34 μs. To make $L < Q$ such that the CP can be cancelled at the BSs, we assume that the maximum number of resolvable paths is $L = 200$. Moreover, we consider $M = 4$ BSs in the network, while each BS is randomly assigned with $N/M = 825$ sub-carriers such that $\mathcal{N}_m \bigcap \mathcal{N}_u = \emptyset$, $\forall m \neq u$, i.e., $\Upsilon_m = \emptyset$, $\forall m$. Under this setup, we randomly generate 10^5 independent localization realizations of the $M = 4$ BSs and K targets, following uniform distribution over a 200 m $\times$ 200 m square. Given the values of the BS-target distance, we can know the delay in terms of OFDM sample periods from BS m to target k back to BS m, $\forall m, k$, according to (2.6). Define $\mathcal{L}_m$ as the set of K true delay values in terms of OFDM sample periods caused by the K targets to BS m, $\forall m$. Then, we estimate the channels $\boldsymbol{h}_{m,m}$'s by solving problem (2.13), and define $\bar{\mathcal{L}}_m = \{l | \bar{h}_{m,m,l} \neq 0, l = 1, \ldots, L\}$ as the set of estimated delay values at BS m, $\forall m$. If there exists at least an m such that $\mathcal{L}_m \neq \bar{\mathcal{L}}_m$, we say that the range estimation is in error in this realization. Fig. 2.6 shows the range estimation error probability versus the number of targets, K (ranging from 2 to 8), where the BS transmit power is set as 6 Watt (W) and 8 W, respectively. It is observed that the range estimation error probability is very low under our proposed scheme, and can be significantly reduced by increasing the transmit power.

After $\bar{d}_{m,\bar{k}_{m,l}}$'s and the range sets $\mathcal{D}_m$'s are obtained, we need to study how the BSs can cooperate with each other to localize the K targets based on $\mathcal{D}_m$'s. As discussed at the end of Section 2.3, the main challenge here lies in the lack of information about $g_{m,k}$'s, i.e., each BS m does not know how to match the ranges in $\mathcal{D}_m$ with the right targets, which may lead to the detection of ghost targets instead of the true targets. In the following, we will first consider the ideal case without error in estimating the values of the distance between the BSs and targets, i.e., $\bar{d}_{m,k} = d_{m,k}$, $\forall m, k$, and investigate the fundamental limit of the ghost target detection probability in Section 2.5. Then, in Section 2.6, we will focus on the practical case with possible error in estimating $d_{m,k}$'s, and propose an ML algorithm to find a good matching solution $g_{m,k}$'s at each BS so as to minimize the target localization error.

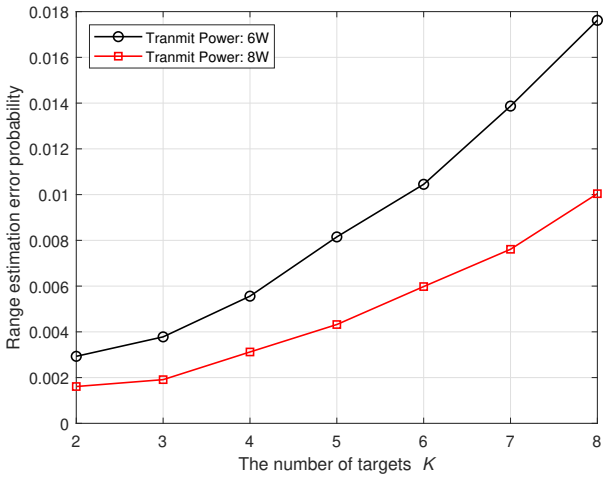

Figure 2.6: Range estimation error probability versus the number of targets.

2.5 Phase II: Localization with Perfect Range Estimation

In this section, we introduce the target localization in Phase II, assuming that the range estimation based on (2.7) is perfect, i.e., $\bar{d}_{m,k} = d_{m,k}$, $\forall m,k$, in order to derive the fundamental limits and draw essential insights. This corresponds to the ideal case of an infinite channel bandwidth such that $\Delta d = 0$ in (2.8).

Note that in device-based sensing where each BS can distinguish the ranges of different targets, the locations of the targets can be estimated by solving the following equations:

$$\sqrt{(a_m - x_k)^2 + (b_m - y_k)^2} = d_{m,k}, \quad \forall m,k. \tag{2.14}$$

It is well-known that three BSs are sufficient to localize the targets. However, in our considered device-free sensing where each BS cannot distinguish the ranges of different targets, the BSs need to solve the following equations to estimate the target locations:

$$\sqrt{(a_m - x_k)^2 + (b_m - y_k)^2} = \mathcal{D}_m(g_{m,k}), \quad \forall m,k, \tag{2.15}$$

$$g_{1,k} = k, \quad \forall k, \tag{2.16}$$

$$\{g_{m,1}, \ldots, g_{m,K}\} = \mathcal{K}, \quad \forall m > 2. \tag{2.17}$$

Different from the device-based sensing equations in (2.14), under device-free sensing, $g_{m,k}$'s are also unknown variables in (2.15) that need to satisfy conditions (2.16) and (2.17), i.e., different ranges for each BS belong to different targets. In (2.16), we define target k as the target

whose distance to BS 1 is the k-th largest element in $\mathcal{D}_1$, i.e., $d_{1,k} = \mathcal{D}_1(k)$, $\forall k \in \mathcal{K}$. The reason is to mitigate the ambiguity in target indexing. To illustrate this, let us consider Example 2.1 in Section 2.4. In Fig. 2.4 (a), under the matching solution of $g_{1,1} = 1$, $g_{2,1} = 2$, $g_{3,1} = 2$, $g_{1,2} = 2$, $g_{2,2} = 1$, $g_{3,2} = 1$, the location of target 1 is $(2,-2)$, while that of target 2 is $(-2,2)$. However, if we consider the matching solution of $g_{1,1} = 2$, $g_{2,1} = 1$, $g_{3,1} = 1$, $g_{1,2} = 1$, $g_{2,2} = 2$, $g_{3,2} = 2$, the location of target 1 is $(-2,2)$, while that of target 2 is $(2,-2)$. In fact, these two matching solutions lead to the same localization result. Thus, we add constraint (2.16) to avoid the above ambiguity.

It is worth noting that in device-free sensing, the target locations may not be accurately estimated by three BSs because there may be multiple solutions to equations (2.15), (2.16), and (2.17) when $M = 3$, which leads to the existence of *ghost targets*, as shown in Example 1. In the following, we propose an algorithm to detect the existence of ghost targets, and derive the fundamental limit of ghost target existence.

2.5.1 Definition of Ghost Targets

First, we present the rigourous definition of ghost targets.

Definition 2.1. Define $\mathcal{X} = \{(x_1, y_1), \ldots, (x_K, y_K)\}$ as the set of coordinates for all the K targets. Then, consider another coordinate set $\mathcal{X}^{\mathrm{G}} = \{(x_1^{\mathrm{G}}, y_1^{\mathrm{G}}), \ldots, (x_K^{\mathrm{G}}, y_K^{\mathrm{G}})\} \neq \mathcal{X}$ and define

$$d_{m,k}^{\mathrm{G}} = \sqrt{(a_m - x_k^{\mathrm{G}})^2 + (b_m - y_k^{\mathrm{G}})^2}, \quad \forall m,k, \tag{2.18}$$

$$\mathcal{D}_m^{\mathrm{G}} = \{d_{m,1}^{\mathrm{G}}, \ldots, d_{m,K}^{\mathrm{G}}\}, \quad \forall m. \tag{2.19}$$

We say K ghost targets exist with the coordinates shown in the set X^{G} if and only if

$$\mathcal{D}_m = \mathcal{D}_m^{\mathrm{G}}, \quad \forall m. \tag{2.20}$$

In other words, besides $\mathcal{X}$, $\mathcal{X}^{\mathrm{G}}$ is another solution to equations (2.15), (2.16), and (2.17).

2.5.2 Algorithm to Detect the Existence of Ghost Targets

Based on Definition 2.1, given any particular BS locations (a_m, b_m)'s and range sets $\mathcal{D}_m$'s, we can efficiently check whether ghost targets exist as follows. First, since three BSs can

locate any target if the matching solution is given, we can fix the matching solution for BS 1 as (2.16) and list all the feasible matching solutions for BSs 2 and 3 that satisfy condition (2.17). In total, there are $(K!)^2$ feasible matching solutions for BSs 2 and 3. Moreover, a feasible matching solution for BSs 1, 2, and 3 should also satisfy the following triangle inequalities for each target k:

$$|\mathcal{D}_{m_1}(g_{m_1,k}) - \mathcal{D}_{m_2}(g_{m_2,k})| \leq d^{\mathrm{BS}}_{m_1,m_2},\ \forall m_1, m_2 \in \{1,2,3\}, \tag{2.21}$$

$$|\mathcal{D}_{m_1}(g_{m_1,k}) + \mathcal{D}_{m_2}(g_{m_2,k})| \geq d^{\mathrm{BS}}_{m_1,m_2},\ \forall m_1, m_2 \in \{1,2,3\}. \tag{2.22}$$

To summarize, we can define a set consisting of all the feasible matching solutions for BSs 1, 2, and 3 as follows:

$$\begin{aligned}\mathcal{H} =& \{\{g_{1,k}, g_{2,k}, g_{3,k}\}_{k=1}^K | \{g_{1,k}, g_{2,k}, g_{3,k}\}_{k=1}^K \text{ satisfies (2.16)},\\ & \text{(2.17)}, \text{ and } (g_{1,k}, g_{2,k}),\ (g_{1,k}, g_{3,k}),\ (g_{2,k}, g_{3,k}) \text{ satisfy}\\ & \text{(2.21)},\ \text{(2.22)},\ \forall k\}.\end{aligned} \tag{2.23}$$

Usually, the cardinality of $\mathcal{H}$ is much smaller than $(K!)^2$ thanks to the utilization of the triangle inequalities (2.21) and (2.22) to eliminate the infeasible matching solutions.

Then, for each matching solution for BSs 1, 2, and 3 in the set $\mathcal{H}$, which is given by $\bar{g}_{m,k}$'s, $m = 1,2,3$ and $\forall k$, we check whether there is a localization solution to the following equations:

$$\sqrt{(a_m - x_k)^2 + (b_m - y_k)^2} = \mathcal{D}_m(\bar{g}_{m,k}), m = 1,2,3,\ \forall k. \tag{2.24}$$

If there is no solution, we can conclude that under all the matching solutions for all the BSs where the matching solution to BSs 1, 2, and 3 is $g_{m,k} = \bar{g}_{m,k}$, $m = 1,2,3$ and $k = 1,\ldots,K$, no ghost target exists. Otherwise, if there is a solution denoted by $\{(\bar{x}_k, \bar{y}_k)\}_{k=1}^K$ to the above equations, we can use this solution to calculate $\bar{\mathcal{D}}_m$, $\forall m > 3$, the elements of which are $\sqrt{(a_m - \bar{x}_k)^2 + (b_m - \bar{y}_k)^2}$'s, $k \in \mathcal{K}$. If there exists an $\bar{m} > 3$ such that $\bar{\mathcal{D}}_{\bar{m}} \neq \mathcal{D}_{\bar{m}}$, then we can conclude that under all the matching solutions for all the BSs where the matching solution to BSs 1, 2, and 3 is $g_{m,k} = \bar{g}_{m,k}$, $m = 1,2,3$ and $k = 1,\ldots,K$, no ghost targets exist. Otherwise, if $\bar{\mathcal{D}}_m = \mathcal{D}_m$, $\forall m > 3$, then $\{(\bar{x}_k, \bar{y}_k)\}_{k=1}^K$ is defined as a feasible localization solution, which may be the locations of either the true targets or the ghost targets. After searching over all the feasible matching solutions for BSs 1, 2, and 3 in the set $\mathcal{H}$, if only one feasible solution of $\{(\bar{x}_k, \bar{y}_k)\}_{k=1}^K$ is found, it indicates that given this particular (a_m, b_m)'s and $\mathcal{D}_m$'s, no ghost target

Algorithm 1: Algorithm to Check Whether Ghost Target Exists

Input: (a_m, b_m)'s and $\mathcal{D}_m$'s, $\forall m \in \mathcal{M}$.
Initialization: Obtain the feasible matching solutions for BSs 1, 2, and 3 in $\mathcal{H}$ given in (2.23). Define $\mathcal{H}(t)$ as the t-th matching solution in $\mathcal{H}$. Set $t = 1$ and $\tau = 0$.
Repeat:

1. Set $\mathcal{H}(t)$ as the matching solution of BSs 1, 2, and 3, denoted by $\bar{g}_{m,k}$'s, $m = 1,2,3$ and $k = 1,\ldots,K$;
2. Check whether there exists a localization solution to equations (2.24) given the above matching solution. If there exists a solution, which is denoted by $\{(\bar{x}_k, \bar{y}_k)\}_{k=1}^K$, then:
   2.1 For each BS $m > 3$, set $\bar{\mathcal{D}}_m = \{\sqrt{(a_m - \bar{x}_k)^2 + (b_m - \bar{y}_k^2)} | k = 1,\ldots,K\}$;
   2.2 Check whether $\bar{\mathcal{D}}_m = \mathcal{D}_m$, $\forall m > 3$, holds. If this is true, set $\tau = \tau + 1$.
3. Set $t = t + 1$.

Until $t = |\mathcal{H}|$.
Output: If $\tau = 1$, no ghost target exists; otherwise, if $\tau > 1$, ghost target exists.

exists. Otherwise, if multiple feasible solutions of $\{(\bar{x}_k, \bar{y}_k)\}_{k=1}^K$ are found, then ghost targets exist given this (a_m, b_m)'s and $\mathcal{D}_m$'s. A summary of this algorithm is given in Algorithm 1.

2.5.3 Fundamental Limit for Existence of Ghost Target

Note that Algorithm 1 can help us determine whether ghost target exists given any (a_m, b_m)'s and $\mathcal{D}_m$'s. In the following, we aim to show some stronger results about the fundamental limit of the ghost target detection probability merely given the BS locations, i.e., (a_m, b_m)'s, but regardless of the range sets $\mathcal{D}_m$'s. To achieve this goal, given any target coordinate set $\mathcal{X}$ and another set $\mathcal{X}^{\mathrm{G}} \neq \mathcal{X}$ consisting of K pairs of coordinates, define

$$\mathcal{X}^{\mathrm{C}} = \mathcal{X} \bigcap \mathcal{X}^{\mathrm{G}}, \tag{2.25}$$

$$\tilde{\mathcal{X}} = \mathcal{X} / \mathcal{X}^{\mathrm{C}}, \tag{2.26}$$

$$\tilde{\mathcal{X}}^{\mathrm{G}} = \mathcal{X}^{\mathrm{G}} / \mathcal{X}^{\mathrm{C}}, \tag{2.27}$$

where $\mathcal{A}/\mathcal{B} = \{x | x \in \mathcal{A} \text{ and } x \notin \mathcal{B}\}$. As a result, $\mathcal{X}^{\mathrm{C}}$ is the set of common coordinates in $\mathcal{X}$ and $\mathcal{X}^{\mathrm{G}}$, while $\tilde{\mathcal{X}}$ and $\tilde{\mathcal{X}}^{\mathrm{G}}$ consist of the distinct parts in $\mathcal{X}$ and $\mathcal{X}^{\mathrm{G}}$. Then, define

$$\mathcal{S}_{k,q} = \{m | d_{m,k} = d_{m,q}^{\mathrm{G}}, \forall m\}, \quad \forall k, q, \tag{2.28}$$

as the set of BSs whose distance values to (x_k, y_k) and $(x_q^{\mathrm{G}}, y_q^{\mathrm{G}})$ are the same, where $d_{m,q}^{\mathrm{G}}$ is given in (2.18). Note that if $(x_k, y_k) = (x_q^{\mathrm{G}}, y_q^{\mathrm{G}}) \in \mathcal{X}^{\mathrm{C}}$, then $\mathcal{S}_{k,q} = \mathcal{M}$. Otherwise, if $(x_k, y_k) \in \tilde{\mathcal{X}}$ and $(x_q^{\mathrm{G}}, y_q^{\mathrm{G}}) \in \tilde{\mathcal{X}}^{\mathrm{G}}$ such that $(x_k, y_k) \neq (x_q^{\mathrm{G}}, y_q^{\mathrm{G}})$, then all the BSs in the set $\mathcal{S}_{k,q}$ must be on the perpendicular bisector of the line segment connecting (x_k, y_k) and $(x_q^{\mathrm{G}}, y_q^{\mathrm{G}})$. In the following, we provide one BS deployment topology where ghost target never exists no matter where the true targets are.

Theorem 2.2. *Suppose that range estimation is perfect at all BSs. If $M \geq 2K+1$ and any three of the BSs are not deployed on the same line, then no matter where the K targets are, ghost target does not exist.*

Proof. We prove Theorem 2.2 by contradiction. Suppose that there exists a coordinate set for the K true targets $\mathcal{X} = \{(x_1, y_1), \ldots, (x_K, y_K)\}$ such that K ghost targets exist with a coordinate set $\mathcal{X}^{\mathrm{G}} = \{(x_1^{\mathrm{G}}, y_1^{\mathrm{G}}), \ldots, (x_K^{\mathrm{G}}, y_K^{\mathrm{G}})\} \neq \mathcal{X}$. Let us consider a coordinate $(x_k, y_k) \in \mathcal{X}$ which however does not appear in $\mathcal{X}^{\mathrm{G}}$, i.e., $(x_k, y_k) \in \tilde{\mathcal{X}}$ defined in (2.26). In this case, the BSs in the set $\mathcal{S}_{k,q}$ should be on the perpendicular bisector of the line segment connecting (x_k, y_k) and $(x_q^{\mathrm{G}}, y_q^{\mathrm{G}})$, $\forall q \in \mathcal{K}$. Since any three BSs are not deployed on the same line, we have $|\mathcal{S}_{k,p}| = 0$, 1, or 2, $\forall q \in \mathcal{K}$. It thus follows that $\sum_{q=1}^{K} |\mathcal{S}_{k,q}| \leq 2K < M$. In other words, $\bigcup_{q \in \mathcal{K}} \mathcal{S}_{k,q} \neq \mathcal{M}$, and there exists an $m \in \mathcal{M}$ such that $m \notin \bigcup_{q \in \mathcal{K}} \mathcal{S}_{k,q}$. This indicates that $d_{m,k}$ is not in the set $\mathcal{D}_m^{\mathrm{G}}$ and $\mathcal{D}_m \neq \mathcal{D}_m^{\mathrm{G}}$, which contradicts (2.20) in Definition 2.1. Therefore, if $M \geq 2K+1$ and any three BSs are not deployed on the same line, then there never exist ghost targets no matter where the K true targets are. Theorem 2.2 is thus proved. □

The key condition for Theorem 2.2 is $M \geq 2K+1$. It is worth noting that if this condition does not hold, there may exist some target locations that can lead to ghost targets, as shown in Example 2.1, where $M = 3$ and $K = 2$. Interestingly, the following theorem shows that even if $M < 2K+1$, when the targets are located independently and uniformly in the network, the probability that these targets happen to be at the locations that can lead to ghost targets is *zero*.

Theorem 2.3. *Suppose that range estimation is perfect at all BSs. If $M \geq 4$ and any three of the BSs are not deployed on the same line, then given any finite number of targets, ghost target does not exist almost surely when the true targets are located independently and uniformly in the network.*

Proof. Please refer to Appendix 7.1. □

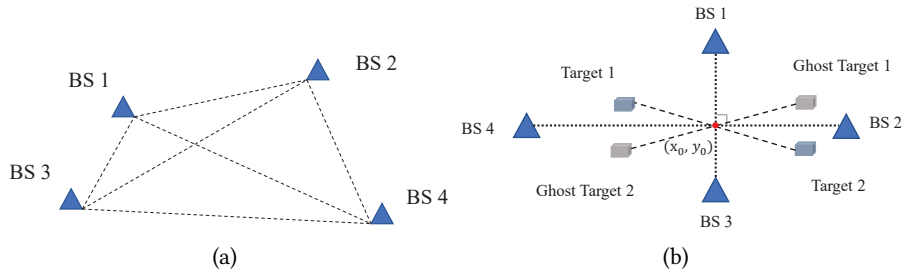

Figure 2.7: Examples of the BS deployment strategies shown in Lemma 2.4 for detecting $K = 2$ targets with $M = 4$ BSs.

In the following, we provide a toy example with $M = 4$ BSs and $K = 2$ targets to help understand Theorem 2.3.

Lemma 2.4. *Suppose that range estimation is perfect at all BSs. Consider the case of $M = 4$ and $K = 2$, where any three of the BSs are not deployed on the same line. If the line connecting any two BSs is not perpendicular to the line connecting the other two BSs, then no matter where the K true targets are, there never exist ghost targets. If there exist two BSs such that the line connecting them is perpendicular to the line connecting the other two BSs with an intersection point (x_0, y_0), then there exist ghost targets only when the coordinates of the two true targets satisfy $x_1 + x_2 = 2x_0$ and $y_1 + y_2 = 2y_0$, i.e., the intersection point (x_0, y_0) is the middle point of the line segment connecting the two true targets.*

Proof. Please refer to Appendix 7.2. □

The BS deployment strategies of Lemma 2.4 are shown in Fig. 2.7 with $M = 4$ BSs, where ghost targets never exist regardless of the location of the $K = 2$ true targets under the strategy shown in Fig. 2.7(a), and may exist given some special target location, i.e., $x_1 + x_2 = 2x_0$ and $y_1 + y_2 = 2y_0$, under the strategy shown in Fig. 2.7(b). Lemma 2.4 indicates that even if the BSs are deployed as in Fig. 2.7 (b), ghost targets do not exist almost surely if the targets are located independently and uniformly in the network, because the probability of the event of $x_1 + x_2 = 2x_0$ and $y_1 + y_2 = 2y_0$ is zero in a four-dimension space constructed by x_1, x_2, y_1, y_2.

We also implement tremendous Monte Carlo simulations to verify Theorem 2.3, where we set $M = 4$ and K up to 20. For each value of K, we generate 10^5 realizations, where BS and target locations are generated independently and randomly under the uniform distribution in each realization, similar to the setup for Fig. 2.6. Based on the generated locations of BSs and

targets, we use Algorithm 1 to check whether ghost target exists. It is observed that no ghost target is detected in any realization.

Theorems 2.2 and 2.3 provide a theoretical guarantee to the performance of our proposed two-phase device-free sensing framework. Specifically, compared to device-based sensing, a key issue in device-free sensing is the potential existence of ghost targets as pointed out in the above. However, Theorems 2.2 and 2.3 imply that this issue is actually not the bottleneck under our considered framework, since the ghost target never exists, or does not exist almost surely, depending on the relationship between the number of BSs and that of the targets.

Despite the above results, matching each range with the right target is a main technical challenge for implementing device-free sensing compared to implementing device-based sensing, although such a matching will not degrade the fundamental performance as explained above. In the next section, we study the range matching at the BSs for localization for the practical case with imperfect range estimation in Phase I.

2.6 Phase II: Localization with Imperfect Range Estimation

In this section, we consider the practical case when the range estimation is imperfect in Phase I due to the limited bandwidth, i.e., $\bar{d}_{m,k}$ shown in (2.7) is not equal to $d_{m,k}, \forall m,k$. In this case, we propose an ML-based algorithm to estimate the locations of the targets based on the knowledge of the BS locations, i.e., (a_m, b_m)'s, and the target range sets, i.e., $\mathcal{D}_m$'s.

2.6.1 Algorithm Design

Similar to [44, 59], in the rest of this paper, we assume that the estimated range shown in (2.7) follows

$$\bar{d}_{m,k} = d_{m,k} + \varepsilon_{m,k}, \forall m,k, \tag{2.29}$$

where $\varepsilon_{m,k} \sim \mathcal{CN}(0, \sigma^2_{m,k})$ denotes the error for estimating $d_{m,k}$ and $\varepsilon_{m,k}$'s are independent over m and k. Based on the above range estimation model, for each BS m and target k, the conditional probability for the event that $\bar{d}_{m,k}$ is the $g_{m,k}$-th largest element in $\mathcal{D}_m$, i.e., $\bar{d}_{m,k} = \mathcal{D}_m(g_{m,k})$,

given (x_k, y_k) and $g_{m,k}$, is

$$\begin{aligned} & f_{m,k}(\mathcal{D}_m(g_{m,k})|x_k, y_k, g_{m,k}) \\ =& \frac{1}{\sqrt{2\pi}\sigma_{m,k}} e^{-\frac{(\mathcal{D}_m(g_{m,k})-\sqrt{(a_m-x_k)^2+(b_m-y_k)^2})^2}{2\sigma_{m,k}^2}}, \ \forall m,k. \end{aligned} \tag{2.30}$$

Define $\mathcal{G} = \{g_{m,k}|m = 1,\ldots,M, k = 1,\ldots,K\}$. Then, the ML problem to estimate the locations of all the K targets can be formulated as

$$\begin{aligned} \underset{\mathcal{X},\mathcal{G}}{\text{maximize}} \ & \prod_{k=1}^{K}\prod_{m=1}^{M} f_{m,k}(\mathcal{D}_m(g_{m,k})|x_k, y_k, g_{m,k}) \\ \text{subject to } & (2.16), (2.17). \end{aligned} \tag{2.31}$$

Note that different from the device-based sensing problem, the matching solutions $g_{m,k}$'s need to be jointly optimized with the target locations in our considered device-free sensing problem, since each BS m does not know the matching between the elements in $\mathcal{D}_m$ and the targets.

Based on (2.30), problem (2.31) can be simplified into the following problem

$$\begin{aligned} \underset{\mathcal{X},\mathcal{G}}{\text{minimize}} \ & \sum_{k=1}^{K}\sum_{m=1}^{M} \frac{(\mathcal{D}_m(g_{m,k})-\sqrt{(a_m-x_k)^2+(b_m-y_k)^2})^2}{\sigma_{m,k}^2} \\ \text{subject to } & (2.16), (2.17). \end{aligned} \tag{2.32}$$

Problem (2.32) is a non-convex optimization problem, which is thus difficult to solve. Nevertheless, it is worth noting that given any matching solution satisfying conditions (2.16) and (2.17), denoted by $g_{m,k} = \bar{g}_{m,k}, \forall m,k$, problem (2.32) can be decoupled into K subproblems, each being formulated as follows for estimating the location of target k:

$$\underset{x_k,y_k}{\text{minimize}} \ \sum_{m=1}^{M} \frac{(\mathcal{D}_m(\bar{g}_{m,k}) - \sqrt{(a_m-x_k)^2+(b_m-y_k)^2})^2}{\sigma_{m,k}^2}. \tag{2.33}$$

Similar to the device-based localization scenario, problem (2.33) given the matching solution is a nonlinear least squared problem, which can be solved efficiently by using the Gauss-Newton algorithm [63, 64]. As a result, problem (2.32) can be solved in a straightforward manner based on the exhaustive search method. Specifically, given any matching solution $g_{m,k} = \bar{g}_{m,k}$'s satisfying (2.16) and (2.17), we can solve problem (2.33) to obtain the locations of all the targets and check the corresponding objective value of problem (2.32). Then, after all the matching

solutions satisfying (2.16) and (2.17) are searched, we can select the matching solution that minimizes the objective function of problem (2.32). However, the above approach based on exhaustive search is of prohibitively high complexity in practice. Specifically, there are $(K!)^{M-1}$ different matching solutions for $g_{m,k}$'s satisfying (2.16) and (2.17). Moreover, given each feasible matching solution, we need to solve the complex optimization problem (2.33) for K times (each corresponding to one target). This thus motivates us to propose a low-complexity algorithm for solving problem (2.32).

To this end, we first note that some matching solutions can be easily determined to be infeasible with very high probability under imperfect range estimation. For instance, for any two range sets $\mathcal{D}_{m_1}$ and $\mathcal{D}_{m_2}$, if $\mathcal{D}_{m_1}(g_{m_1,k})$ and $\mathcal{D}_{m_2}(g_{m_2,k})$ do not satisfy the triangle inequalities for target k, i.e.,

$$|\mathcal{D}_{m_1}(g_{m_1,k}) - \mathcal{D}_{m_2}(g_{m_2,k})| \leq d^{\mathrm{BS}}_{m_1,m_2} + \delta_0, \ \forall m_1, m_2, \tag{2.34}$$

$$|\mathcal{D}_{m_1}(g_{m_1,k}) + \mathcal{D}_{m_2}(g_{m_2,k})| \geq d^{\mathrm{BS}}_{m_1,m_2} - \delta_0, \ \forall m_1, m_2, \tag{2.35}$$

where $\delta_0 > 0$ is some given value, then $(g_{m_1,k}, g_{m_2,k})$ is not a feasible matching solution for target k with very high probability. Note that different from (2.21) and (2.22) for the case of perfect range estimation, we put a margin δ_0 here considering the imperfect estimation of $d_{m,k}$'s.

Inspired by the above property, we propose a low-complexity algorithm to solve problem (2.32) as follows. First, we just consider BSs 1, 2, and 3. Define the set of feasible matching solutions for these 3 BSs as

$$\begin{aligned}\mathcal{G}^{(3)} = \{\{g_{1,k}, g_{2,k}, g_{3,k}\}_{k=1}^K | \{g_{1,k}, g_{2,k}, g_{3,k}\}_{k=1}^K \text{ satisfies} \\ (2.16),\ (2.17),\ \text{and } (g_{1,k}, g_{2,k}),\ (g_{1,k}, g_{3,k}),\ (g_{2,k}, g_{3,k}) \\ \text{satisfy } (2.34),\ (2.35),\ \forall k\}.\end{aligned} \tag{2.36}$$

Next, given any $\{\bar{g}_{1,k}, \bar{g}_{2,k}, \bar{g}_{3,k}\}_{k=1}^K \in \mathcal{G}^{(3)}$, we solve problem (2.33) by setting $M = 3$ to find the location of target k, $\forall k$. Let $(x_k^{(3)}, y_k^{(3)})$'s, $k = 1, \ldots, K$, denote the obtained solutions. Then, given these solutions, we can check the distance from any target k to any BS $m > 3$ as

$$\bar{d}_{m,k}^{(3)} = \sqrt{(a_m - x_k^{(3)})^2 + (b_m - y_k^{(3)})^2}. \tag{2.37}$$

Note that for any BS $m > 3$, it does not know which element in $\mathcal{D}_m$ is the distance of target k to it. If BS $m > 3$ decides that $g_{m,k} = \tilde{k}$, then we define a cost for this decision as

$$\Delta d_{m,k,\tilde{k}} = |\mathcal{D}_m(\tilde{k}) - \bar{d}^{(3)}_{m,k}|, \ \forall k, \tilde{k}, \text{ and } m > 3. \tag{2.38}$$

As a result, the cost for BS $m > 3$ to select $g_{m,k} = \tilde{k}$ is the error for using $\bar{d}^{(3)}_{m,k}$ to replace $\mathcal{D}_m(\tilde{k})$.

Define the indicator functions for matching as follows:

$$\beta_{m,k,\tilde{k}} = \begin{cases} 1, & \text{if } g_{m,k} \text{ is set to be } \tilde{k}, \\ 0, & \text{otherwise}, \end{cases} \quad \forall k, \tilde{k}, m > 3. \tag{2.39}$$

Note that for each BS $m > 3$, (2.17) indicates that any $\tilde{k}$ can only be assigned to one target. Moreover, for any target k, only one $\tilde{k}$ can be assigned to it. As a result, we have the following constraints for the indicator functions:

$$\sum_{k=1}^{K} \beta_{m,k,\tilde{k}} = 1, \quad \forall \tilde{k} \text{ and } m > 3, \tag{2.40}$$

$$\sum_{\tilde{k}=1}^{K} \beta_{m,k,\tilde{k}} = 1, \quad \forall k \text{ and } m > 3. \tag{2.41}$$

Define $\mathcal{B}_m = \{\beta_{m,k,\tilde{k}} | \forall k, \tilde{k} \in \mathcal{K}\}, \forall m > 3$. Given the estimated target locations $(x^{(3)}_k, y^{(3)}_k)$'s, we aim to find a matching solution for each BS $m > 3$ such that the overall mismatch between $\bar{d}_{m,k}$'s and $\bar{d}^{(3)}_{m,k}$'s for all the targets is minimized, for which we formulate the following optimization problem for any BS $m > 3$:

$$\begin{aligned} &\underset{\mathcal{B}_m}{\text{minimize}} \sum_{k=1}^{K} \sum_{\tilde{k}=1}^{K} \beta_{m,k,\tilde{k}} \Delta d_{m,k,\tilde{k}} \\ &\text{subject to } (2.40), (2.41). \end{aligned} \tag{2.42}$$

Problem (2.42) is an *assignment problem*, which can be efficiently solved by the Hungarian algorithm [65]. After solving problem (2.42) for all the BSs $m > 3$, we can find the matching solutions of $g_{m,k}$'s for these BSs based on (2.39).

Given any feasible matching solutions for BSs 1, 2, and 3 denoted by $\{\bar{g}_{1,k}, \bar{g}_{2,k}, \bar{g}_{3,k}\}_{k=1}^{K} \in \mathcal{G}^{(3)}$, after the assignment problem (2.42) is solved for the other BSs, the matching solutions for all the M BSs, denoted by $\{\bar{g}_{1,k}, \ldots, \bar{g}_{M,k}\}_{k=1}^{K}$, are known. Then, by plugging these matching

solutions of all the M BSs into problem (2.33), we can get a better estimation of the K target locations, which is denoted by $(x_k^{(M)}, y_k^{(M)})$, $k = 1, \ldots, K$. According to (2.32), the overall cost for choosing the matching solutions of BSs 1, 2, and 3 as $\{\bar{g}_{1,k}, \bar{g}_{2,k}, \bar{g}_{3,k}\}_{k=1}^K \in \mathcal{G}^{(3)}$ is defined as

$$\begin{aligned} &\Gamma(\{\bar{g}_{1,k}, \bar{g}_{2,k}, \bar{g}_{3,k}\}_{k=1}^K) \\ &= \sum_{m=1}^{M} \sum_{k=1}^{K} \frac{(\mathcal{D}_m(\bar{g}_{m,k}) - \sqrt{(a_m - x_k^{(M)})^2 + (b_m - y_k^{(M)})^2})^2}{\sigma_{m,k}^2}. \end{aligned} \tag{2.43}$$

At last, after searching all the feasible matching solutions of BSs 1, 2, and 3 in the set $\mathcal{G}_K^{(3)}$, we can select the one that can minimize the above overall error as follows

$$\begin{aligned} &\{g_{1,k}^*, g_{2,k}^*, g_{3,k}^*\}_{k=1}^K \\ &= \arg \min_{\{g_{1,k}, g_{2,k}, g_{3,k}\}_{k=1}^K \in \mathcal{G}^{(3)}} \Gamma(\{g_{1,k}, g_{2,k}, g_{3,k}\}_{k=1}^K). \end{aligned} \tag{2.44}$$

Then, the optimal matching solution of the other BSs and the optimal location solution of all the targets can be obtained via solving problem (2.42) and problem (2.33), respectively.

The above procedure for solving problem (2.32) is summarized in Algorithm 2. As compared to the exhaustive search based method, the complexity of Algorithm 2 is significantly reduced. First, instead of searching over all the $(K!)^{(M-1)}$ matching solutions of all the BSs that satisfy (2.16) and (2.17), under our proposed algorithm, we merely search over the feasible matching solutions of BSs 1, 2, and 3, i.e., $\mathcal{G}^{(3)}$ given in (2.36), as shown in problem (2.44). Note that there are at most $(K!)^2$ solutions in $\mathcal{G}^{(3)}$ satisfying constraints (2.16) and (2.17); moreover, under constraints (2.34) and (2.35), the number of matching solutions in $\mathcal{G}^{(3)}$ is usually much smaller than $(K!)^2$. Second, under our proposed algorithm, given any matching solutions for BSs 1, 2, and 3, each BS $m > 3$ can independently obtain its own matching solution by solving problem (2.42), instead of collaborating with the other BSs to jointly obtain their matching solutions.

2.6.2 Numerical Examples

In the following, we provide numerical examples to verify the effectiveness of Algorithm 2 for target localization, under the setup with $M = 4$ BSs and $2 \leq K \leq 7$ targets.

Algorithm 2: ML-Based Algorithm to Solve Problem (2.32) for Target Localization

Input: (a_m, b_m)'s and $\mathcal{D}_m$'s, $\forall m \in \mathcal{M}$.

Initialization: Obtain the feasible matching solutions for BSs 1, 2, and 3 in $\mathcal{G}^{(3)}$ given in (2.36). Define $\mathcal{G}^{(3)}(t)$ as the t-th matching solution in $\mathcal{G}^{(3)}$. Set $t = 1$.

Repeat:

1. Set $\mathcal{G}^{(3)}(t)$ as the matching solutions of BSs 1, 2, and 3, denoted by $\{\bar{g}_{1,k}, \bar{g}_{2,k}, \bar{g}_{3,k}\}_{k=1}^{K}$;
2. Solve problem (2.33) via the Gauss-Newton algorithm by setting $M = 3$ to get an estimation of target locations via BSs 1, 2, and 3, denoted by $\{(x_k^{(3)}, y_k^{(3)})\}_{k=1}^{K}$;
3. Calculate $\Delta d_{m,k,\tilde{k}}$'s based on (2.38), $\forall k, \tilde{k}, m > 3$, and solve problem (2.42) via the Hungarian algorithm to obtain the matching solution of BSs $4, \ldots, M$, denoted by $\{\bar{g}_{4,k}, \ldots, \bar{g}_{M,k}\}_{k=1}^{K}$;
4. Solve problem (2.33) given $\{\bar{g}_{1,k}, \ldots, \bar{g}_{M,k}\}_{k=1}^{K}$ to get a better estimation of target locations via all the BSs, denoted by $\{(x_k^{(M)}, y_k^{(M)})\}_{k=1}^{K}$;
5. Calculate $\Gamma(\{\bar{g}_{1,k}, \ldots, \bar{g}_{3,k}\}_{k=1}^{K})$ based on (2.43);
6. Set $t = t + 1$.

Until $t = |\mathcal{G}^{(3)}|$.

Output:

1). Obtain the optimal matching solutions for BSs 1, 2, and 3 via solving problem (2.44), denoted by $\{g_{1,k}^*, g_{2,k}^*, g_{3,k}^*\}_{k=1}^{K}$.

2). Obtain the optimal matching solutions for BSs $4, \ldots, M$ via solving problem (2.42), denoted by $\{g_{4,k}^*, \ldots, g_{M,k}^*\}_{k=1}^{K}$.

3). Obtain the optimal locations of all the K targets via solving problem (2.33), denoted by $\{(x_k^*, y_k^*)\}_{k=1}^{K}$.

First, we consider the case where the channel bandwidth is $B = 100$ MHz at the sub-6G band [57], and the worst-case range estimation error shown in (2.8) is $\Delta d = 0.75$ m. We assume that the BSs and targets are uniformly and randomly located in a 240 m $\times$ 240 m square, and generate 10^5 independent realizations of their locations. In each realization, we first estimate $\mathcal{D}_m$'s based on (2.7), and then localize the targets by Algorithm 2 given $\mathcal{D}_m$'s, where an error event for localizing a target is defined as the case that the estimated location is not lying within a radius of r m from the true target location. Let N_{error} denote the total number of error events in these 10^5 realizations. Then, the location estimation error probability is defined as $\frac{N_{\text{error}}}{K \times 10^5}$. Note that Algorithm 2 is designed based on the range estimation model in (2.29), where the estimation error is modeled as a Gaussian random variable, rather than the true range model in (2.7). To show that (2.29) is a good approximation of (2.7), in each realization, we also generate $\mathcal{D}_m$'s based on (2.29) with $\sigma_{m,k}^2 = \sigma^2$, $\forall m, k$, as the input of Algorithm 2, and evaluate the corresponding location estimation error probability.

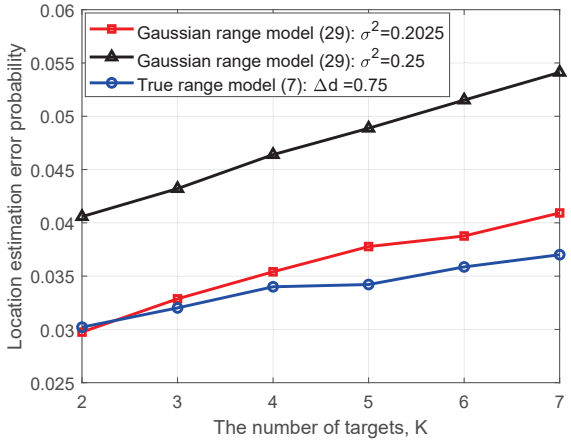

(a) $r = 1.5$ m

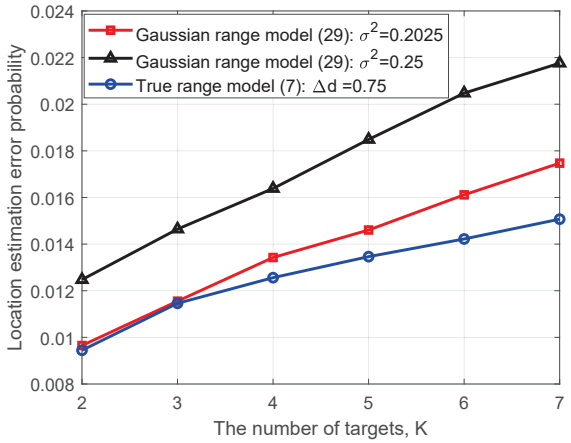

(b) $r = 2.5$ m

Figure 2.8: Location estimation error probability versus the number of targets with $B = 100$ MHz.

Considering $r = 1.5$ m and $r = 2.5$ m, Fig. 2.8 shows the location estimation error probability achieved by Algorithm 2 under the true range estimation model in (2.7) with worst-case error of $\Delta d = 0.75$ m and the approximated model in (2.29) with $\sigma^2 = 0.2025$ or $\sigma^2 = 0.25$. It is observed that under the true range estimation model, the error probability to estimate the locations of $K = 7$ targets is below 4% and 1.6% with $r = 1.5$ m and $r = 2.5$ m, respectively. Therefore, the estimation accuracy of our proposed scheme is in the order of meter with a probability higher than 95% when the channel bandwidth is $B = 100$ MHz. Moreover, it is observed that when $\sigma^2 = 0.2025$ in model (2.29), the performance achieved under this approximated model is very close to that achieved under the true range model (2.7). Thus, it is reasonable to use the Gaussian range model (2.29) in Algorithm 2 for localization in practical systems.

Next, we consider the case where the channel bandwidth is $B = 400$ MHz at the mmWave

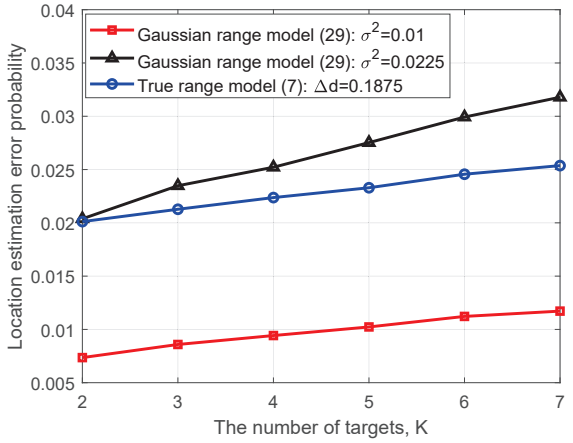

(a) $r = 0.6$ m

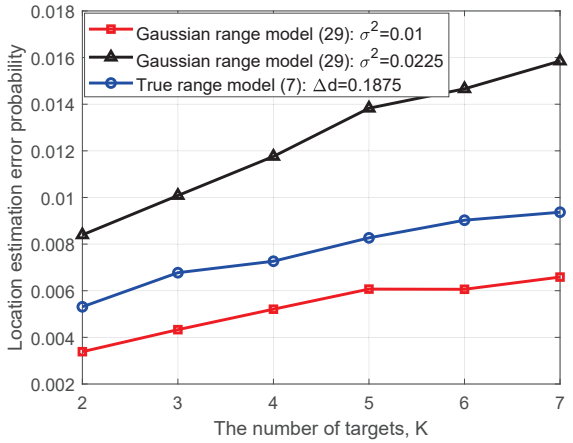

(b) $r = 1$ m

Figure 2.9: Location estimation error probability versus the number of targets with $B = 400$ MHz.

band [57]. In this case, the worst-case range estimation error shown in (2.8) is reduced to $\Delta d = 0.1875$ m, and the length of CP is 0.585 μs according to [62]. We assume that the BSs and users are located uniformly in an 80 m $\times$ 80 m square.[5] Moreover, we set $r = 0.6$ m and $r = 1$ m, respectively. Under the above setup, Fig. 2.9 shows the location estimation error probability achieved by Algorithm 2 under the true range estimation model (2.7) with worst-case error of $\Delta d = 0.1875$ m and the approximated model (2.29) with $\sigma^2 = 0.01$ or $\sigma^2 = 0.0225$. It is observed that the estimation accuracy of our proposed scheme is in the order of decimeter with a probability higher than 95% when the channel bandwidth is $B = 400$ MHz, thanks to the reduced worst-case estimation error due to the increased bandwidth.

[5]In this case, the maximum value of distance between a target and a BS such that the delay spread can be compensated by the CP (i.e., $L < Q$) is $0.585 \times 10^{-6} \times c_0/2 = 87.75$ m, thus we consider an 80 m $\times$ 80 m region.

2.7 Concluding Remarks

In this paper, we proposed a novel two-phase framework for device-free sensing in an OFDM cellular network to achieve ISAC. In Phase I, the delay of each BS-target-BS path is obtained based on the OFDM channel estimation technique for range estimation; while in Phase II, each BS matches each estimated range with the right target such that the locations of the targets can be estimated based on their values of distance with different BSs. Compared with existing device-free sensing techniques, the proposed framework does not depend on any specific channel model for range estimation in Phase I. Moreover, different from the legacy device-based sensing techniques, this paper proposed a range matching algorithm in Phase II to avoid the detection of ghost targets and analytically proved that the ghost target issue actually is not a fundamental limitation for device-free sensing.

There are a number of directions along which the device-free sensing framework proposed in this paper can be further enriched. For example, it is interesting to investigate how to deploy the BSs in the cellular network not only to improve the communication throughput, but also to reduce the ghost target existence probability when the range estimation is imperfect. Moreover, in practice, signals reflected by other objects, e.g., buildings, may also be received by the sensing receive antennas. It is thus crucial to explore clutter suppression techniques to avoid such interference under the proposed framework.

Chapter 3

Joint LOS Identification and Data Association for 6G-Enabled Networked Device-Free Sensing

In Chapter 2, we focus on the case that merely line-of-sight (LOS) paths exist between the targets and the BSs. In this Chapter, we explores networked device-free sensing in an OFDM cellular system with a multipath environment, where non-line-of-sight (NLOS) paths exist and the cooperative BSs are not synchronized. Similarly, a two-phase protocol is considered, where target range information and time offsets among BSs are estimated in Phase I, and target locations are estimated in Phase II.

3.1 Introduction

3.1.1 Background and Motivations

Recently, integrated sensing and communication (ISAC) has been listed as one of the six key usage scenarios in the future sixth-generation (6G) cellular network by International Telecommunication Union (ITU)[66]. Under the ISAC technology, a common radio signal can be used for conveying messages and sensing the environment simultaneously. It is expected that the ISAC technology can play an active role in traffic monitoring at Smart Transportation, fall detection at Smart Hospital, robot tracking at Smart Factory, etc.

Motivated by the significance of the ISAC technology in the 6G network, a lot of attempts for this emerging direction have been made. Many prior works focus on investigating the performance balance between the capacity of communication and the estimation distortion in radar systems[38, 67, 68], because the optimal waveforms for the communication signals and the sensing signals are quite different [20]. Apart from the performance optimization, there are also works investigating practical signal processing techniques for embedding the sensing function into the 6G cellular network. For instance, efficient algorithms have been proposed such that a BS can extract the range/angle/Doppler information of the targets based on the OFDM signals [29, 30], the orthogonal time frequency space (OTFS) signals [27], and the millimeter wave signals [31], that are reflected by these targets. Moreover, [32, 33] have devised powerful estimation schemes such that a mobile user can utilize the cellular signals for realizing simultaneous localization and mapping (SLAM).

It is worth noting that the above works mainly consider the scenario where localization is performed with one transmitter and one collocated/separate receiver, as in the monostatic/bistatic radar systems. Inspired by cooperative communication techniques such as cloud radio access network (C-RAN) [69–71], we are interested in the networked device-free sensing setup [72–74], where the targets passively reflect the OFDM signals emitted by the BSs for downlink communication, and the BSs share the local sensing information obtained from their received echoes to jointly localize these targets, as shown in Fig. 3.1. The goal of this paper is to provide practical solutions for incorporating the sensing functions into the cellular network, such that ubiquitous sensing can also be realized in future 6G cellular networks.

3.1.2 Prior Works

There are many interesting and important explorations made for network-level sensing, as discussed in the following.

3.1.2.1 Networked Device-based Sensing

In networked device-based sensing, the targets are able to transmit signals actively such that the mapping between the measurements at each BS and the targets can be known based on the signal signature[72]. In this case, if LOS paths can be identified, all BSs can cooperatively localize each target, e.g., time-of-arrival (ToA) based method and angle-of-arrival (AoA) based

method [75]. Therefore, it is important to mitigate NLOS paths in networked device-based sensing, which has been well surveyed in various works [76–78]. The simplest way is that the LOS path is assumed to be the shortest and/or the strongest one among all paths, but it may be affected by obstacles in the environment[76]. In [79], it is observed that the AoA/ToA of the LOS path has a smaller variation over several continuous packets than that of the NLOS path, which is leveraged for identifying the LOS path. The distance bias of NLOS path caused by other objects is modeled as some certain probability distribution[80, 81]. By leveraging the modeled probability distribution, the maximum likelihood (ML) based algorithm is proposed to estimate the locations of targets. Moreover, the prior knowledge of statistics of LOS path and NLOS path is assumed to be known in [82]. Then, the likelihood-ratio tests for LOS/NLOS identification are conducted to localize the target.

3.1.2.2 Network Device-free Sensing

When the targets are passive and not equipped with communication functions, device-free sensing is leveraged to estimate their locations. For example, when monitoring unregistered UAVs in the sky, each UAV will have LOS paths to most BSs and they can only be localized via signal echoes. Similarly, the LOS paths between targets and BSs should also be identified for target localization. On the other hand, as pointed out by [83] where there is no NLOS path or LOS blockage, the data association between ranges of LOS paths and targets also needs to be addressed in networked device-free sensing. Specifically, each BS does not know which (range of) LOS path belongs to which target, since the signatures of signals reflected by all targets are the same. To associate measurements with targets, plenty of pioneering and excellent algorithms have been presented in previous works. One straightforward way is the nearest neighbor (NN) method, which directly associates the most likely measurement to each target. However, the same measurement may be allocated to two or more targets, which is not applicable to the case that one measurement is associated with at most one target, e.g., when any two targets can be distinguished in the range/angle domain. The problem of globally assigning the measurements to the targets can be formulated as a multi-dimensional assignment (MDA) problem[84, 85]. When the dimension of the MDA problem is two, it is a linear assignment problem, which can be solved in polynomial time via the Hungarian algorithm[65]. When the dimension exceeds two, it is an NP-hard problem, which can be solved by branch and bound algorithm and Lagrangian relaxation algorithm [84, 85]. Instead of only retaining the best data association in the MDA method, the PDA and JPDA methods consider each kind of possible

data association hypothesis [86, 87]. Different from considering data association hypotheses at one snapshot, the hypotheses over several consecutive snapshots are jointly taken into account in the MHT method[88].

However, these works mainly focus on multiple target tracking (MTT), where prior information about target locations is available for associating measurements with targets at each time slot. With prior target locations as a reference, each BS can individually associate its measurements with these targets. Nevertheless, the locations of targets are unknown in our considered framework, where all BSs need to jointly localize passive targets only based on the obtained measurements. More importantly, LOS identification and data association are coupled together in networked device-free sensing, because each BS does not know either the mapping between paths and targets or that between ranges of LOS paths and targets. In detail, each BS should not only mitigate NLOS paths and identify which BSs have the range information about a particular target, but also perform data association between ranges of identified LOS paths and targets. To our best knowledge, there is a lack of research works that jointly consider the LOS identification and data association problem under networked device-free sensing. Multiple passive target localization in a multi-path environment is studied in [89], but the mapping constraint between targets and ranges is ignored. Specifically, it is assumed that each range can be associated with multiple targets due to low range resolution, which will lead to a high probability of the existence of undesired targets. Motivated by this, we propose to jointly tackle the issues of LOS identification and data association under networked device-free sensing, where any two targets can be distinguished in the range domain thanks to the high range resolution provided in the future 6G cellular network.

3.1.3 Main Contributions

In this paper, we study the networked device-free sensing technique in the OFDM cellular network. As shown in Fig. 1, multiple BSs transmit downlink OFDM signals to convey messages to mobile users. At the same time, each target reflects the OFDM signals to the BSs via the NLOS paths and/or LOS paths. Under this setup, we consider a two-phase protocol to perform networked sensing via BS cooperation. In Phase I, based on its received signals emitted by various BSs, each BS estimates the ranges of all the LOS paths and NLOS paths to it. In Phase II, all the BSs transmit their range information obtained in Phase I to the cloud over the

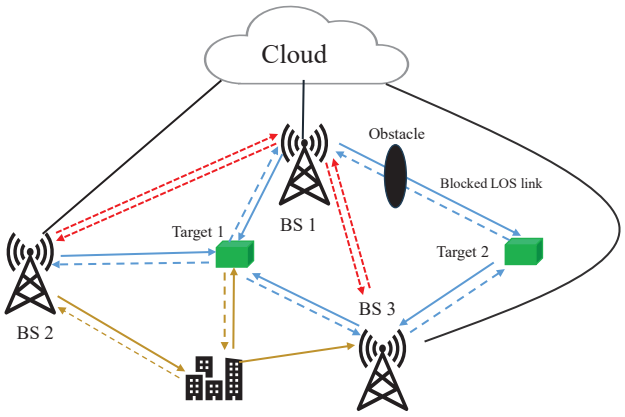

Figure 3.1: System model of our considered networked device-free sensing architecture. The BSs are connected to the central processor via fronthaul links to share the range estimations. For wireless propagation, there are Type I paths (e.g., the path from BS 1 to BS 3), Type II paths (e.g., the path from BS 1 to Target 1 to BS 2), Type III paths (e.g., the path from BS 2 to the building to Target 1 back to BS 3), and LOS blockage (Target 2 cannot be detected by BS 1 due to the obstacle).

optical fibers, such that the global range information can be utilized to estimate the number and the locations of the targets. Our contributions are summarized as follows.

- First, in practice, the BSs are not perfectly synchronized. The difference between the clocks at two BSs is defined as the sampling timing offset (STO). For OFDM communication, it is known that as long as the STO is shorter than the length of the cyclic prefix (CP), the effect of STO on communication can be mitigated by removing the CP [90, 91]. However, such an approach cannot mitigate the effect of STO on sensing. Specifically, due to the STO, the estimated propagation delay from a transmitting BS to a target to the receiving BS is the sum of the true propagation delay and the STO between the transmitting and the receiving BSs. Therefore, STO will affect the accuracy of range estimation in Phase I. In this paper, we design an efficient method that can estimate both the STO and the effective propagation delay including the STO based on the sparse optimization technique. Therefore, the true propagation delay can be efficiently estimated when the BSs are not perfectly synchronized.

- In Phase II, we pointed out three challenges to performing target localization based on the range information obtained in Phase I. The first challenge is that the LOS path between a target and a BS may not exist due to the blockage. Therefore, some useful range information is missing at each BS. Besides, due to the multipath environment, a target's

echo signal can be received by a BS over the NLOS path. Therefore, some range information obtained by the BSs is not useful. The last one is that at each BS, it does not directly know how to match one estimated range to the right target. This is the data association issue for networked device-free sensing [83]. Due to the first two challenges, it is difficult to estimate the number of targets based on the cardinality of the range set at each BS. Due to the second and third challenges, we need to jointly perform NLOS mitigation and data association. In other words, for each range estimated in Phase I, we should determine whether it is obtained via a LOS path, and if yes, which target it will belong to.

- To decouple the above three challenges in Phase II, we propose a novel algorithm. Suppose that the number of BSs is M. Under this algorithm, at the first iteration, we aim to estimate the number and locations of the targets that have LOS paths to all M BSs, and in the second iteration, we aim to estimate the number and locations of the targets that have LOS paths just to $M-1$ BSs, and so on. This architecture can tackle the first challenge because at each iteration, we just consider the targets that have LOS paths to a set of the BSs. Next, at each iteration of this algorithm, we propose an efficient method to perform NLOS mitigation and data association to localize the targets that do not have the LOS blockage issue to the considered set of BSs.

The rest of this paper is organized as follows. The system model and the sensing signal model are described in Section 3.2. Section 3.3 first introduces how to eliminate the synchronization error between any two BSs. Then, the true delays (ranges) of all paths between the BSs can be estimated. In Section 3.4, an efficient algorithm is proposed to jointly tackle the issues of LOS identification and data association to estimate the number and the locations of targets. The numerical results in Section 3.5 verify the effectiveness of the proposed algorithm in localizing targets in the multi-path environment. In the end, Section 3.6 concludes the paper.

Notations: Boldface lower-case and boldface upper-case letters are used to represent vectors and matrices, respectively. Denote superscripts $(\cdot)^T$ and $(\cdot)^H$ by the transpose and the Hermitian operators, respectively. Let $\text{diag}(\cdot)$ and $[\cdot]_{i,j}$ denote the diagonal matrix with the vector being the main diagonal and (i,j)-th entry of a matrix, respectively. Denote $\|\cdot\|_1$ by the l_1 norm of a vector and $|\cdot|$ by the absolute value of a scalar. We use $\binom{n}{k}$ for k-combinations of the set with n elements, $|\mathcal{A}|$ for the cardinality of the set $\mathcal{A}$, $\mathbb{C}$ for the set of complex values,

$\mathbb{C}^{N\times N}$ for the set of complex-value matrices of size $N\times N$, and $\boldsymbol{I}_N$ for the identity matrix of size $N\times N$.

3.2 System Model

In this paper, we consider a 6G-enabled ISAC system consisting of M BSs, K targets to be localized (the value of K is unknown and needs to be estimated), and I users for communication, as shown in Fig. 3.1. Since the communication technology is very mature in the cellular network, we mainly focus on the sensing function in this ISAC system. Let (a_m, b_m) and (x_k, y_k) denote the 2D coordinates of the m-th BS and the k-th target, respectively, $m = 1,\ldots,M$, $k = 1,\ldots,K$. Then, the direct distance between the m-th BS and the k-th target is given by

$$\begin{aligned} d_{m,k} &= f(x_k, y_k, a_m, b_m) \\ &= \sqrt{(a_m - x_k)^2 + (b_m - y_k)^2},\ \forall m,k. \end{aligned} \tag{3.1}$$

Moreover, the sum of the distance between the u-th BS and the k-th target and that between the k-th target and the m-th BS is

$$d_{u,m,k} = d_{u,k} + d_{m,k},\ \forall u,m,k. \tag{3.2}$$

In the downlink, the BSs will transmit the OFDM signals to the information receivers, while these signals can be reflected by the targets to different BSs as well. In practice, each target may have LOS links to some BSs while having no LOS links to the other BSs, as shown in Fig. 3.1. Define $\mathcal{M}_k$ as the set of BSs that have the LOS links to the k-th target.[1] If there exists a LOS link between target k and BS m, we may estimate their distance, i.e., $d_{m,k}$, based on the propagation delay from BS m to target k back to BS m. Moreover, if there exist LOS links from target k to both BS m and BS $u \neq m$, then we can also estimate $d_{u,m,k}$ based on the propagation delay from BS u to target k to BS m. Last, each target can be localized based on these distance values obtained from the LOS links.

Specifically, let $\boldsymbol{s}_m = [s_{m,1},\ldots,s_{m,N}]^T$ denote one frequency-domain OFDM symbol at the m-th BS, $\forall m$, where $s_{m,n}$ is the signal at the n-th sub-carrier and N is the number of sub-carriers. Then, the time-domain modulated signal of BS m over one OFDM symbol consisting

[1] In our paper, it is assumed that each target is detected by at least three BSs, i.e., $|\mathcal{M}_k| \geq 3$, $\forall k$.

of N samples is given by $\boldsymbol{\chi}_m = [\chi_{m,1}, ..., \chi_{m,N}]^T = \sqrt{p}\boldsymbol{W}^H \boldsymbol{s}_m, \forall m$, where p denotes the common transmit power for all the BSs, and $\boldsymbol{W} \in \mathbb{C}^{N\times N}$ denotes the discrete Fourier transform (DFT) matrix with $\boldsymbol{W}\boldsymbol{W}^H = \boldsymbol{W}^H\boldsymbol{W} = \boldsymbol{I}$. After inserting the CP consisting of Q OFDM samples, the time-domain signal transmitted by BS m over one OFDM symbol period is given by $\bar{\boldsymbol{\chi}}_m = [\bar{\chi}_{m,-Q}, \ldots, \bar{\chi}_{m,-1}, \bar{\chi}_{m,0}, \ldots, \bar{\chi}_{m,N-1}]$, where if $n > 0$, $\bar{\chi}_{m,n} = \chi_{m,n+1}$ denotes the useful signal, and if $n \leq 0$, $\bar{\chi}_{m,n} = \chi_{m,N+n+1}$ denotes the CP.

Because the BSs are not perfectly synchronized in practice, define the STO between BS u and BS m as $\tau_{u,m}$ OFDM sample periods[2], $\forall u, m$, i.e., if the local clock time at BS m is t_m, then that at BS u is $t_u = t_m + \tau_{u,m}$. In other words, for BSs m and u that are not perfectly synchronized, $\tau_{u,m} > 0$ if the clock time at BS m is earlier, while $\tau_{u,m} < 0$ otherwise. Then, define the maximum absolute STO in the network as $\tau_{\max} = \max_{u,m}|\tau_{u,m}|$. Moreover, define $\boldsymbol{h}_{u,m} = [h_{u,m,0}, \ldots, h_{u,m,L-1}]^T$ as the L-tap multi-path channel from BS u to BS m, where $h_{u,m,l}$ denotes the complex channel coefficient of the path with a delay of l OFDM sample periods and L denotes the maximum number of resolvable paths. Then, the received time-domain OFDM signal at the m-th BS in the n-th OFDM sample period, which is contributed by the signals transmitted by the m-th BS itself as well as the other $M-1$ BSs that are not perfectly synchronized with the m-th BS, can be expressed as

$$y_{m,n} = \sum_{u=1}^{M}\sum_{l=0}^{L-1} h_{u,m,l}\bar{\chi}_{u,n-l-\tau_{u,m}} + z_{m,n}, \ \forall m, n, \tag{3.3}$$

where $z_{m,n} \sim \mathcal{CN}(0, \sigma_z^2)$ denotes the noise at the m-th BS in the n-th OFDM sample period. Note that each BS m can potentially receive the signals transmitted by BS u via three types of paths - **Type I path**: the LOS path[3] from BS u to BS m; **Type II path**: the combination of the LOS path from BS u to some target and that from this target to BS m; **Type III path**: the NLOS path, e.g., the path from BS u to BS m via not only some target but also some reflector/scatter. Thereby, $h_{u,m,l} \neq 0$ indicates that there exists a Type I/II/III path from BS u to BS m, whose propagation delay is of l OFDM sample periods. Specifically, if $h_{u,m,l} \neq 0$ for a particular l is contributed by a Type I path from BS u to BS m, then the propagation delay, i.e.,

$$l_{u,m} = \left\lfloor \frac{N\Delta f\sqrt{(a_u - a_m)^2 + (b_u - b_m)^2}}{c_0} \right\rceil, \ \forall u, m, \tag{3.4}$$

[2]There are also carrier frequency offset and sampling frequency offset in the network, but we assume that they have been estimated and mitigated by existing methods[90, 91].

[3]We assume that a Type I path exists between any two BSs because BSs are deployed at high locations such that there is no blockage among them.

should be of $l_{u,m} = l$ OFDM sample periods, where c_0 is the speed of the light and $\lfloor \cdot \rfloor$ denotes the floor function; if $h_{u,m,l} \neq 0$ is contributed by a Type II path from BS u to some target k to BS m, then the propagation delay of this path, i.e., $\lfloor d_{u,m,k}/c_0 \rfloor$, is equal to l OFDM sample periods. As will be shown later in this paper, Type I paths are useful for estimating the STOs among the BSs, Type II paths are useful for localizing the targets, while Type III paths are not beneficial to localization and their impact should be mitigated.

Based on the above observation, in this paper, we adopt a two-phase networked device-free sensing protocol. Specifically, in Phase I, each BS m first estimates the channels $h_{u,m,l}$'s based on its received signals, and then sends its delay (thus range) information to a central processor. The main challenge that will be tackled here lies in the unknown STOs $\tau_{u,m}$'s, because if the clocks at different BSs are not perfectly synchronized, the estimated delays will be shifted by STOs. Then, in Phase II, the central processor will estimate the number and the locations of the targets based on the range information sent by all the BSs. Specifically, for each target, we need to first identify the BSs that have the LOS links to this target, and then find the useful LOS range information (corresponding to Type II paths) for localization by mitigating the NLOS range information (corresponding to Type III paths). In the following two sections, we show the details of Phase I and Phase II under the above protocol.

3.3 Phase I: Range Estimation

It is challenging to apply the conventional OFDM channel estimation techniques to estimate $h_{u,m,l}$'s based on (3.3) because the STOs, i.e., $\tau_{u,m}$'s, are unknown. In this section, we show that even when the BSs are not perfectly synchronized, the channel estimation problem can still be formulated as a sparse signal recovery problem, which can be efficiently solved by the standard compressed sensing techniques, such as LASSO [61]. Then, we will propose an efficient approach that can jointly estimate the STOs and the range of each path based on the estimated channels.

Specifically, we reformulate the received signals given in (3.3) as

$$\begin{aligned} y_{m,n} &\overset{(a)}{=} \sum_{u=1}^{M} \sum_{l=l_{u,m}}^{L-1} h_{u,m,l} \bar{\chi}_{u,n-l-\tau_{u,m}} \\ &= \sum_{u=1}^{M} \sum_{l=l_{u,m}+\tau_{u,m}}^{L+\tau_{u,m}-1} h_{u,m,l-\tau_{u,m}} \bar{\chi}_{u,n-l} \\ &= \sum_{u=1}^{M} \sum_{l=0}^{L+\tau_{\max}-1} \tilde{h}_{u,m,l} \bar{\chi}_{u,n-l} + z_{m,n}, \ \forall m,n, \end{aligned} \tag{3.5}$$

where $l_{u,m}$ is the propagation delay for the Type I path between BS u and BS m as given in (3.4), and $\tilde{h}_{u,m,l}$ is defined as

$$\tilde{h}_{u,m,l} = \begin{cases} h_{u,m,l-\tau_{u,m}}, & \text{if } l \in [l_{u,m}+\tau_{u,m}, L+\tau_{u,m}-1], \\ 0, & \text{otherwise.} \end{cases} \tag{3.6}$$

Therefore, $\tilde{h}_{u,m,l}$ can be interpreted as the virtual channel corresponding to a path from BS u to BS m whose delay is believed by the imperfectly synchronized BSs to be of l OFDM sample periods but actually is of $l-\tau_{u,m}$ OFDM sample periods. In other words, if $\tilde{h}_{u,m,l} \neq 0$, then there is a path from BS u to BS m, whose propagation delay is of $l-\tau_{u,m}$ OFDM sample periods. Note that in (3.5), (a) holds because no path with a delay of $l < l_{u,m}$ OFDM sample periods exists between BS u and BS m, i.e., $h_{u,m,l} = 0$, $\forall l \in [0, l_{u,m})$. To guarantee that all the inter-symbol interference (ISI) from the last OFDM symbol is received within the CP of the current OFDM symbol for all the BSs, we assume that the length of the CP satisfies $Q > L + \tau_{\max}$. Besides, it is assumed that $l_{u,m} + \tau_{u,m} \geq 0$, $\forall u, m$, such that BS m sees no ISI from the next OFDM symbol sent by BS u even when BS u's clock time is earlier than that at BS m, i.e., $\tau_{u,m} < 0$. Note that the maximum absolute STO of 5G networks is within 130 ns[92]. Therefore, as long as the distance between any two BSs is larger than 39 m, which is true in practice, then $l_{u,m} + \tau_{u,m} \geq 0$ will hold, $\forall u, m$.

Because $\tilde{h}_{u,m,l}$'s are defined as (3.6), we do not have STOs, i.e., $\tau_{u,m}$'s, in the new received signal model (3.5), indicating that $\tilde{h}_{u,m,l}$'s can be estimated based on the conventional OFDM channel estimation techniques. However, the cost is the shifted delay estimation for each path - if $\tilde{h}_{u,m,l} \neq 0$, there is a path from BS u to BS m with a delay of $l-\tau_{u,m}$, rather than l, OFDM sample periods. If the STOs are unknown, then the delay/range estimation is always incorrect.

Interestingly, we can efficiently tackle the above issue by utilizing the LOS signals between any two BSs. Specifically, among all the paths from BS u to BS m, the Type I path, i.e., the LOS

path between them, is of the minimum range. Therefore, let us define

$$l'_{u,m} = \min\{l | \forall l \text{ with } \tilde{h}_{u,m,l} \neq 0\}, \forall u \neq m. \tag{3.7}$$

Then, the imperfectly synchronized BSs u and m estimate the delay of their LOS path as $l'_{u,m}$ OFDM sample periods. However, we know that the true delay of this LOS path is of $l_{u,m}$ OFDM sample periods, as defined in (3.4). Therefore, the STOs can be determined as

$$\tau_{u,m} = l'_{u,m} - l_{u,m}, \forall u \neq m. \tag{3.8}$$

After STOs are known, we can correct the delay estimation made from $\tilde{h}_{u,m,l}$'s. In the following, we show how to achieve the above goals in Phase I of our considered protocol.

According to (3.5), the frequency-domain signal received at BS m over all the N sub-carriers can be expressed as [83, 93]

$$\bar{\boldsymbol{y}}_m = \sqrt{p} \sum_{u=1}^{M} \text{diag}(\boldsymbol{s}_u) \boldsymbol{G} \tilde{\boldsymbol{h}}_{u,m} + \bar{\boldsymbol{z}}_m = \sqrt{p} \tilde{\boldsymbol{G}} \tilde{\boldsymbol{h}}_m + \bar{\boldsymbol{z}}_m, \ \forall m, \tag{3.9}$$

where $\tilde{\boldsymbol{h}}_m = [\tilde{\boldsymbol{h}}_{1,m}, \ldots, \tilde{\boldsymbol{h}}_{M,m}]^T$ with $\tilde{\boldsymbol{h}}_{u,m} = [\tilde{h}_{u,m,0}, \ldots, \tilde{h}_{u,m,L+\tau_{max}-1}]^T$, $\boldsymbol{G} \in \mathbb{C}^{N \times (L+\tau_{max})}$ with the (n,l)-th element being $G_{n,l} = e^{\frac{-j2\pi(n-1)(l-1)}{N}}$, $\tilde{\boldsymbol{G}} = [\text{diag}(\boldsymbol{s}_1)\boldsymbol{G}, \ldots, \text{diag}(\boldsymbol{s}_M)\boldsymbol{G}]$, and $\bar{\boldsymbol{z}}_m = [\bar{z}_{m,1}, \ldots, \bar{z}_{m,N}]^T = \boldsymbol{W}\boldsymbol{z}_m \sim \mathcal{CN}(0, \sigma_z^2 \boldsymbol{I})$.

In this paper, we assume that all the BSs know $\boldsymbol{s}_1, \ldots, \boldsymbol{s}_M$ sent by the BSs. For example, in the channel estimation phase for communication, $\boldsymbol{s}_m$'s are pilot signals and can be known by all the BSs. In the data transmission phase, the BSs can exchange the messages $\boldsymbol{s}_m$'s with each other over the fronthaul links as in the cloud radio access network [94]. Hence, $\tilde{\boldsymbol{G}}$ in (3.9) is known by all the BSs. Moreover, due to the limited number of targets, reflectors, and scatters, very few elements in $\tilde{\boldsymbol{h}}_m$'s are non-zero, i.e., $\tilde{\boldsymbol{h}}_m$ is a sparse channel vector, $\forall m$. This motivates us to utilize the LASSO technique to estimate the time-domain channels [61]. Therefore, given any penalty parameter $\alpha > 0$, the problem of channel estimation is formulated as

$$\underset{\tilde{\boldsymbol{h}}_m}{\text{minimize}} \ \frac{1}{2} \|\bar{\boldsymbol{y}}_m - \sqrt{p}\tilde{\boldsymbol{G}}\tilde{\boldsymbol{h}}_m\|_2^2 + \alpha \|\tilde{\boldsymbol{h}}_m\|_1. \tag{3.10}$$

Note that the above problem is convex and can be solved efficiently by CVX [95].

Let $\bar{\boldsymbol{h}}_m = [\bar{\boldsymbol{h}}_{1,m}, \ldots, \bar{\boldsymbol{h}}_{M,m}]^T$ denote the optimal solution to problem (3.10), where $\bar{\boldsymbol{h}}_{u,m} = [\bar{h}_{u,m,0}, \ldots, \bar{h}_{u,m,L+\tau_{max}-1}]^T$, $u, m = 1, \ldots, M$. If $\bar{h}_{u,m,l} \neq 0$ for some l, then there exists a path from

BS u to BS m whose delay is estimated as $l-\tau_{u,m}$ OFDM sample periods. As shown in the method described in (3.7) and (3.8), define

$$\bar{l}'_{u,m}=\min\{l|\forall l \text{ with } \bar{h}_{u,m,l}\neq 0\},\ \forall u\neq m, \tag{3.11}$$

as the estimated propagation delay of the Type I path between BS u and BS m. Then, the STOs can be estimated as

$$\bar{\tau}_{u,m}=\begin{cases}\bar{l}'_{u,m}-l_{u,m}, & \text{if } u\neq m,\\ 0, & \text{if } u=m.\end{cases} \tag{3.12}$$

Once the STOs are estimated, if $\bar{h}_{u,m,l}\neq 0$ with $l\neq\bar{l}'_{u,m}$, we claim that there exists a Type II/III path from BS u to BS m with a range of

$$\bar{r}_{u,m,l}=\frac{(l-\bar{\tau}_{u,m})c_0}{N\Delta f}+\frac{c_0}{2N\Delta f}. \tag{3.13}$$

Based on the definitions of Type II and Type III paths in Section 3.2, we can know that

$$\bar{r}_{u,m,l}=\begin{cases}d_{u,m,k_{u,m,l}}+\varepsilon_{u,m,k_{u,m,l}}, & \text{Type II path},\\ d_{u,m,k_{u,m,l}}+\varepsilon_{u,m,k_{u,m,l}}+\eta_{u,m,l}, & \text{Type III path},\end{cases} \tag{3.14}$$

where $k_{u,m,l}$ denotes the index of the target which reflects the signal from BS u to BS m with a delay of l OFDM sample periods, $\varepsilon_{u,m,k_{u,m,l}}$ denotes the error caused by the estimation shown in (3.13), and $\eta_{u,m,l}$ denotes the bias introduced by the NLOS propagation. Note that under the above estimation rule, the worst-case range estimation error for each target is given by

$$|\bar{d}_{u,m,k_{u,m,l}}-d_{u,m,k_{u,m,l}}|\leq\frac{c_0}{2N\Delta f}\triangleq\Delta d. \tag{3.15}$$

For example, in 5G OFDM systems, the channel bandwidth can be up to $B=400$ MHz at the mmWave band according to 3GPP Release 15 [57]. In this case, the worst-case range estimation error is 0.375 m. Since Δd is practically very small, we assume in the sequel that the values of distance for any two Type II paths originated from one BS and reflected back to another BS by two different targets differ by more than $2\Delta d$, thus the corresponding paths are resolvable. Therefore, any two targets will not generate the same ranges of Type II paths in our considered framework.

To summarize, after Phase I of our considered two-phase networked device-free sensing protocol, each BS m will possess M range estimation sets

$$\mathcal{D}_{u,m} = \{\bar{r}_{u,m,l} | \forall l \text{ with } \bar{h}_{u,m,l} \neq 0 \text{ and } l \neq \bar{l}'_{u,m}\}, \\ u = 1, \cdots, M. \tag{3.16}$$

Then, each BS m will transmit the above M range sets, i.e., $\mathcal{D}_{1,m}, \ldots, \mathcal{D}_{M,m}$, to the central processor via the fronthaul links. The job of the central processor in Phase II is to first identify the ranges belonging to Type II paths in $\mathcal{D}_{u,m}$'s and then utilize these ranges for estimating the number and the locations of the targets. However, there are some challenges to achieving the above goal. First, for each target, its LOS range information to some BSs may be missing because as shown in Fig. 3.1, in practice, the Type II paths between some targets and some BSs may be blocked. We thus need to identify which BSs have the LOS range information for a particular target to localize it. Second, even if a target's LOS ranges corresponding to Type II paths are known to be contained in some $\mathcal{D}_{u,m}$'s, they are mixed with many NLOS ranges corresponding to Type III paths. We thus need to mitigate the effects of NLOS propagation for localization. Last, even if $\bar{r}_{u,m,l}$ is identified to be the range estimation associated with a Type II path from BS u to BS m via some target, we do not know whether $\bar{r}_{u,m,l}$ is an estimation of $d_{u,m,1}$ for target 1, ..., or $d_{u,m,K}$ for target K. We thus need to perform data association such that each useful range of a Type II path can be matched to the right target for localizing it[83]. In the next section, we will show how the central processor can tackle the above challenges in Phase II to estimate the number and the locations of the targets based on $\mathcal{D}_{u,m}$'s.

3.4 Phase II: Target Number and Location Estimation

With the range sets $\mathcal{D}_{u,m}$'s, $\forall u, m$, the objectives of the central processor in Phase II are two-fold. First, it needs to estimate the number of targets in the network, i.e., K. Second, it needs to estimate the coordinates of the K targets, i.e., (x_k, y_k), $k = 1, \ldots, K$. To achieve the above goals, in this section, we will first formulate a problem for joint target number and location estimation. Then, we will propose an efficient LOS identification and data association algorithm to solve the above problem.

For convenience, given any set $\mathcal{D}$, let $\mathcal{D}(g)$ denote its g-th smallest element. If the Type II LOS path from BS u to target k and to BS m exists and the estimation of $d_{u,m,k}$ is contained in the

set $\mathcal{D}_{u,m}$, then define $g_{u,m,k} > 0$ as an integer such that $\mathcal{D}_{u,m}(g_{u,m,k})$ is the estimation of $d_{u,m,k}$. Otherwise, define $g_{u,m,k} = 0$. Note that $g_{m,m,k} > 0$ and $g_{u,u,k} > 0$ is equivalent to $g_{u,m,k} > 0$ and vice versa. Moreover, define

$$\mathcal{G}_k = \{g_{u,m,k}, \forall u, m\} \tag{3.17}$$

as the solution of LOS identification and data association for target k to all the M BSs, $k = 1, \ldots, K$. This is because (i) among all the elements in $\mathcal{D}_{u,m}$, only $\mathcal{D}_{u,m}(g_{u,m,k})$'s, $\forall k$ with $g_{u,m,k} > 0$, are the estimated ranges for Type II LOS paths; (ii) if $g_{u,m,k} > 0$, then $\mathcal{D}_{u,m}(g_{u,m,k})$ is the estimated range of a Type II path for target k. Therefore, if $\mathcal{G}_k$'s are known, we can know which BSs have the LOS links to target k, i.e., the set of BSs that can detect target k is given by

$$\mathcal{M}_k = \mathcal{M}(\mathcal{G}_k) = \{m | g_{m,m,k} > 0, \forall g_{m,m,k} \in \mathcal{G}_k\}. \tag{3.18}$$

Furthermore, we can find the range estimations belonging to Type II LOS paths from $\mathcal{D}_{u,m}$'s and associate them with the right targets.

For convenience, define $\bar{\mathcal{G}}_k$ as the set containing all the positive integer elements in $\mathcal{G}_k$, $\forall k$. If $\mathcal{G}_1, \ldots, \mathcal{G}_K$ can be found out, then the number of the targets can be directly known because one mapping corresponds to one target and vice versa. Further, given $\mathcal{G}_k$, the location of each target k can be estimated based on its range information $\mathcal{D}_{u,m}(g_{u,m,k})$'s, $\forall u, m$, i.e., trilateration or multilateration localization. In the following, we show how to estimate the number of the targets and their locations via solving the mapping solution $\mathcal{G}_1, \ldots, \mathcal{G}_K$.

3.4.1 Problem Formulation

First, we define the conditions that a feasible mapping solution of $\mathcal{G}_1, \ldots, \mathcal{G}_K$ should satisfy. Given u, m, the number of elements in the range set $\mathcal{D}_{u,m}$ is denoted by $N_{u,m} = |\mathcal{D}_{u,m}|$. Since the range associated with each target must originate from the range sets, the elements in $\mathcal{G}_1, \ldots, \mathcal{G}_K$ should satisfy

$$g_{u,m,k} \in \{0, 1, \ldots, N_{u,m}\}, \ \forall u, m, k. \tag{3.19}$$

Moreover, if one range estimation in $\mathcal{D}_{u,m}$ is matched to target k, then it cannot be matched to another user $\bar{k} \neq k$, i.e.,

$$g_{u,m,k} \neq g_{u,m,\bar{k}},\ \forall g_{u,m,k} \in \bar{\mathcal{G}}_k, g_{u,m,\bar{k}} \in \bar{\mathcal{G}}_{\bar{k}}. \tag{3.20}$$

Another condition that $\mathcal{G}_1, \ldots, \mathcal{G}_K$ should satisfy arises from (3.2): the length of the Type II path from BS u to target k to BS m, i.e., $d_{u,m,k}$, is equal to the sum of the distance between BS u and target k, i.e., $d_{u,k}$, and that between BS m and target k, i.e., $d_{m,k}$. Note that the imperfect estimations of $d_{u,m,k}$, $d_{u,k}$, and $d_{m,k}$'s are $\mathcal{D}_{u,m}(g_{u,m,k})$ (also $\mathcal{D}_{m,u}(g_{m,u,k})$), $\mathcal{D}_{u,u}(g_{u,u,k})/2$, and $\mathcal{D}_{m,m}(g_{m,m,k})/2$. Therefore, we set the following constraints for $\mathcal{G}_1, \ldots, \mathcal{G}_K$:

$$\left| \frac{\mathcal{D}_{u,u}(g_{u,u,k})}{2} + \frac{\mathcal{D}_{m,m}(g_{m,m,k})}{2} - \mathcal{D}_{u,m}(g_{u,m,k}) \right| \leq \delta, \tag{3.21}$$
$$\left| \frac{\mathcal{D}_{u,u}(g_{u,u,k})}{2} + \frac{\mathcal{D}_{m,m}(g_{m,m,k})}{2} - \mathcal{D}_{m,u}(g_{m,u,k}) \right| \leq \delta,$$
$$\forall g_{u,m,k} \in \bar{\mathcal{G}}_k, \tag{3.22}$$

where $\delta > 0$ is a given threshold. The last constraint about $\mathcal{G}_1, \ldots, \mathcal{G}_K$ is on the localization residual associated with this solution of LOS identification and data association. Specifically, given $\mathcal{G}_k$, the location of target k is estimated by solving the following nonlinear least squared (NLS) problem

$$\begin{aligned} \text{(P1)} \ \underset{x_k, y_k}{\text{minimize}} \ & \sum_{(u,m): g_{u,m,k} \in \bar{\mathcal{G}}_k} (f(x_k, y_k, a_u, b_u) \\ & + f(x_k, y_k, a_m, b_m) - \mathcal{D}_{u,m}(g_{u,m,k}))^2,\ \forall k, \end{aligned}$$

where $f(x_k, y_k, a_m, b_m)$'s are given in (3.1). Problem (P1) is a non-convex problem. We can adopt the Gauss-Newton method to solve it [63]. Given $\mathcal{G}_k$ for target k, define $R(\mathcal{G}_k)$ as the value of problem (P1) achieved by the Gauss-Newton method. Therefore, $R(\mathcal{G}_k)$ can be interpreted as the residual for localizing target k given $\mathcal{G}_k$. If $\mathcal{G}_k$ is the right solution, then the localization residual $R(\mathcal{G}_k)$ should be small, $\forall k$, because the correct ranges are associated with each target. For example, when the range estimation error is zero, the localization residual will also be zero if the correct ranges are utilized for localizing each target. We thus set the following residual constraints about $\mathcal{G}_k$'s:

$$R(\mathcal{G}_k) \leq \beta,\ k = 1, \ldots, K, \tag{3.23}$$

where $\beta > 0$ is some given threshold.

To summarize, any $\mathcal{G}_1, \ldots, \mathcal{G}_K$ satisfying constraints (3.19)-(3.23) can be a feasible solution for LOS identification and data association. Hence, we need to decide which one is optimal among all feasible mapping solutions. When there are K targets, it is not likely that the range data estimated from the NLOS paths at various BSs can be well matched such that more than K targets can be detected. In other words, the probability that the number of mappings satisfying constraints (3.19)-(3.23) is larger than that of the true targets (mappings) is low[96–98]. Therefore, we want to maximize the number of targets whose locations can be estimated in this paper. Specifically, the solution of LOS identification and data association can be found by solving the following problem

$$\begin{aligned} (\text{P2}) \quad & \underset{K, \mathcal{G}_1, \ldots, \mathcal{G}_K}{\text{maximize}} \; K \\ & \text{subject to } (3.19) - (3.23). \end{aligned} \tag{3.24}$$

Next, we focus on solving problem (P2) to estimate the number of targets and the mapping solutions. With the obtained mapping solution, the location of each target can be estimated by solving problem (P1).

3.4.2 The Proposed Algorithm

There are three challenges to solve problem (P2). The first challenge is that a target may have no LOS paths to some BSs. Therefore, the range information of many Type II paths is missing in the range set of each BS, i.e., there are $K_{u,m} \leq K$ targets detected by BS u and BS m, $\forall u, m$. The number of possibilities for assigning the $N_{u,m}$ ranges in $\mathcal{D}_{u,m}$ to the detected $K_{u,m}$ out of K targets is $\binom{N_{u,m}}{K_{u,m}}\binom{K}{K_{u,m}}(K_{u,m}!)$. When there is no LOS blockage, i.e., $K_{u,m} = K$, $\forall u, m$, there are $\binom{N_{u,m}}{K}(K!)$ assignment possbilities. However, when there is LOS blockage, i.e., $K_{u,m}$ ranges from 0 to K, the number of possibilities is $\sum_{K_{u,m}=0}^{K}\binom{N_{u,m}}{K_{u,m}}\binom{K}{K_{u,m}}(K_{u,m}!)$, which is much larger than the case without LOS blockage. The second one is that a target may reflect the signals to the BSs via NLOS paths. Due to the Type III paths, the cardinality of the range set at each BS is larger, i.e., $N_{u,m}$ is larger, such that the number of assignment probabilities for the range set $\mathcal{D}_{u,m}$ also increases. Furthermore, we have to mitigate the range information of the Type III paths, which are not beneficial for target localization. The last one is that given the range of a Type II path, how to match it to the corresponding target is also a big challenge. Moreover, the above three

challenges are coupled together. To localize each target, we need to jointly determine which BSs have LOS paths to it, and for these BSs, which ranges in the range sets belong to this target. In the following, we propose an iterative algorithm to decouple Challenge 1 from Challenges 2 and 3. Specifically, the targets can be classified into the following categories: the targets that have LOS paths to exactly M BSs, the targets that have LOS paths to exactly $M-1$ BSs, and so on. The last category will be the targets that have LOS paths to exactly 3 BSs[4].

Define the number of targets that have LOS paths to exactly l BSs as K_l, $l = 3, \ldots, M$. Then, we have

$$K = \sum_{l=3}^{M} K_l. \tag{3.25}$$

Under our proposed algorithm, at the first iteration, we aim to localize all the targets that have LOS paths to exactly M BSs, while at the second iteration, we aim to localize all the targets that have LOS paths to exactly $M-1$ BSs, and so on. Note that at each iteration of our proposed algorithm, we do not face Challenge 1, because when we localize some targets, we only consider the BSs that have LOS paths to them. Specifically, the problem of localizing the targets that have LOS paths to l BSs can be formulated as

$$(\text{P3}-l) \quad \underset{K_l, \mathcal{G}_1^{(l)}, \ldots, \mathcal{G}_{K_l}^{(l)}}{\text{maximize}} \; K_l \tag{3.26}$$

$$\text{subject to} \quad |\mathcal{M}(\mathcal{G}_k^{(l)})| = l, \; k = 1, \ldots, K_l, \tag{3.27}$$

$$(3.19) - (3.23).$$

where $\mathcal{G}_k^{(l)}$ denotes the mapping for target k that can be detected by l BSs and $\mathcal{M}(\mathcal{G}_k^{(l)})$ is given in (3.18). In the following, we first focus on how to deal with problem (P3$-l$), $\forall l$. Then, based on (3.25), the solutions to problem (P3$-l$), $l = M, \ldots, 3$, are used for solving problem (P2) such that the number of targets and the mapping solutions can be estimated. Last, with the obtained mapping solution, the location of each target can be estimated by solving problem (P1).

Problem (P3$-l$) can be solved by exhaustive search, i.e., given each K_l and $\mathcal{G}_1^{(l)}, \ldots, \mathcal{G}_{K_l}^{(l)}$, we check whether conditions (3.19)-(3.23) and (3.27) hold. However, such an approach needs to solve the non-convex problem (P1) many times, which is of high complexity. To resolve this issue, we first ignore constraints (3.20) and (3.23) in problem (P3$-l$), and find the feasible

[4]We do not consider the targets that have LOS paths to only one or two BSs because they cannot be localized based on the range information.

region that any mapping $\mathcal{G}_k$ should satisfy constraints (3.19), (3.21), (3.22), and (3.27), i.e.,

$$\bar{\mathcal{G}}^{(l)} = \{\mathcal{G}_k^{(l)} | \mathcal{G}_k^{(l)} \in \mathcal{G}^{(l)} \text{ satisfies (3.21) and (3.22)}\}. \tag{3.28}$$

where

$$\mathcal{G}^{(l)} = \{\mathcal{G}_k^{(l)} | \mathcal{G}_k^{(l)} \text{ satisfies (3.19) and (3.27)}\}. \tag{3.29}$$

Due to the constraints (3.21) and (3.22), the size of $\bar{\mathcal{G}}^{(l)}$ is generally small, because the probability that (3.21) and (3.22) holds for Type III paths is very small. Then, we just need to check which mappings in $\bar{\mathcal{G}}^{(l)}$ rather than $\mathcal{G}^{(l)}$ satisfy the constraint (3.23). As a result, the number of times to solve problem (P1) is significantly reduced compared to the exhaustive search approach to problem (P3$-l$). Define

$$\tilde{\mathcal{G}}^{(l)} = \{\mathcal{G}_k^{(l)} | \mathcal{G}_k^{(l)} \in \bar{\mathcal{G}}^{(l)} \text{ and } R(\mathcal{G}_k^{(l)}) \leq \beta\}. \tag{3.30}$$

In other words, by removing $\mathcal{G}_k^{(l)}$'s that do not satisfy condition (3.23) from $\bar{\mathcal{G}}^{(l)}$, we can obtain $\tilde{\mathcal{G}}^{(l)}$. Note that each element contained in $\tilde{\mathcal{G}}^{(l)}$ satisfies conditions (3.19), (3.21)-(3.23), i.e., it is a feasible solution of LOS identification and data association to localize one target. However, for two mappings $\mathcal{G}_k^{(l)} \in \tilde{\mathcal{G}}^{(l)}$ and $\mathcal{G}_{\bar{k}}^{(l)} \in \tilde{\mathcal{G}}^{(l)}$, it is possible that $g_{u,m,k} \in \mathcal{G}_k^{(l)}$ is equal to $g_{u,m,\bar{k}} \in \mathcal{G}_{\bar{k}}^{(l)}$ for some u, m, i.e., in these two solutions, some estimated range at BS m is matched to both target k and target $\bar{k}$. Therefore, the last step to solve problem (P3$-l$) is to select the maximum number of elements in $\tilde{\mathcal{G}}$ such that condition (3.20) can be satisfied. Such a problem can be formulated as

$$\text{(P4)} \quad \underset{K_l, \mathcal{G}_1^{(l)}, \ldots, \mathcal{G}_K^{(l)}}{\text{maximize}} \; K_l \tag{3.31}$$

$$\text{subject to } \mathcal{G}_k^{(l)} \in \tilde{\mathcal{G}}^{(l)}, k = 1, \ldots, K_l, \tag{3.32}$$

$$(3.20).$$

One way to solve problem (P4) is the exhaustive search method. For a given K_l, we need try $\binom{N_{\tilde{\mathcal{G}}^{(l)}}}{K_l}$ possiblities to see whether (3.20) is satisfied, where $N_{\tilde{\mathcal{G}}^{(l)}}$ denotes the cardinality of $\tilde{\mathcal{G}}^{(l)}$. Because we do not know the exact value of K_l, we need to try each possible value of K_l, which is quite computationally prohibitive. To alleviate the complexity, we can divide $\tilde{\mathcal{G}}^{(l)}$ into

$N_{1,1}+1$ subsets based on the value of $g_{1,1,k}$, i.e.,

$$\tilde{\mathcal{G}}^{(l)} = \tilde{\mathcal{G}}_0^{(l)} \cup \tilde{\mathcal{G}}_1^{(l)} \cup \ldots \cup \tilde{\mathcal{G}}_{N_{1,1}}^{(l)}, \tag{3.33}$$

where

$$\tilde{\mathcal{G}}_i^{(l)} = \{\mathcal{G}_k^{(l)} | \mathcal{G}_k^{(l)} \in \tilde{\mathcal{G}}^{(l)} \text{ and } g_{1,1,k} = i \text{ with } g_{1,1,k} \in \mathcal{G}_k^{(l)}\}$$
$$i = 0, 1, \ldots, N_{1,1}. \tag{3.34}$$

As a consequence, at most one mapping $\mathcal{G}_k^{(l)}$ can be selected from each $\tilde{\mathcal{G}}_i^{(l)}$ to make sure (3.20) is satisfied. In other words, some $\tilde{\mathcal{G}}_i^{(l)}$'s contain the mappings $\mathcal{G}_k^{(l)}$'s, while others do not. Note that the number of $\tilde{\mathcal{G}}_i^{(l)}$'s containing the mappings $\mathcal{G}_k^{(l)}$'s is equal to K_l, i.e., the K_l constraints in (3.32). Motivated by this, we aim at finding the indexes of $\tilde{\mathcal{G}}_i^{(l)}$'s that contain the mappings $\mathcal{G}_k^{(l)}$'s. As a result, problem (P4) can be transformed into

$$\text{(P5)} \quad \underset{\Omega, \mathcal{G}_1^{(l)}, \ldots, \mathcal{G}_{|\Omega|}^{(l)}}{\text{maximize}} \ |\Omega| \tag{3.35}$$

$$\text{subject to} \ \ \Omega \subseteq \{0, 1, \ldots, N_{1,1}\}, \tag{3.36}$$

$$\mathcal{G}_k^{(l)} \in \tilde{\mathcal{G}}_{\Omega(k)}^{(l)}, \ k = 1, \ldots, |\Omega|, \tag{3.37}$$

$$(3.20).$$

Given Ω in problem (P5), there may be multiple feasible mapping solutions that satisfy (3.37) and (3.20). Compared with problem (P4), problem (P5) is of lower complexity, since the cases that two or more mappings $\mathcal{G}_k^{(l)}$'s belong to the same $\tilde{\mathcal{G}}_i^{(l)}$ need not be considered. However, it is still of high complexity for large $N_{\tilde{\mathcal{G}}^{(l)}}$. To tackle this issue, we greedily maximize $|\Omega|$ iteratively. At the beginning, we initialize $\Omega^{(0)} = \{\}$. At the t-th iteration, we try to increase $|\Omega|$ by 1. Specifically, we set $\Omega = \Omega^{(t-1)} \cup \{t-1\}$ in problem (P5) to see whether there exists a mapping solution $\mathcal{G}_1^{(l)}, \ldots, \mathcal{G}_{|\Omega|}^{(l)}$ that satisfies (3.20) and (3.37). If such a mapping solution do exist, we update $\Omega^{(t)} = \Omega^{(t-1)} \cup \{t-1\}$; otherwise, $\Omega^{(t)} = \Omega^{(t-1)}$. By repeating the above procedure until $t > N_{1,1}+1$, we can get the solution of problem (P5), denoted by $\hat{\Omega} = \Omega^{(N_{1,1}+1)}$.

Note that if $\mathcal{G}_1^{(l)}, \ldots, \mathcal{G}_{|\Omega^{(t)}|}^{(l)}$ is a mapping solution for $\Omega = \Omega^{(t)} = \Omega^{(t-1)} \cup \{t-1\}$ in problem (P5), then $\mathcal{G}_1^{(l)}, \ldots, \mathcal{G}_{|\Omega^{(t-1)}|}^{(l)}$ is a solution for $\Omega = \Omega^{(t-1)}$. This can be utilize to simplify finding $\mathcal{G}_1^{(l)}, \ldots, \mathcal{G}_{|\Omega|}^{(l)}$ at the t-th iteration. Denote $\mathcal{G}_{n_t}^{(t)} = \{\mathcal{G}_{n_k}^{(l)}\}_{k=1}^{|\Omega^{(t)}|}$ by the n_t-th mapping solution for $\Omega = \Omega^{(t)}$ in problem (P5) at the t-th iteration. Then, we just need to check whether there

Algorithm 3: Algorithm for Solving Problem (P3$-l$)

Input: (a_m, b_m)'s, $\mathcal{D}_{u,m}$'s, $\forall u, m$, and l

Procedure:

1. Find $\tilde{\mathcal{G}}^{(l)}$ based on (3.30) and get $\tilde{\mathcal{G}}_i^{(l)}$'s according to (3.34);
2. Initialize $t = 1$ and $\Omega^{(0)} = \{\}$; Get $\mathcal{G}_1^{(0)} = \{\}$; Set $k = 1$;
3. **Repeat**:
   - 3.1. For each $\mathcal{G}_{n_{t-1}}^{(t-1)}$, check whether there exists $\mathcal{G}_k^{(l)} \in \tilde{\mathcal{G}}_{t-1}^{(l)}$ that satisfies (3.20) with any mapping in $\mathcal{G}_{n_{t-1}}^{(t-1)}$;
   - 3.2. If such $\mathcal{G}_k^{(l)}$ and $\mathcal{G}_{n_{t-1}}^{(t-1)}$ exist or $\mathcal{G}_{n_{t-1}}^{(t-1)}$ is empty, add $\mathcal{G}_{n_t}^{(t)} = \mathcal{G}_{n_{t-1}}^{(t-1)} \cup \{\mathcal{G}_k^{(l)}\}$ as the mapping solution for $\Omega = \Omega^{(t-1)} \cup \{t-1\}$. After finding all such $\mathcal{G}_{n_t}^{(t)}$'s, update $\Omega^{(t)} = \Omega^{(t-1)} \cup \{t-1\}$ and $k = k+1$; otherwise, only update $\Omega^{(t)} = \Omega^{(t-1)}$ and $\mathcal{G}_{n_t}^{(t)} = \mathcal{G}_{n_{t-1}}^{(t-1)}$ for each $\mathcal{G}_{n_{t-1}}^{(t-1)}$;
   - 3.3. Update $t = t+1$;

   Until $t > N_{1,1} + 1$.
4. Get the index solution to problem (P5), denoted by $\hat{\Omega} = \Omega^{(N_{1,1}+1)}$. If there are multiple mapping solutions, i.e., $\mathcal{G}_{n_{N_{1,1}+1}}^{(N_{1,1}+1)}$'s, $n_{N_{1,1}+1} = 1, 2, \ldots$, select the one minimizing the localization residual as the optimal mapping solution, denoted by $(\mathcal{G}^{(l)})^*$.

Output:
1) Obtain the estimated number and the solution of LOS identification and data association for the targets that are detected by l BSs, denoted by $\hat{K}^{(l)} = |\hat{\Omega}|$ and $\{\hat{\mathcal{G}}_k^{(l)}\}_{k=1}^{\hat{K}} = (\mathcal{G}^{(l)})^*$, respectively;
2) Estimate the target locations by solving problem (P1) given the mapping solution $\hat{\mathcal{G}}_k^{(l)}$'s, denoted by $(\hat{x}_k, \hat{y}_k)$'s, $k = 1, \ldots, \hat{K}$.

exists $\mathcal{G}_k^{(l)} \in \tilde{\mathcal{G}}_{t-1}^{(l)}$ that satisfy (3.20) with any mapping element in $\mathcal{G}_{n_{t-1}}^{(t-1)}$ at the t-th iteration. If such $\mathcal{G}_k^{(l)}$ and $\mathcal{G}_{n_{t-1}}^{(t-1)}$ exist or $\mathcal{G}_{n_{t-1}}^{(t-1)}$ is empty, we can update $\Omega^{(t)} = \Omega^{(t-1)} \cup \{t-1\}$ and add $\mathcal{G}_{n_t}^{(t)} = \mathcal{G}_{n_{t-1}}^{(t-1)} \cup \{\mathcal{G}_k^{(l)}\}$ as a feasible mapping solution for $\Omega = \Omega^{(t)}$; otherwise, we keep $\Omega^{(t)} = \Omega^{(t-1)}$ and update $\mathcal{G}_{n_t}^{(t)} = \mathcal{G}_{n_{t-1}}^{(t-1)}$ for each $\mathcal{G}_{n_{t-1}}^{(t-1)}$ as the mapping solution for $\Omega = \Omega^{(t)}$.

The details of the above process are shown in Algorithm 3. Since there may be multiple mapping solutions, we will try each of them in Step 3.1. If some $\mathcal{G}_{n_{t-1}}^{(t-1)}$'s can lead to $\Omega^{(t)} = \Omega^{(t-1)} \cup \{t\}$ while others cannot, we only update $\mathcal{G}_{n_t}^{(t)} = \mathcal{G}_{n_{t-1}}^{(t-1)} \cup \{\mathcal{G}_k^{(l)}\}$ for these $\mathcal{G}_{n_{t-1}}^{(t-1)}$'s as the mapping solutions for $\Omega = \Omega^{(t)} = \Omega^{(t-1)} \cup \{t-1\}$. If no $\mathcal{G}_{n_{t-1}}^{(t-1)}$ can lead to $\Omega^{(t)} = \Omega^{(t-1)} \cup \{t-1\}$, then we keep $\mathcal{G}_{n_t}^{(t)} = \mathcal{G}_{n_{t-1}}^{(t-1)}$ for each $\mathcal{G}_{n_{t-1}}^{(t-1)}$ as the mapping solution for $\Omega = \Omega^{(t)} = \Omega^{(t-1)}$. In the end, there may be multiple mapping solutions for $\Omega = \hat{\Omega}$ in problem (P5). For the n-th mapping solution, denoted by $\{\hat{\mathcal{G}}_{n_k}^{(l)}\}_{k=1}^{|\hat{\Omega}|}$, its localization residual, i.e., $\sum_{k=1}^{|\hat{\Omega}|} \mathcal{R}(\hat{\mathcal{G}}_{n_k}^{(l)})$, is calculated. Then,

we select the one with the smallest localization residual as the optimal mapping solution for the estimated $|\hat{\Omega}|$ targets, denoted by $\{\hat{\mathcal{G}}_k^{(l)}\}_{k=1}^{|\hat{\Omega}|}$.

Next, we show how to get the solution problem (P2) by iteratively solving problem (P3$-l$). We sequentially solve problem (P3$-l$) for l from M to 3 and obtain the mapping solutions for each l, denoted by $\{\hat{\mathcal{G}}_k^{(l)}\}_{k=1}^{\hat{K}_l}$. In this process, the ranges corresponding to $\{\hat{\mathcal{G}}_k^{(l+1)}\}_{k=1}^{\hat{K}_{l+1}}$ are removed from the range sets before solving problem (P3-l), $\forall l$. As a result, we can find the targets that are exactly detected by l BSs when solving problem (P3$-l$) for each l. Specifically, at the t-th step, $t = 1,\ldots,M-2$, we find the mapping solution for the targets that can be detected by $M_t = M - t + 1$ BSs based on Algorithm 3. Denote the obtained solution at the t-th step by $\hat{K}_{M_t}$ and $\hat{\mathcal{G}}_1^{(M_t)},\ldots,\hat{\mathcal{G}}_{\hat{K}_{M_t}}^{(M_t)}$, which are regarded as the estimated number and the mapping solution for the targets that are exactly detected by M_t BSs. Then, we remove these assigned ranges, $\mathcal{D}_{u,m}(\hat{g}_{u,m,k})$'s, $\forall \hat{g}_{u,m,k} \in \hat{\mathcal{G}}_k^{(M_t)}$ with $\hat{g}_{u,m,k} > 0$, $k = 1,\ldots,\hat{K}_{M_t}$, from $\mathcal{D}_{u,m}$'s, $\forall u,m$, because each range is associated with at most one target and these assigned ranges should not be considered at the next step. As mentioned above, the complexity will be further reduced at the $(t+1)$-th step, because each $\mathcal{D}_{u,m}$ has a smaller number of ranges such that the size of the feasible region $\tilde{\mathcal{G}}^{(M_{t+1})}$ becomes smaller. Then, we update $t = t+1$ to go into the next step. By repeating the above procedure until $t > M-2$, we can obtain the estimated number of targets and the mapping solution for problem (P2). In the end, with the estimated mapping solutions for all targets, the location of each target can be estimated by solving problem (P1).

The details of the above process are shown in Algorithm 4. Note that solving problem (P2) is decoupled into sequentially finding the solution to problem (P3$-l$). Thus, Algorithm 3 can be applied to each step of Algorithm 4. Moreover, if there are multiple mapping solutions at the t-th step, the one minimizing the localization residual is selected as the optimal solution. After finding the mapping solution for the targets that are exactly detected by $M-t+1$ BSs at the t-th step, the corresponding ranges are removed from $\mathcal{D}_{u,m}$'s and should not be considered at the next step.

The complexity of solving problem (P3-l) depends on the times of solving problem (P1), because we need to check the constraint (3.23) for each mapping $\mathcal{G}_k^{(l)}$, $k = 1,\ldots,K_l$. If the constraints (3.21) and (3.22) are not utilized to filter those ineffective mappings, we may solve problem (P1) many times to check whether (3.23) holds for each mapping element in $\mathcal{G}^{(l)}$, whose cardinality is much larger than that of $\bar{\mathcal{G}}^{(l)}$. On the other hand, the complexity of problem (P4) is derermined by the cardinality of $\tilde{\mathcal{G}}^{(l)}$, which is generally small after applying constrains

Algorithm 4: Algorithm for estimating the mapping and location solutions of all targets

Input: (a_m, b_m)'s, $\mathcal{D}_{u,m}$'s, $\forall u, m$

Initialize: $t = 1$, $\hat{K} = 0$ and $\hat{\mathcal{G}} = \{\}$;

Repeat:

1. Apply Algorithm 3 to solve problem (P3) and obtain the solution $\hat{K}_{M_t}$ and $\hat{\mathcal{G}}_1^{(M_t)}, \ldots, \hat{\mathcal{G}}_{K_{M_t}}^{(M_t)}$;
2. Remove $\mathcal{D}_{u,m}(\hat{g}_{u,m,k})$ from $\mathcal{D}_{u,m}$, $\forall \hat{g}_{u,m,k} \in \hat{\mathcal{G}}_k^{(M_t)}$ with $\hat{g}_{u,m,k} > 0$, $k = 1, \ldots, \hat{K}_{M_t}$, $\forall u, m$;
3. Infer the mapping solution for the $\hat{K}_{M_t}$ new detected targets, denoted by $\hat{\mathcal{G}}_{\hat{K}+1}, \ldots, \hat{\mathcal{G}}_{\hat{K}+K_{M_t}}$
4. Update $\hat{\mathcal{G}} = \hat{\mathcal{G}} \cup \{\hat{\mathcal{G}}_{\hat{K}+1}, \ldots, \hat{\mathcal{G}}_{\hat{K}+K_{M_t}}\}$, $\hat{K} = \hat{K} + \hat{K}_{M_t}$, and $t = t + 1$;

Until $t > M - 2$.

Output:

1) Obtain the estimated number of targets and the solution of LOS identification and data association, respectively, i.e., $\hat{K}$ and $\hat{\mathcal{G}} = \{\hat{\mathcal{G}}_k\}_{k=1}^{\hat{K}}$;

2) Estimate the target locations by solving problem (P1) given the mapping solution $\hat{\mathcal{G}}_k$'s, denoted by $(\hat{x}_k, \hat{y}_k)$'s, $k = 1, \ldots, \hat{K}$.

(3.21)-(3.23). In Section 3.5, we provide numerical results about the cardinalities of $\mathcal{G}^{(l)}$, $\bar{\mathcal{G}}^{(l)}$, and $\tilde{\mathcal{G}}^{(l)}$ to prove the reduction of computational complexity. Moreover, the complexity of the proposed algorithm can be further reduced by transforming problem (P4) into problem (P5), since the data association possibilities that any two mappings belonging to the same $\tilde{\mathcal{G}}_i^{(l)}$ will not be considered in problem (P5). Denote the cardinality of $\tilde{\mathcal{G}}_i^{(l)}$ by $N_i^{(l)}$ in (3.34). Specifically, we just need to try at most $\prod_{i=0}^{N_{1,1}} N_i^{(l)}$ data association possibilities to check whether (3.20) holds in problem (P5). In exhaustive search method to problem (P4), the number of data association possibilities in problem (P4) is $\binom{N_{\bar{\mathcal{G}}^{(l)}}}{K_l}$ for a given K_l such that the total $\sum_{n=K_l}^{N_{\bar{\mathcal{G}}^{(l)}}} \binom{N_{\bar{\mathcal{G}}^{(l)}}}{n}$ data association possibilities need to be numerated.

Remark 3.1. It is worth noting that there may be error propagation in the proposed Algorithm 4. Define the error propagation event as that before the last step, i.e., $M_t > 3$, a spurious mapping $\mathcal{G}_{k_t}^{(M_t)}$ occurs, which satisfies

$$|\{g_{m,m,k} | g_{m,m,k} > 0, g_{m,m,k} \in \mathcal{G}_k, g_{m,m,k} \in \mathcal{G}_{k_t}^{(M_t)}\}| \leq 2, \ \forall k. \tag{3.38}$$

In other words, the spurious target k_t with the mapping $\mathcal{G}_{k_t}^{(M_t)}$ shares at most two same direct ranges with any true target k. The error propagation event is most likely to happen when $M_t = 4$, because there will be more constraints arising from (3.22) to prevent errors when M_t is larger. Then, there will be two cases for the target k_t when $M_t = 4$: (i) the target k_t shares at

most one direct range with any true target; (ii) the target k_t shares two direct ranges with some true target k. Case (i) indicates that the four direct ranges are independent of each other and should satisfy (3.23) to lead to one target. Besides, there should exist sum ranges that satisfy (3.21) and (3.22) with these direct ranges. As for Case (ii), the two direct ranges corresponding to the true target k give rise to two possible locations with one being the location of the true target k and the other one being that of the target k_t. In this case, the other two direct ranges should be matched with the location of the target k_t. Similarly, there should also exist sum ranges that can be associated with the target k_t. Therefore, the probability that Case (i) or Case (ii) happens in our proposed algorithm is quite low. In summary, the error propagation will not significantly degrade the performance of target localization.

3.5 Numerical Results

In this section, we provide the numerical results to verify the effectiveness of our proposed two-phase protocol for networked device-free sensing. In the network, we consider $M = 4$ BSs and $2 \leq K \leq 7$ targets over a 80 m $\times$ 80 m square. To account for LOS blockage, we denote P_b by the probability that the LOS path between a target and a BS is blocked. As for Type III paths, we assume that the number of Type III paths for each target between any two BSs follows a Binomial distribution. In detail, the probabilities that there is/is not one Type III path for each target are P_{nl} and $1 - P_{\text{nl}}$, respectively. Besides, the range of the Type III path is randomly generated in our setup.

3.5.1 Joint STO and Range Estimation in Phase I

In this part, we provide a numerical example to evaluate the range estimation performance of our proposed algorithm in Phase I. Specifically, we set $N = 3300$ and $\Delta f = 120$ kHz such that $B = 400$ MHz [57]. According to [62], with $\Delta f = 120$ kHz, the length of the CP is 0.59 μs. Besides, the STOs between any two BSs are randomly generated in the interval $[-\tau_{\max}, \tau_{\max}]$, where $\tau_{\max}$ is set as 10. To make $L + \tau_{\max} < Q$ such that all the ISI is received within the CP, we assume that the maximum number of resolvable paths is $L = 200$. Moreover, P_{b} and P_{nl} are set as 0.1 and 0.5, respectively. Under this setup, we randomly generate 10^5 independent location realizations of BSs and targets, which are uniformly distributed in the considered area. Given the coordinates of BSs and targets, we can know the delays in terms of OFDM sample periods

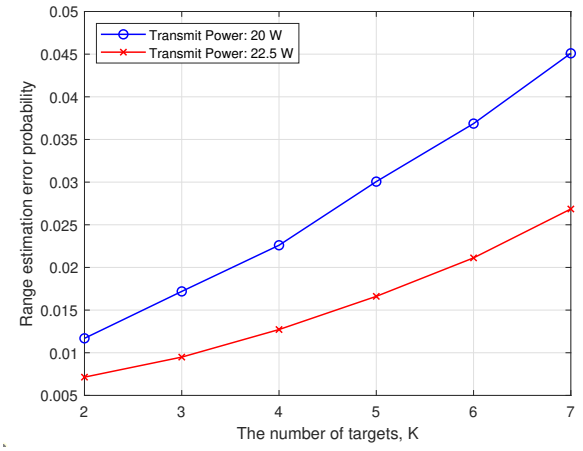

Figure 3.2: Range estimation error probability versus the number of targets.

for Type I and Type II paths. Define $\mathcal{L}_{u,m}$ as the set consisting of the indices of the non-zero channel coefficients in $\boldsymbol{h}_{u,m}$, $\forall u, m$. Then, we estimate the channels $\tilde{\boldsymbol{h}}_{u,m}$'s by solving problem (3.10), and define the set consisting of the indices of the non-zero channel coefficients in $\bar{\boldsymbol{h}}_{u,m}$ as $\bar{\mathcal{L}}_{u,m}$. Based on the estimated channels and the true range between any two BSs, we can estimate the STOs between any two BSs based on (3.11) and (3.12). With the estimated STO $\bar{\tau}_{u,m}$'s, we will substract each element in $\bar{\mathcal{L}}_{u,m}$ by $\bar{\tau}_{u,m}$ to get $\hat{\mathcal{L}}_{u,m}$, $\forall u, m$., i.e., STO compensation in (3.13). If there exist u and m such that $\mathcal{L}_{u,m} \neq \hat{\mathcal{L}}_{u,m}$, we say that the range estimation is in error in this realization. The range estimation error probability versus the number of targets, i.e., K, is shown in Fig. 3.2, where the BS transmit power is set as 20 Watt (W) and 22.5 W, respectively. It is observed that the range estimation error probability is very low under our proposed scheme, and can be significantly reduced by increasing the transmit power.

3.5.2 Localization Accuracy of Two-Phase Protocol

In this part, we provide numerical examples to verify the effectiveness of the overall two-phase protocol for target localization. To show the effectiveness of our proposed algorithm, we adopt the following schemes as benchmark schemes for performance comparison.

- *Benchmark Scheme 1:* Under this benchmark scheme, range estimation in Phase I is the same as our method in Section 3.3, while in Phase II, there is no constraint (3.20) for multiple target localiztion[89]. In other words, each range can be associated with multiple targets. Therefore, each mapping that satisfies the contraints (3.19), and (3.21)-(3.23) is

used for target localization. Specifically, given each mapping element in $\tilde{\mathcal{G}}^{(l)}$, $\forall l$, problem (P1) is solved for estimating the location of the target corresponding to the mapping.

- *Benchmark Scheme 2:* Under this benchmark scheme, range estimation in Phase I is the same as our method in Section 3.3, while in Phase II, we assume that data association is perfectly known, and we just need to perform LOS identification to localize the targets. As a result, this scheme can serve as an error probability lower bound. With the known data association solution, given each target, each BS knows which ranges estimated in Phase I belong to this range. For these ranges belonging to some target, the job of each BS is to identify the ones of Type I/Type II paths if it has the LOS path to this target. We adopt the LOS identification scheme proposed in [80] to tackle the above challenge.

To compare the performance of the proposed scheme and benchmark schemes, we generate 10^4 independent location realizations of BSs and targets, which are distributed in the considered area. The setup is same as that introduced in the last sub-section, i.e., $\tau_{\max} = 10$, $L = 200$, $B = 400$ MHz, $P_{\text{nl}} = 0.5$, and $P_{\text{b}} = 0.1$. Besides, the transmit power is set as 20 W. In each realization, we first estimate channels by solving problem (10) to obtain $\mathcal{D}_{u,m}$'s based on (3.16), and then estimate the number and the locations of targets by Algorithm 4, Benchmark 1, and Benchmark 2, respectively. A target is said to be localized correctly if the distance between its estimated location and its true location is no larger than r m. Denote N_i and K_i as the numbers of the correctly localized targets and the detected targets in the i-th realization, respectively. Then, miss detection (MD) and false alarm (FA) error probabilities over the 10^4 realizations, which are defined as $P_{\text{MD}} = \frac{\sum_{i=1}^{10^4}(K-N_i)}{K\times 10^4}$ and $P_{\text{FA}} = \frac{\sum_{i=1}^{10^4}(K_i-N_i)}{K\times 10^4}$, respectively, are used to characterize the target localization performance for each method.

Fig. 3.3 gives the comparison between the benchmarks and the proposed algorithm in terms of P_{MD} and P_{FA} with different values of r. It is observed that under our proposed scheme, the probabilities of miss detection and false alarm are below 12% and 9% when K ranges from 2 to 7 and with $r = 0.375$ m and $r = 0.5$ m, respectively. We can also see that the proposed algorithm outperforms Benchmark 1 in terms of both miss detection and false alarm error probabilities when K ranges from 2 to 7. Moreover, there is merely a small performance gap between the proposed algorithm and Benchmark 2, where data association is assumed to be known. Therefore, the performance of our proposed joint data association and LOS identification scheme is very close to the localization error probability lower bound.

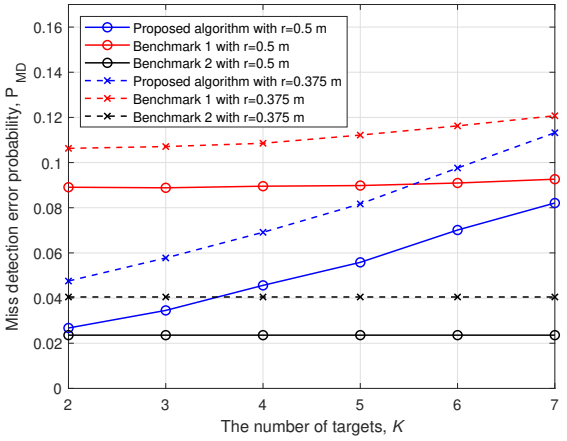

(a) Miss detection probability P_{MD}

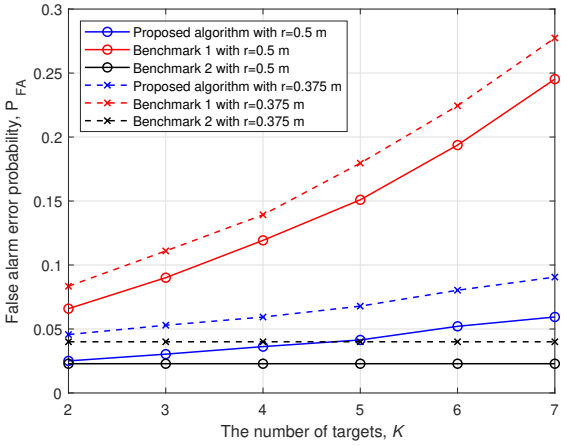

(b) False alarm probability P_{FA}

Figure 3.3: The comparison of location estimation error probability between the benchmark and the proposed algorithm with different r when $B = 400$ MHz, $P_{\mathrm{b}} = 0.1$, and $P_{\mathrm{nl}} = 0.5$.

As for the complexity, the three methods are compared in terms of the average running time in seconds (s) over the 10^4 realizations, which is depicted in Fig. 3.4. We can see that the average running time for the proposed scheme is less than 0.16 seconds in each realization when K ranges from 2 to 7. Considering each BS will have much more computational resources, the actual running time will be lower. Besides, the running time for Benchmark 1 is longer than that of our proposed algorithm when the number of targets is small. There are two reasons, (i) since all possible mappings satisfying constraints (3.19), and (3.21)-(3.23) will be retained, the times of solving problem (P1) in Benchmark 1 is more than that in the proposed algorithm; (ii) the complexity of solving problem (P5) will not be high in the proposed algorithm when the number of targets is small. However, when the number of targets is larger, e.g., $K = 7$, the complexity of solving problem (P5) will be higher such that the running time for the proposed

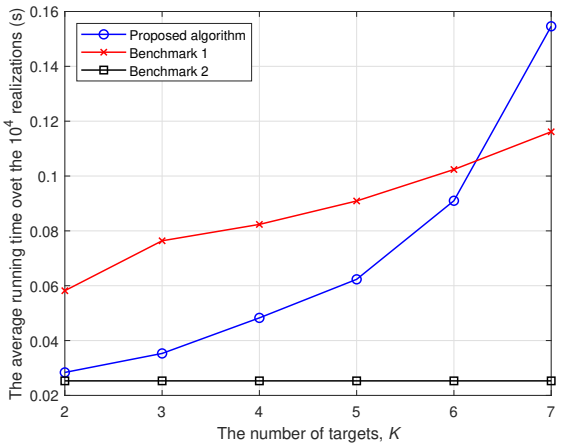

Figure 3.4: The comparison of the average running time for the benchmarks and the proposed algorithm when $B = 400$ MHz, $P_{\mathrm{b}} = 0.1$, and $P_{\mathrm{nl}} = 0.5$.

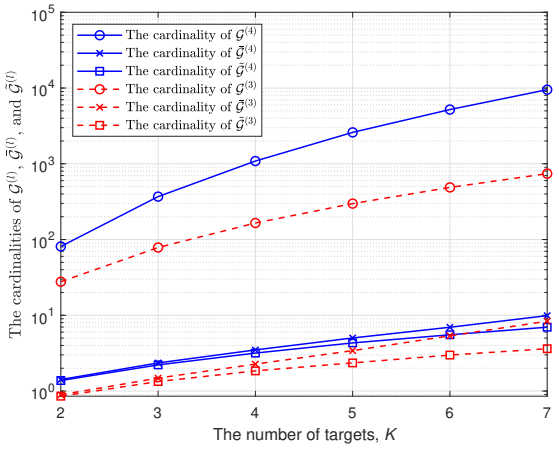

Figure 3.5: The cardinalities of $\mathcal{G}^{(l)}$, $\bar{\mathcal{G}}^{(l)}$, and $\tilde{\mathcal{G}}^{(l)}$ for the proposed algorithm when $B = 400$ MHz, $P_{\mathrm{b}} = 0.1$, and $P_{\mathrm{nl}} = 0.5$.

algorithm is longer.

On the other hand, we also provide the simulation results for the average cardinalities of $\mathcal{G}^{(l)}$, $\bar{\mathcal{G}}^{(l)}$, and $\tilde{\mathcal{G}}^{(l)}$ over the 10^4 realizations, as shown in Fig. 3.5. It is observed that via utilizing (3.21) and (3.22), the cardinality of $\bar{\mathcal{G}}^{(l)}$ is much smaller than that of $\mathcal{G}^{(l)}$, $\forall l \in \{3,4\}$. In other words, the sum distance constraints can efficiently remove the bad data association solutions in $\mathcal{G}^{(l)}$, $\forall l \in \{3,4\}$. Therefore, thanks to constraints (3.21)-(3.23), the utilizations of solving problem (P1) can be greatly reduced. Moreover, the number of possible mapping solutions can be further reduced by (3.23), i.e., the cardinality of $\tilde{\mathcal{G}}^{(l)}$ is fewer than that of $\bar{\mathcal{G}}^{(l)}$, $\forall l \in \{3,4\}$, which can reduce the complexity for solving problem (P4).

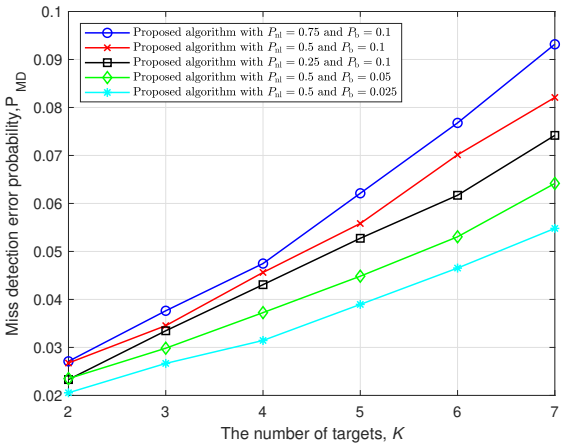

(a) Miss detection probability P_{MD}

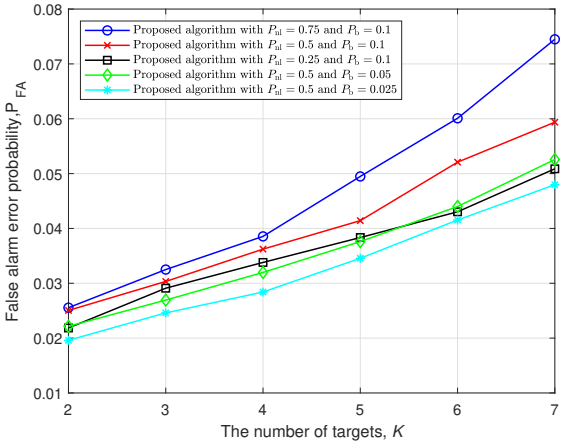

(b) False alarm probability P_{FA}

Figure 3.6: The comparison of location estimation error probability between the benchmark and the proposed algorithm with different P_{b} and P_{nl} when $B = 400$ MHz and $r = 0.5$ m.

3.5.3 Effect of LOS Blockage, NLOS Paths, and Bandwidth on Performance

In this sub-section, we show the impact of LOS blockage, NLOS paths, and bandwidth on target localization. Specifically, the probability that determines the number of Type III paths, i.e., P_{nl}, is set as 0.75, 0.5, and 0.25, respectively. The bandwidth that determines the range resolution, i.e., B, is set as 400 MHz and 300 MHz, respectively. The probability that the LOS path between a target and a BS is blocked, i.e., P_{b}, is set as 0.1, 0.05, and 0.025, respectively.

The effect of bandwidth, LOS blockage, and NLOS paths on target localization for the proposed method is shown in Fig. 3.6 and Fig. 3.7 with $r = 0.5$ m. It is depicted that the location error probability will be lower when the probability P_{b} is decreased, since the additional LOS path information is beneficial for target localization. Moreover, we can see that when the

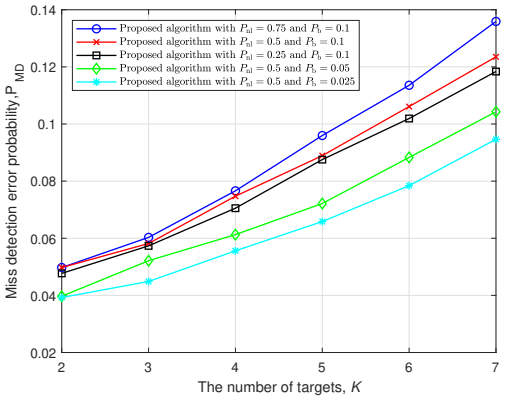

(a) Miss detection probability P_{MD}

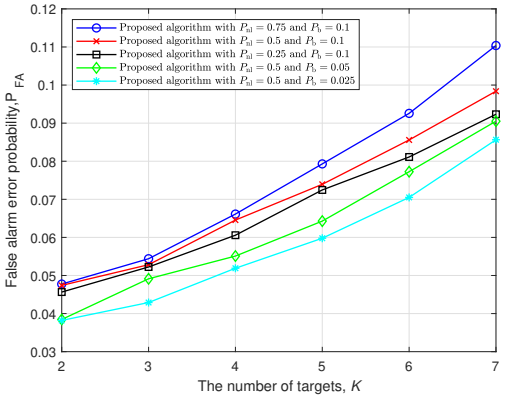

(b) False alarm probability P_{FA}

Figure 3.7: The comparison of location estimation error probability between the benchmark and the proposed algorithm with different P_{b} and P_{nl} when $B = 300$ MHz and $r = 0.5$ m.

probability of the existence of NLOS paths P_{nl} is increased, the location error probabilities of our proposed algorithm increase as well. The reason is that the NLOS paths will increase the probability of the existence of spurious mappings such that the localization performance is degraded. It is observed from Fig. 3.6 and Fig. 3.7 that the target localization performance can be improved by increasing the system bandwidth from 300 MHz to 400 MHz. Because the larger bandwidth can bring a higher range resolution, the accuracy of target localization in our proposed algorithm will be enhanced.

3.6 Conclusion

In this paper, we study networked device-free sensing based on the echoes of the transmitted downlink communication signals in a multi-path environment, where the BSs are not

perfectly synchronized but will share the communication and sensing information. A two-phase protocol was adopted. In the first phase, each BS estimated the direct distances from targets to itself and the sum distances from other BSs to targets to itself. Since the range of the LOS path between any two BSs is known, it is utilized to estimate the STOs such that the range of each path between any two BSs can be accurately estimated. In the second phase, all BSs collaboratively localized targets based on range estimations obtained in Phase I. Nevertheless, there are issues of range interference arising from NLOS paths, LOS blockage for some BSs and some targets, and the unknown mapping between ranges of LOS paths and targets, which are coupled together. To tackle the above challenges, an efficient algorithm was proposed to iteratively localize the targets that are exactly detected by a given number of BSs. In this way, we can decouple the issue of LOS blockage from the problem of NLOS paths and data association. As a result, the number and the locations of targets can be efficiently estimated. Numerical results showed that the proposed strategy can achieve high accuracy of target localization, thanks to BS coordination and large bandwidth in the 6G cellular network.

Chapter 4

A 6G-Based Multi-View Reconstruction Approach

4.1 Introduction

Reconstruction is the process of capturing the shape and appearance of real objects. It finds wide applications in practice, such as object detection, activity monitoring, and vehicle navigation[99]. Currently, reconstruction mainly relies on the camera technology, and there are lots of excellent computer vision based methods proposed in the literature[100, 101]. Despite the high resolution of the camera, the vision based method poses stringent requirements on light and weather conditions[102]. Moreover, there are privacy concerns in vision based systems, because too many details of the sensed objects may be exposed to unauthorized parties.

To overcome the above issues arising from vision based reconstruction technique, this paper aims to investigate an alternative - radio signal based reconstruction technique. Specifically, integrated sensing and communication (ISAC) is a main use scenario of the future 6G cellular technology[72, 83, 103–105]. This brings a paradigm shift to cellular systems, because ISAC also promises many sensing applications such as target detection, drone navigation, etc. In particular, the high range resolution brought by the millimeter wave (mmWave) and Terahertz (THz) techniques and the high angle resolution brought by the massive multiple-input multiple-output (MIMO) technique make it possible to leverage 6G signals to perform reconstruction. Compared to vision based counterpart, 6G-based reconstruction can work in any

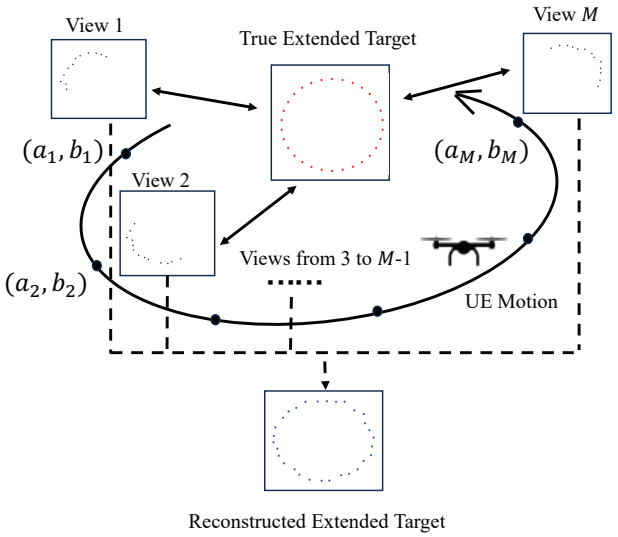

Figure 4.1: The illustration of a 6G-based multi-view reconstruction system. A mobile UE moves to different known locations to image a static extended target from different angles.

light and weather condition. Moreover, 6G-based reconstruction belongs to textureless (here, texture includes but is not limited to the granularity, regularity, and roughness of the extended target) sensing techniques, because it can merely recover the shape of the target. It is thus more appealing than the conventional vision based reconstruction technique in applications where privacy is a main concern. Another drawback is that quite a lot of vision based methods rely on deep learning. As a result, these deep learning models may lack good generalization to different environments and leads to poor performance of target reconstruction. We believe that 6G-based textureless reconstruction can be used in myriad applications such as pose recognition, object tracking, etc.

Motivated by the above, this paper will explore the 6G-based technique to reconstruct the shape of an extended target consisting of many adjacent point targets. Specifically, a user equipment (UE), e.g., drone, robot, etc., is merely equipped with the radio transceiver (without requiring extra space to carry a camera) and emits orthogonal frequency division multiplexing (OFDM) signals for both communication and reconstruction purposes. Particularly, we are interested in the *multi-view* reconstruction technique. As shown in Fig. 4.1, at each time slot, the UE first moves to a known location, then emits the OFDM signals, and records the echo signals reflected by the point targets belonging to the extended target. After observing the target from sufficient angles, we will fuse all the echo signals received at all time slots and localize the point targets for the reconstruction purpose. Specifically, the multi-view data is used to build a probability density map, on which each grid represents the probability of

the existence of a point target of the extended target. Numerical results show that the image obtained based on our proposed multi-view technique is of much higher resolution than that observed from each angle based on the single-view technique.

A related work is [106], where a high-resolution single-view imaging system, named mm-Eye, was presented based on the 69GHz Wi-Fi technique. However, as shown in [106], many point targets are not detected based on the proposed imaging technique. The multi-view technique can overcome this issue because the point targets that are not detected from one angle can be detected from other angles. In the existing literature, multi-view reconstruction was mainly studied in the field of computer vision [107–111]. Quite a lot of deep learning based techniques have been proposed based on texture information, e.g., color, edge, and corner, which is not available under the 6G imaging technique. However, our proposed textureless algorithm merely relies on the location information of the point targets for target reconstruction.

4.2 System Model

We consider a 6G-based reconstruction system consisting of a mobile UE (e.g., a drone, a robot, etc.) that is equipped with N_T transmit antennas and N_R receive antennas and a static passive extended target that is modeled as a collection of K adjacent point targets. The location of the k-th point target of the extended target is denoted by (x_k, y_k), $k = 1, \ldots, K$. Moreover, towards any direction θ, let $\boldsymbol{a}(\theta, N_T) \in \mathbb{C}^{N_T \times 1}$ and $\boldsymbol{b}(\theta, N_R) \in \mathbb{C}^{N_R \times 1}$ denote the transmit and receive steering vectors of the mobile UE, respectively. For example, under the uniform linear array (ULA) model, the transmit and receive steering vectors are respectively

$$\boldsymbol{a}(\theta, N_T) = [1, e^{-\frac{j2\pi d_A \sin\theta}{\lambda}}, \ldots, e^{-\frac{j2\pi(N_T-1)d_A \sin\theta}{\lambda}}]^T, \tag{4.1}$$

and

$$\boldsymbol{b}(\theta, N_R) = [1, e^{-\frac{j2\pi d_A \sin\theta}{\lambda}}, \ldots, e^{-\frac{j2\pi(N_R-1)d_A \sin\theta}{\lambda}}]^T, \tag{4.2}$$

where d_A is the antenna spacing and λ is the signal wavelength. We consider M time slots, and at the m-th time slot, the UE first moves to a known location $(a^{(m)}, b^{(m)})$, then emits OFDM communication signals, and last receives the echo signals from the extended target. After

collecting the echo signals received over all the M time slots, our goal is to reconstruct the shape of the extended target, which is equivalent to precisely localizing all the K point targets of the extended target.

Specifically, at the m-th time slot, define $\boldsymbol{s}_{n_T}^{(m)} = [s_{n_T,1}^{(m)}, \ldots, s_{n_T,N}^{(m)}]^T$ as one frequency-domain OFDM symbol for transmit antenna n_T, where N is the number of sub-carriers of the transmitted OFDM signals and $s_{n_T,n}^{(m)}$ is the signal at the n-th sub-carrier. Then, the time-domain modulated signal of the UE at the m-th time slot over one OFDM symbol consisting of N samples is given by $\boldsymbol{\chi}_{n_T}^{(m)} = [\boldsymbol{\chi}_{n_T,1}^{(m)}, \ldots, \boldsymbol{\chi}_{n_T,N}^{(m)}]^T = \sqrt{p}\boldsymbol{W}^H \boldsymbol{s}_{n_T}^{(m)}, \forall m, n_T$, where p denotes the transmit power for the UE and $\boldsymbol{W} \in \mathbb{C}^{N\times N}$ denotes the the discrete Fourier transform (DFT) matrix with $\boldsymbol{W}\boldsymbol{W}^H = \boldsymbol{W}^H\boldsymbol{W} = \boldsymbol{I}_N$. After inserting the cyclic prefix (CP) consisting of Q OFDM samples, the time-domain signal for transmit antenna n_T over one OFDM symbol period is given by $\bar{\boldsymbol{\chi}}_{n_T}^{(m)} = [\bar{\boldsymbol{\chi}}_{n_T,-Q}^{(m)}, \ldots, \bar{\boldsymbol{\chi}}_{n_T,-1}^{(m)}, \bar{\boldsymbol{\chi}}_{n_T,0}^{(m)}, \ldots, \bar{\boldsymbol{\chi}}_{n_T,N-1}^{(m)}]^T$, where when $n \geq 0$, $\bar{\boldsymbol{\chi}}_{n_T,n}^{(m)} = \boldsymbol{\chi}_{n_T,n+1}^{(m)}$ denotes the useful signal, and when $n < 0$, $\bar{\boldsymbol{\chi}}_{n_T,n}^{(m)} = \boldsymbol{\chi}_{n_T,N+n+1}^{(m)}$ denotes the CP.

Moreover, the distance and angle between the k-th point target and the UE at the m-th time slot are respectively

$$d_k^{(m)} = \sqrt{(a^{(m)} - x_k)^2 + (b^{(m)} - y_k)^2}, \tag{4.3}$$

and

$$\theta_k^{(m)} = \text{atan}\frac{y_k - b^{(m)}}{x_k - a^{(m)}}, \tag{4.4}$$

where atan$(\cdot)$ is the arctan function. On one hand, the line-of-sight (LOS) channel between the k-th point target and the UE at the m-th time slot can be expressed as

$$\hat{\boldsymbol{H}}_k^{(m)} = \alpha_k^{(m)} \boldsymbol{b}(\theta_k^{(m)}, N_R)\boldsymbol{a}^T(\theta_k^{(m)}, N_T), \ \forall k \in \mathcal{K}_m^{\text{det}}, \tag{4.5}$$

where $\alpha_k^{(m)}$ denotes the attenuation coefficient caused by the path loss and radar cross section (RCS) between the UE and point target k at time slot m, and $\mathcal{K}_m^{\text{det}} \subseteq \{1, \ldots, K\}$ consists of the point targets that have the LOS paths to the UE at the m-th time slot. Under the Swerling target model, $\alpha_k^{(m)}$'s are Gaussian distributed and independent over m and k, i.e., $\alpha_k^{(m)} \sim \mathcal{CN}(0, \sigma_{m,k}^2)$. On the other hand, define $\tau_k^{(m)} = \lfloor \frac{2N\Delta f d_k^{(m)}}{c_0} \rfloor$ as the propagation delay (in terms of OFDM sample periods) from the UE to point target k and back to the UE at the m-th time slot, where Δf is the sub-carrier spacing of the transmitted OFDM signals and c_0 is the speed of light. Then,

under an L-tap multi-path propagation environment, at the m-th time slot, define the set that consists of all the point targets that cause signal delay of l OFDM sample periods as

$$\Omega_l^{(m)} = \{k : \tau_k^{(m)} = l \text{ and } k \in \mathcal{K}_m^{\text{det}}\},\ \forall m, l. \tag{4.6}$$

Therefore, at time slot m, the channel associated with the l-th tap of the multi-path environment from the transmit antennas of the UE to the receive antennas of the UE via the extended target is modeled as

$$\tilde{\boldsymbol{H}}_l^{(m)} = \sum_{k \in \Omega_l^{(m)}} \hat{\boldsymbol{H}}_k^{(m)} \in \mathbb{C}^{N_R \times N_T}, \forall m, l. \tag{4.7}$$

Note that if $\Omega_l^{(m)} \neq \emptyset$, then $\tilde{\boldsymbol{H}}_l^{(m)}$ is a function of $d_k^{(m)}$'s and $\theta_k^{(m)}$'s for the point targets in $\Omega_l^{(m)}$; while if $\Omega_l^{(m)} = \emptyset$, then $\tilde{\boldsymbol{H}}_l^{(m)} = \boldsymbol{0}$.

Hence, the time-domain signal at receive antenna n_R for the n-th sampling period at the m-th time slot can be expressed as

$$y_{n_R,n}^{(m)} = \sum_{n_t=1}^{N_T} \sum_{l=0}^{L-1} h_{n_R,n_T,l}^{(m)} \bar{\chi}_{n_T,n-l}^{(m)} + z_{n_R,n}^{(m)},\ \forall n_R, n, m, \tag{4.8}$$

where $h_{n_R,n_T,l}^{(m)}$ is the element at the n_R-th row and n_T-th column of $\tilde{\boldsymbol{H}}_l^{(m)}$ and represents the channel of path from transmit antenna n_T to receive antenna n_R with a delay of l OFDM samples at the m-th time slot, and $z_{n_R,n}^{(m)} \sim \mathcal{CN}(0, \sigma_z^2)$ denotes the noise at the n_R-th receive antenna in the n-th OFDM sample period at the m-th time slot.

After collecting the received signals given in (4.8) over all the M time slots, we adopt a two-phase method to estimate the locations of the K point targets and reconstruct the shape of the extended target. In Phase I, we estimate the distances and angles from point targets to the UE at each time slot, i.e., $d_k^{(m)}$ and $\theta_k^{(m)}$, $\forall k \in K_m$, $\forall m$. Note that each pair of distance and angle estimations can localize one point target. At each time slot m, we can construct a textureless image of the extended target by putting all the point targets detected at this time slot together. Therefore, after Phase I, we have M single-view textureless images. However, each image obtained at each time slot may be of quite low quality due to the following two reasons. First, as shown in (4.7) and (4.8), the received signal at each time slot m is only contributed by the point targets in $\mathcal{K}_m^{\text{det}}$, and the corresponding single-view image cannot contain all the information about the extended target. Second, at each time slot m, even for the point targets in

$\mathcal{K}_m^{\text{det}}$, their range and angle estimations are subject to errors. Therefore, the mismatch between each single-view image and the extended target can be large. In Phase II, we aim to fuse the M single-view images in an effective way so as to better reconstruct the shape of the extended target. This is possible because 1. a point target that cannot be detected at one time slot can be detected at other time slots; 2. each point target is usually detected in multiple time slots, and the estimation of its location can be more accurate based on all these observations. In the rest of this paper, we introduce how to devise Phase I and Phase II to perform multi-view reconstruction.

4.3 Phase I: Range and Angle Estimation

In this section, we show how to obtain the range and angle information of the point targets based on the signals received at each time slot. By removing the first Q CP samples, the time-domain received signal for the n_R-th receive antenna over one OFDM symbol at the m-th time slot is given by [83]

$$\begin{aligned}\boldsymbol{y}_{n_R}^{(m)} &= [y_{n_R,1}^{(m)},\ldots,y_{n_R,N}^{(m)}]^T \\ &= \sqrt{p}\sum_{n_t=1}^{N_T}\boldsymbol{H}_{n_R,n_T}^{(m)}\boldsymbol{\chi}_{n_T}^{(m)}+\boldsymbol{z}_{n_R}^{(m)},\ \forall n_R,m,\end{aligned} \tag{4.9}$$

where $\boldsymbol{H}_{n_R,n_T}^{(m)} \in \mathbb{C}^{N\times N}$ is a circulant matrix with the first row being $[h_{n_R,n_T,0}^{(m)},0,\ldots,0,h_{n_R,n_T,L-1}^{(m)},\ldots,h_{n_R,n_T,2}^{(m)}]^T$, and $\boldsymbol{z}_{n_R}^{(m)} = [z_{n_R,1}^{(m)},\ldots,z_{n_R,N}^{(m)}]^T \sim \mathcal{CN}(\boldsymbol{0},\sigma_z^2\boldsymbol{I}_N)$. After multiplying the time-domain signal by the DFT matrix $\boldsymbol{W}$, the received frequency-domain OFDM signal for the n_R-th receive antenna at the m-th time slot is given by [55]

$$\begin{aligned}\bar{\boldsymbol{y}}_{n_R}^{(m)} &= \boldsymbol{W}\boldsymbol{y}_{n_R}^{(m)} \\ &= \sqrt{p}\sum_{l=0}^{L-1}\tilde{\boldsymbol{G}}_l\tilde{\boldsymbol{h}}_{n_R,l}^{(m)}+\bar{\boldsymbol{z}}_{n_R}^{(m)},\ \forall n_R,m,\end{aligned} \tag{4.10}$$

where $\tilde{\boldsymbol{G}}_l \in \mathbb{C}^{N\times N_T}$ with the (n,n_T)-th element $[\tilde{\boldsymbol{G}}_l]_{n,n_T} = s_{n_T,n}e^{-\frac{-j2\pi(n-1)l}{N}}$, $\tilde{\boldsymbol{h}}_{n_R,l} = [h_{n_R,1,l}^{(m)},\ldots,h_{n_R,N_T,l}^{(m)}]^T \in \mathbb{C}^{N_T\times 1}$, and $\bar{\boldsymbol{z}}_{n_R}^{(m)} = [\bar{z}_{n_R,1}^{(m)},\ldots,\bar{z}_{n_R,N}^{(m)}]^T = \boldsymbol{W}\boldsymbol{z}_{n_R}^{(m)} \sim \mathcal{CN}(\boldsymbol{0},\sigma_z^2\boldsymbol{I}_N)$ since

$\boldsymbol{W}\boldsymbol{W}^H = \boldsymbol{W}^H\boldsymbol{W} = \boldsymbol{I}_N$. By stacking the overall received signal across all the N_R receive antennas and N sub-carriers, it follows that

$$\begin{aligned}\bar{\boldsymbol{y}}^{(m)} =&[(\bar{\boldsymbol{y}}_1^{(m)})^T,\ldots,(\bar{\boldsymbol{y}}_{N_R}^{(m)})^T]^T\\ =&\sqrt{p}\sum_{l=0}^{L-1}[(\tilde{\boldsymbol{G}}_l\tilde{\boldsymbol{h}}_{1,l}^{(m)})^T,\ldots,(\tilde{\boldsymbol{G}}_l\tilde{\boldsymbol{h}}_{N_R,l}^{(m)})^T]^T+\bar{\boldsymbol{z}}^{(m)}\\ =&\sqrt{p}\sum_{l=0}^{L-1}\tilde{\boldsymbol{\Theta}}_l\tilde{\boldsymbol{h}}_l^{(m)}+\bar{\boldsymbol{z}}^{(m)}\\ =&\sqrt{p}\tilde{\boldsymbol{\Theta}}\tilde{\boldsymbol{h}}^{(m)}+\bar{\boldsymbol{z}}^{(m)},\ \forall m,\end{aligned}\tag{4.11}$$

where

$$\tilde{\boldsymbol{\Theta}} =[\tilde{\boldsymbol{\Theta}}_0,\ldots,\tilde{\boldsymbol{\Theta}}_{L-1}]\in\mathbb{C}^{N_RN\times LN_TN_R},\tag{4.12}$$

$$\tilde{\boldsymbol{\Theta}}_l =\begin{bmatrix}\tilde{\boldsymbol{G}}_l & \cdots & \boldsymbol{0}\\ \vdots & \ddots & \vdots\\ \boldsymbol{0} & \cdots & \tilde{\boldsymbol{G}}_l\end{bmatrix}\in\mathbb{C}^{N_RN\times N_TN_R},\ \forall l,\tag{4.13}$$

$$\tilde{\boldsymbol{h}}^{(m)} =[(\tilde{\boldsymbol{h}}_0^{(m)})^T,\ldots,(\tilde{\boldsymbol{h}}_{L-1}^{(m)})^T]^T\in\mathbb{C}^{LN_TN_R\times 1},\tag{4.14}$$

$$\tilde{\boldsymbol{h}}_l^{(m)} =[(\tilde{\boldsymbol{h}}_{1,l}^{(m)})^T,\ldots,(\tilde{\boldsymbol{h}}_{N_R,l}^{(m)})^T]^T\in\mathbb{C}^{N_TN_R\times 1},\ \forall l,\tag{4.15}$$

$$\bar{\boldsymbol{z}}^{(m)} =[(\bar{\boldsymbol{z}}_1^{(m)})^T,\ldots,(\bar{\boldsymbol{z}}_{N_R}^{(m)})^T]^T\in\mathbb{C}^{N_RN\times 1}.\tag{4.16}$$

Note that $\tilde{\boldsymbol{h}}^{(m)}$ is a function of point targets' distances and angle-of-arrivals (AOAs) to the UE at time slot m. The job of the UE is to estimate these location parameters based on the received signals given in (4.11) at each time slot. In the following, we show how to estimate the range information and the AOA information, respectively.

Note that $\tilde{\boldsymbol{h}}_l^{(m)}$ in (4.15) is the vector-form expression of $\tilde{\boldsymbol{H}}_l^{(m)}$ in (4.7). Hence, it can be known from (4.7) that $\tilde{\boldsymbol{h}}_l^{(m)}=\boldsymbol{0}$ (equivalent to $\tilde{\boldsymbol{H}}_l^{(m)}=\boldsymbol{0}$) if there is no point target in the l-th range bin at the m-th time slot, i.e., $\Omega_l^{(m)}=\emptyset$. As a result, there is block sparsity in $\tilde{\boldsymbol{h}}^{(m)}$, which motivates us to employ the group LASSO technique [61] to estimate the OFDM channels based on (4.14). Specifically, given a carefully designed parameter $\rho>0$, the group LASSO problem for estimating each $\tilde{\boldsymbol{h}}^{(m)}$ is formulated as

$$\text{(P1)}\ \underset{\tilde{\boldsymbol{h}}^{(m)}}{\text{minimize}}\ \frac{1}{2}\|\bar{\boldsymbol{y}}^{(m)}-\sqrt{p}\tilde{\boldsymbol{\Theta}}\tilde{\boldsymbol{h}}^{(m)}\|_2^2+\rho\sum_{l=0}^{L-1}\|\tilde{\boldsymbol{h}}_l^{(m)}\|_2,\tag{4.17}$$

which is a convex problem, and thus can be efficiently solved by CVX toolbox [95]. Denote the solution of channel estimation by $\bar{\boldsymbol{h}}^{(m)} = [(\bar{\boldsymbol{h}}_0^{(m)})^T, \ldots, (\bar{\boldsymbol{h}}_{L-1}^{(m)})^T]^T$, $\forall m$, with $\bar{\boldsymbol{h}}_l^{(m)} = [(\bar{\boldsymbol{h}}_{1,l}^{(m)})^T, \ldots, (\bar{\boldsymbol{h}}_{N_R,l}^{(m)})^T]^T = [\bar{h}_{1,1,l}^{(m)}, \ldots, \bar{h}_{1,N_T,l}^{(m)}, \ldots, \bar{h}_{N_R,1,l}^{(m)}, \ldots, \bar{h}_{N_R,N_T,l}^{(m)}]^T$, $\forall l$. Based on the discussion above, if $\bar{\boldsymbol{h}}_l^{(m)} \neq \mathbf{0}$ for some l, then $\Omega_l^{(m)} \neq \emptyset$. In other words, there are some point targets in $\Omega_l^{(m)}$, whose ranges to the UE lie in $[\frac{lc_0}{2N\Delta f}, \frac{(l+1)c_0}{2N\Delta f})$ at the m-th time slot. Hence, the distance from each point target in $\Omega_l^{(m)}$, $\forall l$ with $\bar{\boldsymbol{h}}_l^{(m)} \neq \mathbf{0}$, to the UE can be estimated as

$$\bar{r}_l^{(m)} = \frac{lc_0}{2N\Delta f} + \frac{lc_0}{4N\Delta f}. \tag{4.18}$$

Next, we estimate the AOAs from the $K_l^{(m)} = |\Omega_l^{(m)}|$ point targets in $\Omega_l^{(m)}$ to the UE based on $\bar{\boldsymbol{h}}_l^{(m)}$, $\forall m, l$. Based on (4.7), under the ULA model of the steering vector, we have

$$\begin{aligned} &\bar{h}_{n_R,n_T,l}^{(m)} \\ =&h_{n_R,n_T,l}^{(m)} + \varepsilon_{n_R,n_T,l}^{(m)} \\ =&\sum_{k\in\Omega_l^{(m)}} \alpha_k^{(m)} e^{-\frac{j2\pi(n_R+n_T-2)d_A \sin\theta_k^{(m)}}{\lambda}} + \varepsilon_{n_R,n_T,l}^{(m)}, \end{aligned} \tag{4.19}$$

where $\varepsilon_{n_R,n_T,l} \sim \mathcal{CN}(0, \sigma_\varepsilon^2)$ denotes the channel estimation error for $h_{n_R,n_T,l}^{(m)}$. By defining $\hat{h}_{n_a,l}^{(m)} = \bar{h}_{n_R,n_T,l}^{(m)}$ and $\varepsilon_{n_a,l}^{(m)} = \varepsilon_{n_R,n_T,l}^{(m)}$ with $n_a = n_R + n_T - 1$, it leads to

$$\hat{h}_{n_a,l}^{(m)} = \sum_{k\in\Omega_l^{(m)}} \alpha_k^{(m)} e^{-\frac{j2\pi(n_a-1)d_A \sin\theta_k^{(m)}}{\lambda}} + \varepsilon_{n_a,l}^{(m)}. \tag{4.20}$$

Then, we can get

$$\hat{\boldsymbol{h}}_l^{(m)} = [\hat{h}_{1,l}^{(m)}, \ldots, \hat{h}_{N_a,l}^{(m)}]^T = \boldsymbol{A}_l^{(m)} \boldsymbol{\alpha}_l^{(m)} + \boldsymbol{\epsilon}_l^{(m)}, \tag{4.21}$$

where $N_a = N_R + N_T - 1$, $\boldsymbol{A}_l^{(m)} = [\boldsymbol{a}(\theta_1^{(m)}, N_a), \ldots, \boldsymbol{a}(\theta_{K_l^{(m)}}^{(m)}, N_a)] \in \mathbb{C}^{N_a \times K_l^{(m)}}$ and $\boldsymbol{\alpha}_l^{(m)} = [\alpha_1^{(m)}, \ldots, \alpha_{K_l^{(m)}}^{(m)}]^T \in \mathbb{C}^{K_l^{(m)} \times 1}$ are the steering matrix and the channel coefficient vector for the point targets in $\Omega_l^{(m)}$ at the m-th time slot, respectively, and $\boldsymbol{\epsilon}_l^{(m)} = [\varepsilon_{1,l}^{(m)}, \ldots, \varepsilon_{N_a,l}^{(m)}]^T \sim \mathcal{CN}(\mathbf{0}, \sigma_\varepsilon^2 \boldsymbol{I}_{N_a})$.

In this work, we utilize multiple signal classification (MUSIC) [112] to estimate the angles from the $K_l^{(m)}$ point targets in $\Omega_l^{(m)}$ to the UE at time slot m. The covariance of $\hat{\boldsymbol{h}}_l^{(m)}$ can be

expressed as

$$\begin{aligned}\boldsymbol{R}_{\hat{\boldsymbol{h}}_l^{(m)}} &= \mathbb{E}[\hat{\boldsymbol{h}}_l^{(m)}(\hat{\boldsymbol{h}}_l^{(m)})^H] \\ &= \boldsymbol{A}_l^{(m)}\mathbb{E}[\boldsymbol{\alpha}_l^{(m)}(\boldsymbol{\alpha}_l^{(m)})^H](\boldsymbol{A}_l^{(m)})^H + \mathbb{E}[\boldsymbol{\epsilon}_l^{(m)}(\boldsymbol{\epsilon}_l^{(m)})^H] \\ &= \boldsymbol{A}_l^{(m)}\boldsymbol{R}_{\boldsymbol{\alpha}_l^{(m)}}(\boldsymbol{A}_l^{(m)})^H + \sigma_\varepsilon^2\boldsymbol{I}_{N_a},\end{aligned} \tag{4.22}$$

where $\boldsymbol{R}_{\boldsymbol{\alpha}_l^{(m)}} = \mathrm{diag}(\sigma^2_{m,1},\ldots,\sigma^2_{m,K_l^{(m)}})$ is the covariance of $\boldsymbol{\alpha}_l^{(m)}$ since the attenuation coefficients $\alpha_k^{(m)}$'s are independent over m and k. The eigenvalues $\lambda_1,\ldots,\lambda_{N_a}$ of $\boldsymbol{R}_{\hat{\boldsymbol{h}}_l^{(m)}}$ are sorted in a nonascending order, associated with N_a eigenvectors $\boldsymbol{e}_1,\ldots,\boldsymbol{e}_{N_a}$. Then, the noise subspace can be constructed as $\boldsymbol{E}_n = [\boldsymbol{e}_{K_l^{(m)}+1},\ldots,\boldsymbol{e}_{N_a}]$, where $K_l^{(m)}$ stands for the dimension of the signal subspace. The (pseudo) spatial spectrum for any direction θ can be obtained as

$$P_l^{(m)}(\theta) = \frac{1}{\boldsymbol{a}^H(\theta,N_a)\boldsymbol{E}_n\boldsymbol{E}_n^H\boldsymbol{a}(\theta,N_a)}. \tag{4.23}$$

Large values of the spatial spectrum $P_l^{(m)}(\theta)$ in a specific part of the space would most likely indicate the presence of one or more reflected signals; low values of $P_l^{(m)}(\theta)$ would indicate the absence of such reflections. One critical problem in applying MUSIC is to determine the number of signals $K_l^{(m)}$ that impinge on the array. Akaike information criterion (AIC), a well-known information-theoretic approach for model order selection, is used to estimate $K_l^{(m)}$[113], given by

$$\begin{aligned}&(K_l^{(m)})^\star \\ &= \arg\max_{K_l^{(m)}} \log\left(\frac{\prod_{i=1+K_l^{(m)}}^{N_a}\lambda_i^{1/(\beta_l^{(m)})}}{\sum_{j=1+K_l^{(m)}}^{N_a}\lambda_j/\beta_l^{(m)}}\right)^{\beta_l^{(m)}} \\ &\quad - K_l^{(m)}(N_a+\beta_l^{(m)}),\end{aligned} \tag{4.24}$$

where $\beta_l^{(m)} = N_a - K_l^{(m)}$. Therefore, we can find the $(K_l^{(m)})^\star$ peaks of the spatial spectrum $P_l^{(m)}(\theta)$ to get angle estimations $\{\bar{\theta}_{k_l}^{(m)}\}_{k_l=1}^{(K_l^{(m)})^\star}$ for the point targets in $\Omega_l^{(m)}$.

To summarize, after Phase I of our considered protocol, the UE acquires M measurement sets (single-view textureless images) about the extended target, i.e.,

$$\begin{aligned}\mathcal{D}^{(m)} =&\{(\bar{r}_l^{(m)}, \bar{\theta}_{k_l}^{(m)})|\forall l \text{ with } \bar{\boldsymbol{h}}_l^{(m)} \text{ and} \\ & k_l = 1,\ldots,(K_l^{(m)})^\star\},\ m = 1,\ldots,M. \end{aligned} \tag{4.25}$$

The job of the UE in Phase II is to fuse these M single-view images of measurement to reconstruct the extended target. However, there are two challenges to achieving the above goal. First, each point target may not be detected by the UE at some time slots. In other words, each single-view image may only provide partial information about the extended target. Second, different from vision-based approaches where there is texture information that can be utilized to find the correspondences of point targets across different image views, i.e., *data association*, we can only extract location information about the extended target from the communication signal views. Hence, it is challenging to fuse all the M single-view images of measurement for target reconstruction. In detail, with range and angle information about the point targets, the UE can directly estimate the point targets at each time slot. However, the two point targets of the extended target may be close in our considered case. As a result, it is likely to associate the estimated point target with the wrong nearby point target of the extended target. In other words, the two nearby point targets of the extended target may be thought to be the same point target across different communication signal views. In the next section, we will show how to deal with the above challenges in Phase II to perform passive extended target reconstruction.

4.4 Phase II: Data Fusion

In this section, we fuse the M single-view images of measurement in a grid-based way for target reconstruction[114, 115]. In detail, the whole region of interest (ROI) is divided into multiple grids, and the probability existence of a point target of the extended target at each grid is calculated based on the M measurement sets obtained in Phase I. Then, the probability density map of the target over the whole ROI is leveraged for recovering the extended target.

Based on (4.3) and (4.4), each measurement element $(\bar{r}_l^{(m)}, \bar{\theta}_{k_l}^{(m)})$ in $\mathcal{D}_m$ can be directly used to estimate the location of its corresponding point target. Specifically, given the n-th measurement in $\mathcal{D}_m$, i.e., $(\bar{r}_n^{(m)}, \bar{\theta}_n^{(m)}) \in \mathcal{D}_m$, the location of the corresponding point target can

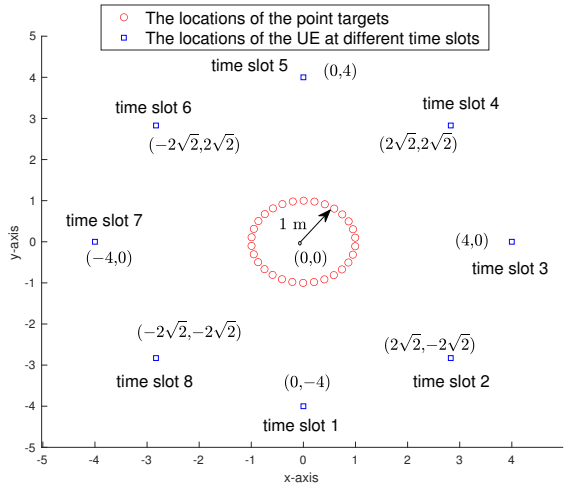

Figure 4.2: Setup of the numerical example. The extended target is modeled as a circle with the center at $(0,0)$ m and the radius $r = 1$ m, and consists of $K = 30$ points. The UE moves to eight sites as shown in the figure at different time slots to sense the extended target.

be estimated as

$$\begin{aligned}&(\bar{x}_n^{(m)}, \bar{y}_n^{(m)})\\ =&(a^{(m)} + \bar{r}_n^{(m)}\cos(\bar{\theta}_n^{(m)}), b^{(m)} + \bar{r}_n^{(m)}\sin(\bar{\theta}_n^{(m)})),\ n = 1,...,N_m,\end{aligned} \tag{4.26}$$

where $N_m = |\mathcal{D}_m|$ is the cardinality of $\mathcal{D}_m$. Therefore, there are N_m estimated point targets for each measurement set $\mathcal{D}_m$ at the m-th time slot.

Next, we show how to calculate the probability density map of the target over the whole ROI based on these estimated point targets, i.e., the probability existence of a point target at each grid. First, the whole ROI is divided into $N_g = N_{g_x} \times N_{g_y}$ grids and the location of the (i,j)-th grid is denoted by $(x_{i,j}^g, y_{i,j}^g)$, $i = 1,\ldots,N_{g_x}$, $j = 1,\ldots,N_{g_y}$. Intuitively, for a particular estimated point target, if one grid is closer to the estimated point target, it is more likely that there is the existence of a point target at this grid. Then, the probability existence of the point target at the (i,j)-th grid, which is contributed by the n-th measurement element in $\mathcal{D}_m$ (the estimated point target $(\bar{x}_n^{(m)}, \bar{y}_n^{(m)})$), is formulated as

$$P_n^{(m)}(i,j) = \eta e^{-\gamma d_{m,n,i,j}^2},\ \forall m,n,i,j, \tag{4.27}$$

where

$$d_{m,n,i,j} = \sqrt{(\bar{x}_n^{(m)} - x_{i,j}^g)^2 + (\bar{y}_n^{(m)} - y_{i,j}^g)^2} \tag{4.28}$$

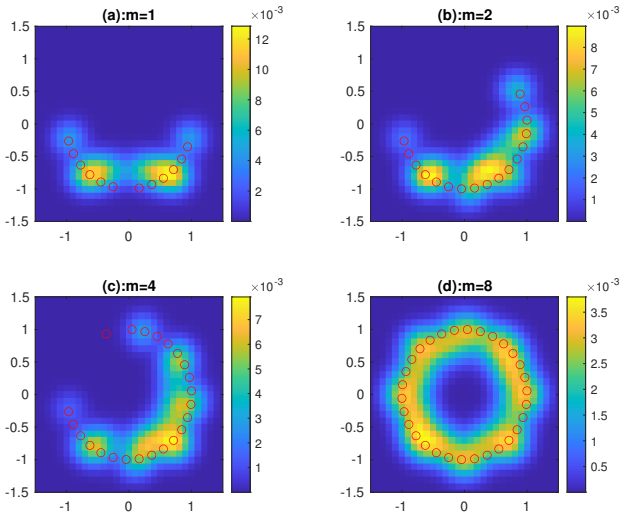

Figure 4.3: The probability density map obtained by our algorithm based on the measurements seen until time slots $m = 1, 2, 4$, and 8. The red small circle in each sub-figure denotes the point targets that can be detected by the UE until the corresponding time slot.

is the range between the (i, j)-th grid and the estimated point target $(\bar{x}_n^{(m)}, \bar{y}_n^{(m)})$, γ is a predefined constant, and η is the normalizing factor such that the sum of the probabilities over all grids is equal to one. Hence, the probability existence of a point target at the (i, j)-th grid, which is contributed by the measurement set $\mathcal{D}_m$, is expressed as

$$P_m(i,j) = \sum_{n=1}^{N_m} P_{m,n}(i,j) = \eta \sum_{n=1}^{N_m} e^{-\gamma d^2_{m,n,i,j}}, \ \forall m, i, j. \tag{4.29}$$

As a result, the probability density map of the target at the (i, j)-th grid based on the measurement sets until the m-th time slot, i.e., $\mathcal{D}_1, \ldots, \mathcal{D}_m$, is given by

$$I_m(i,j) = \sum_{t=1}^{m} P_t(i,j) = \eta \sum_{t=1}^{m} \sum_{n=1}^{N_m} e^{-\gamma d^2_{m,n,i,j}}, \quad m = 1, \ldots, M. \tag{4.30}$$

According to (4.30), we can get the grid-based target reconstruction results based on the measurement sets until any time slot m, $m = 1, \ldots, M$. Note that $I_M(i, j)$'s are leveraged to represent the final reconstructed image of the extended target over all the M time slots.

4.5 Numerical Results

In this section, we evaluate the performance of the proposed two-phase multi-view sensing method. Specifically, we consider a scenario as illustrated in Fig. 4.2, where the UE moves in a counterclockwise direction from $(0,-4)$ m to $(-2\sqrt{2},-2\sqrt{2})$ m over the $M=8$ time slots. The transmit and receive steering vectors of the UE follow the ULA model as shown in (4.1) and (4.2), respectively, where the numbers of transmit and receive antennas are $N_T=N_R=16$, and the antenna spacing is set as $d_A=\frac{\lambda}{2}$. Besides, we set the transmit power as $p=10$ W, the bandwidth as $B=N\Delta f=250$ MHz with $N=256$, and the maximum number of resolvable paths as $L=16$. The extended target is modeled as a circle with the center at $(0,0)$ m and the radius being $r=1$ m, and consists of $K=30$ point targets. At each time slot, only the point targets whose ranges to the UE are less than $\sqrt{15}$ m can be detected with the probability $P_D=0.9$. Moreover, under Phase II, the probability density map is obtained via dividing the 3 m $\times$ 3 m square into 30×30 grids, each of the size 0.1 m $\times$ 0.1 m. In this numerical example, at each time slot, we generate the set of point targets that can be detected, i.e., $\mathcal{K}_m^{\text{det}}$, based on which the channel is generated based on (4.7) and the received signal is generated based on (4.8). Then, we perform the proposed multi-view reconstruction method based on the received signals over all the time slots.

Fig. 4.3 shows the probability density map of the target obtained by our proposed method based on the measurements until time slots $m=1,2,4$, and 8. From Fig. **??** (a), it is observed that the probability density map obtained just based on the measurements at time slot $m=1$ is quite different from the shape of the target. First, many point targets are not detected. Second, with the detected point targets, their positions are subject to some errors. It is seen from Figs. 4.3 (b)-(d) that with observations from more angles, the quality of target reconstruction improves significantly. Particularly, more and more point targets can be detected, and the locations of the detected point targets are more and more accurately estimated. When the measurements of all the $M=8$ time slots are utilized, the probability density map obtained by our method is quite close to the shape of the target.

4.6 Conclusion

In this paper, we considered 6G-based multi-view target reconstruction, where a UE with a radio transceiver moves to different positions at different time slots to emit signals for recovering the shape of an extended target. A two-phase framework was adopted. In Phase I, the range and angle measurements about the extended target towards the position of the UE at each time slot can be obtained via standard OFDM channel estimation technique. In Phase II, the multi-view range and angle values obtained over all the time slots were used to construct the probability density map, on which each grid denotes the probability that a point target exists at this position. Numerical results were provided to show that compared to the single-view counterpart, our proposed multi-view reconstruction method based on 6G signals can recover the shape of the target with significantly improved quality. This verifies the feasibility of leveraging the 6G technique to perform target reconstruction.

Chapter 5

ISAC Prototype

In this chapter, we describe the hardware architecture and the frame structure of the proposed ISAC prototype system. Besides, the experimental results of communication signal based device-free sensing are displayed.

5.1 Hardware Architecture

The architecture of the ISAC-based prototype is shown in Fig. 5.1, which consists of four parts: an arbitrary waveform generator (AWG), an ISAC transmitter, an ISAC receiver, and one oscilloscope. The bandwidth of the optical signals generated by AWG can reach 1 GHz, which enables high data transmission and high range resolution target sensing. The generated optical signals are fed into the transmitter after being converted into electric signals via the photodiode. The ISAC transmitter contains a single RF chain, a mmWave up-and-down frequency converter, and one mmWave phased array. The mmWave phase array adopts a 8×8 UPA analog beamforming architecture. Beamforming can be achieved by controlling the phase shifters in the personal computer (PC). The receiver contains a 1×4 ULA with 4 RF chains. The receive ULA can convert the received RF signal to an intermediate frequency (IF) band and transmit it to the oscilloscope. The IF signals are sampled at the oscilloscope and can be saved in the PC, where we can make programming to perform tasks, such as channel estimation and OFDM constellation display. Noth that the clocks in the transmitter and the receiver are synchronized such that they can transmit/receive the signals at the same time. The specific hardware equipment selection and capabilities are as follows:

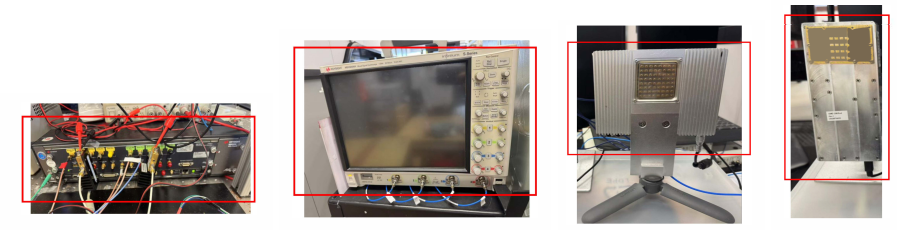

(a) AWG (b) Oscilloscope (c) Transmitter (d) Receiver

Figure 5.1: The components of the ISAC prototype.

- 1) AWG: Keysight AWG-M9502A is fully compatible with the AXIe 1.0 specification. It includes an embedded system module (ESM) that does not take up an instrument slot. This system module performs the chassis management functions contained in the AXIe specification. Additionally, it provides PCI and LAN interfaces for connection to an external computer, external clock and trigger connectors, and Keysight-exclusive, inter-chassis synchronization connectors. The local bus implemented in the M9502A provides the maximum 62 pairs allowed by the AXIe specification.

- 2) mmWave phased array: UME-28TR64 is a 64-elements mmWave Active Phased Array Antenna, with PA, LNA and phase-shifter for each element. The antenna can be controlled by USB port via C DLL command or highspeed digital I/O to perform high-speed 2D beam scanning. The input and output frequency range of UME-28TR64 is 27-29GHz which can be integrated with NI mmWave VST and MTS. It can also be integrated with any IF system with external LO and mixer.

- 3) Receive ULA: The UME-28UDx4 is a four channel version of the UME-28UD, equipped with 4-channel up and down conversion (TDD mode) and 4-channel 12dBi gain antennas, providing higher transmission gain (up to 31dB) and reception gain (up to 33dB). The UME-28UDx4 is a common local oscillator design, with an RF range between channels covering 27.2-29GHz and an intermediate frequency range covering 2-3.8GHz. As a 4-channel up and down converter, the UME-28UDx4 can work with most SDR platforms on the market to expand Sub6G SDR devices to the millimeter wave frequency band. For example, the USRP X410 with a bandwidth of 400MHz and frequency coverage of 1M-7.2GHz can achieve 4-channel millimeter wave frequency band reception/transmission through a single UME-28UDx4.

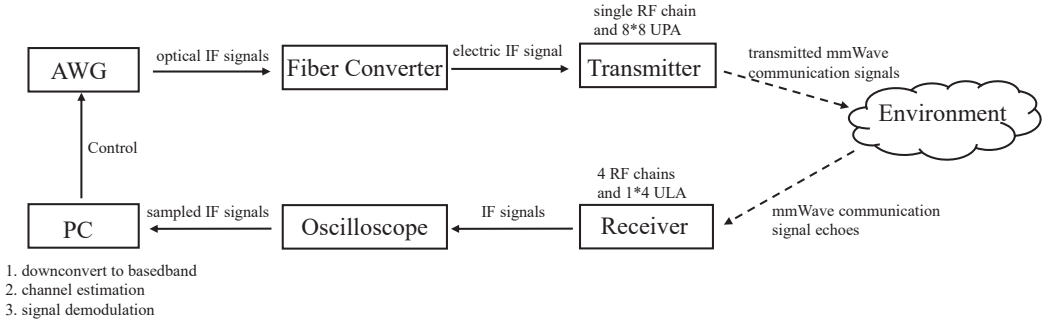

Figure 5.2: The workflow of the ISAC prototype.

5.2 Experimental Setup

5.2.1 Experiment Workflow

The workflow of the ISAC prototype is shown in Fig. 5.2. The transmitted OFDM communication signal is provided by the AWG, where we can design the characteristics of the signals, such as the bandwith, the number of sub-carriers, the sub-carrier spacing, and the frame duration. Note that the generated optical communication signals lie in the IF band. Then, the generated optical signals are transformed into the electric signals, which are fed into the mmWave phase array and upconverted into the RF band. The RF communication signals are sent by the transmitter, and propagates through the environment. The receiver observes the signal echoes reflected by the targets in the environment and downconverts the received signals into the IF band to the oscilloscope. After that, the IF signals will be downconverted to the baseband signal for subsequent signal processing.

5.2.2 Frame Struture

The frame structure of the transmitted signals is illustrated in Fig. 5.3. There are 7 slots in each frame and each slot is composed of 14 OFDM symbols. Specifically, in each subframe, the first 10 OFDM symbols are preamble and the rest symbols are data payload. In each OFDM symbol, the number of sub-carriers and that of CP samples are 1024 and 64, respectively. Besides, the bandwidth of each OFDM symbol is 1 GHz.

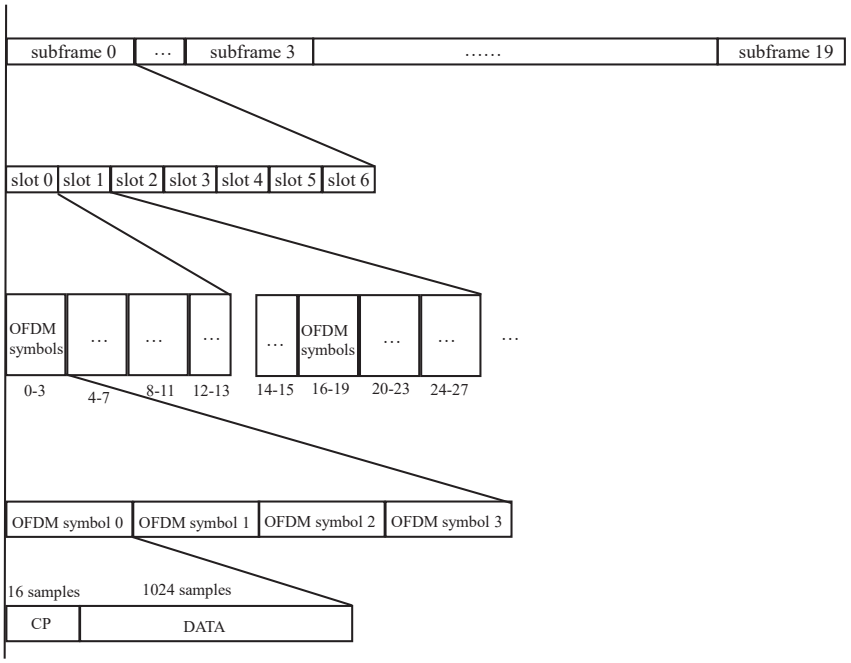

Figure 5.3: The frame structure of the transmitted signals in the ISAC prototype.

5.2.3 Target Localization

The experiment scenario is shown in Fig. 5.4, where the ISAC transmitter and receiver are colocated and synchronized. There are one or multiple targets in the environment. At the beginning, the locations of the targets are unknown. Hence, the transmitter will perform beam scanning and the receiver records the signal echoes sent from different scanning angles. Then, the receiver can estimate the AOD from the transmitter to the targets as the scanning angle with the maximum power of signal echoes. Moroever, the receiver performs the channel estimation based on the receiver signals from the optimal scanning angle. As a result, the range and angle information about the targets can be extracted from the channels, which are utilized to localize the targets.

5.3 Experimental Results

In this section, we give the experiment results for the range and angle estimations of one or multiple targets in the environment.

Figure 5.4: The experiment scenario for target localization via communication signals.

Table 5.1: The comparison between the true and estimated range and angle for one target with known position.

	Ground Truth	Estimation	Error
Target 1	1.607 m, 52°	1.65 m, 53.6°	0.043 m, 1.6°

5.3.1 Known Target Position

In this part, we give the experiment results when the transmitter does not scan the environment. In other words, the target position is known to the transmitter such that the beam is sent towards the targets.

In the first case, there is only one target in the environment, as shown in Fig. 5.5 (a). The distance from the transmitter to the target and that from the target to the receiver are 0.775 m and 0.832 m, respectively, and the AOA of the target with respect to the receiver is 52°. Based on the received signals, the range and angle can be estimated as discussed in Chapter 4. The experiment result is shown in Fig. 5.6, where the sum distance from the transmitter to the target and back to the receiver is estimated as 1.65 m and the AOA is estimated as 53.6°. The above results are summarized in Table. 5.1.

In the second case, there are two targets in the environment, as shown in Fig. 5.5 (b). The distance from the transmitter to the first target and that from the first target to the receiver are 0.500 m and 0.571 m, respectively, and the AOA of the first target is 44°. The distance from the transmitter to the second target and that from the second target to the receiver are 1.189 m

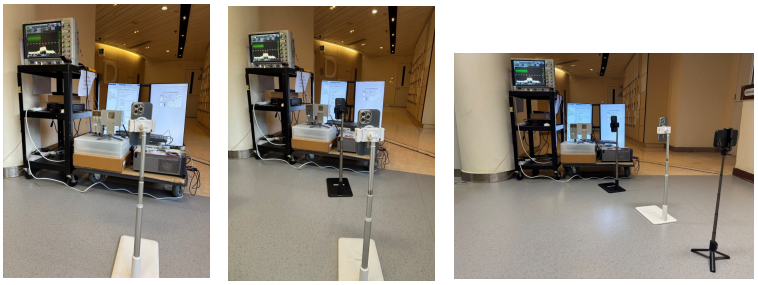

(a) One target (b) Two targets (c) Three targets

Figure 5.5: The experiment scenario with one or more targets and known target position.

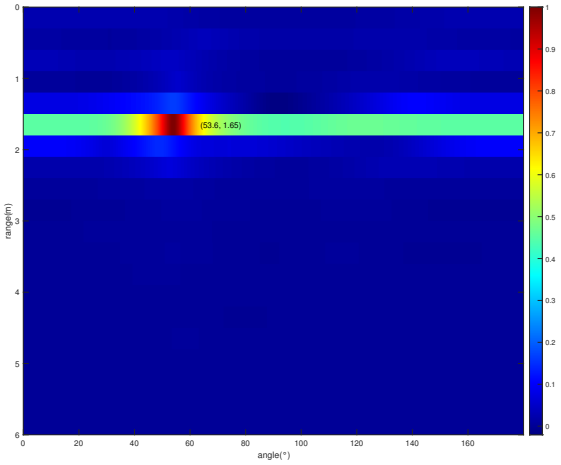

Figure 5.6: The experiment results with one target.

Table 5.2: The comparison between the true and estimated range and angle for two targets with known position.

	Ground Truth	Estimation	Error
Target 1	1.071 m, 44°	1.05 m, 41.8°	0.021 m, 2.2°
Target 2	2.437 m, 53°	2.55 m, 52.9°	0.113 m, 0.1°

and 1.248 m, respectively, and the AOA of the second target is 53°. Similarly, the experiment result is shown in Fig. 5.7. The sum distance and the angle for the first target are estimated as 1.05 m and 41.8°, respectively. Besides, the sum distance and the angle for the second target are estimated as 2.55 m and 52.9°, respectively. The above results are summarized in Table. 5.2.

In the third case, there are three targets in the environment, as shown in Fig. 5.5 (c). The distance from the transmitter to the first target and that from the first target to the receiver are 0.500 m and 0.571 m, respectively, and the AOA of the first target is 44°. The distance

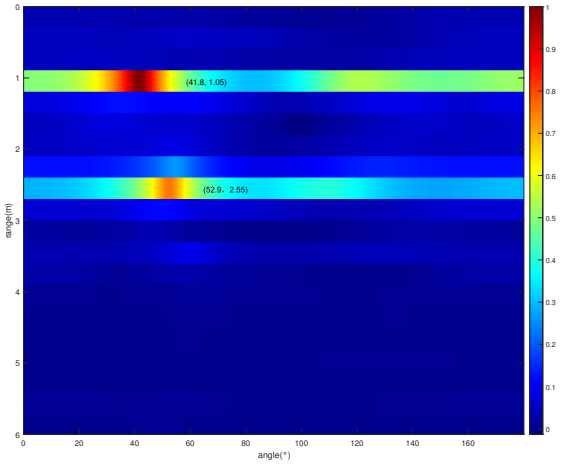

Figure 5.7: The experiment results with two targets.

Table 5.3: The comparison between the true and estimated range and angle for three targets with known position.

	Ground Truth	Estimation	Error
Target 1	1.071 m, 44°	1.05 m, 41.8°	0.021 m, 2.2°
Target 2	2.437 m, 53°	2.55 m, 52.9°	0.113 m, 0.1°
Target 3	3.471 m, 62°	3.45 m, 58.5°	0.021 m, 3.5°

from the transmitter to the second target and that from the second target to the receiver are 1.189 m and 1.248 m, respectively, and the AOA of the second target is 53°. The distance from the transmitter to the third target and that from the third target to the receiver are 1.708 m and 1.763 m, respectively, and the angle of arrival for the first target is 62°. Similarly, the experiment result is shown in Fig. 5.8. The sum distance and the angle for the first target are estimated as 1.05 m and 41.8°, respectively. The sum distance and the angle for the second target are estimated as 2.55 m and 52.9°, respectively. The distance and the angle for the third target are estimated as 3.45 m and 58.5°, respectively. The above results are summarized in Table. 5.3.

5.3.2 Unknown Target Position

In this part, we give the experiment results when the transmitter needs to scan the environment, since the target position is unknown to the transmitter.

In the first case, there are two targets in the environment, as shown in Fig. 5.9 (a). The distance from the transmitter to the first target and that from the first target to the receiver are

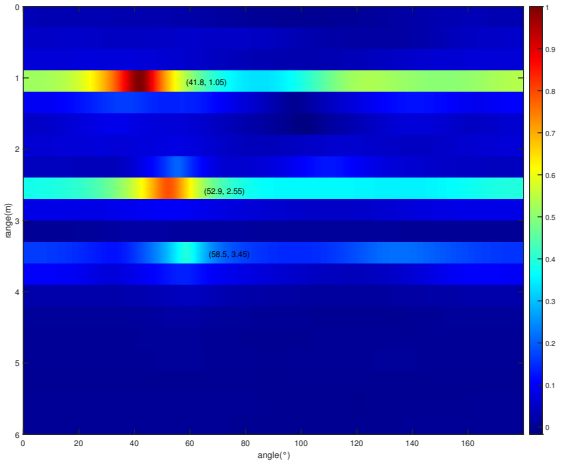

Figure 5.8: The experiment results with three targets.

Table 5.4: The comparison between the true and estimated range and angle for three targets with unknown position.

	Ground Truth	Estimation	Error
Target 1	1.343 m, 103°	1.35 m, 104.1°	0.007 m, 1.1°
Target 2	1.071 m, 44°	1.05 m, 40.5°	0.021 m, 3.5°

0.698m and 0.645 m, respectively, and the angle of arrival for the first target is 103°. The distance from the transmitter to the second target and that from the second target to the receiver are 0.500 m and 0.571 m, respectively, and the angle of arrival for the second target is 44°.

Because the locations of the targets are unknown, the transmitter will adjust the scanning angles from $-30°$ to 30°. The receiver will calculate the received signal strength (RSS) from different scanning angles to measure the angle-of-departure (AOD) of the target with respect to the transmitter. As shown in Fig. 5.10, we can see that there are targets in the environment when the scanning angle is $-20°$ and 27°. Then, based on the received signals when the scanning angle of the transmitted signal is $-20°$, the range and angle estimation result for the first target is shown in Fig. 5.11. The sum distance and the angle for the first target are estimated as 1.35 m and 104.1°, respectively. On the other side, when the scanning angle of the transmitted signal is 27°, the range and angle estimation result for the second target is shown in Fig. 5.12. The sum distance and the angle for the second target are estimated as 1.05 m and 40.5°, respectively. The above results are summarized in Table. 5.4.

In the second case, there are three targets in the environment, as shown in Fig. 5.9 (b). The distance from the transmitter to the first target and that from the first target to the receiver

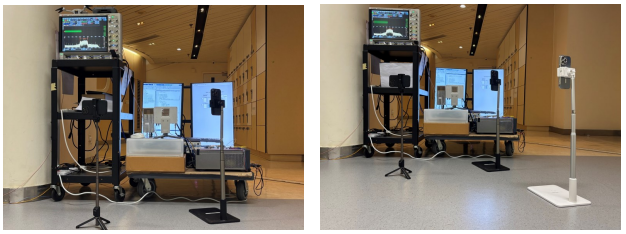

(a) Two targets (b) Three targets

Figure 5.9: The experiment scenario with one or more targets and unknown target position.

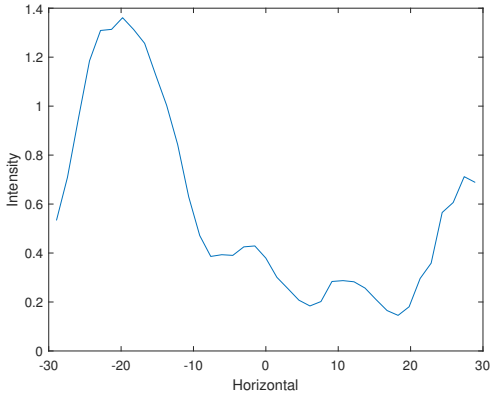

Figure 5.10: RSS over different scanning angles for two targets.

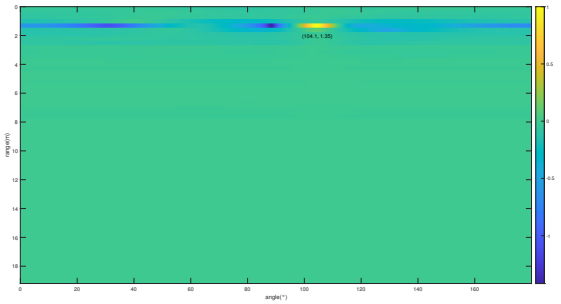

Figure 5.11: The range and angle estimations when the scanning angle is $-20°$.

are 0.698m and 0.645 m, respectively, and the angle of arrival for the first target is 103°. The distance from the transmitter to second target and that from the second target to the receiver are 0.500 m and 0.571 m, respectively, and the angle of arrival for the second target is 44°. The distance from the transmitter to the third target and and that from the third target to the receiver are 1.189 m and 1.248 m, respectively, abd the angle of arrival for the third target is 53°.

As shown in Fig. 5.13, we can see that there are targets in the environment when the scanning angle is $-20°$ and 27° as well. Then, based on the received signals when the scanning

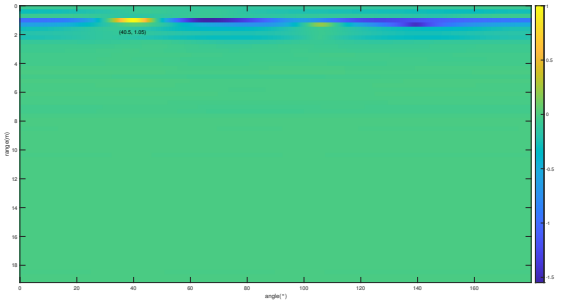

Figure 5.12: The range and angle estimations when the scanning angle is 27°.

Table 5.5: The comparison between the true and estimated range and angle for three targets with unknown position.

	Ground Truth	Estimation	Error
Target 1	1.343 m, 103°	1.35 m, 104.1°	0.007 m, 1.1°
Target 2	1.071 m, 44°	1.05 m, 40.5°	0.021 m, 3.5°
Target 3	2.437 m, 53°	2.55 m, 52.0°	0.113 m, 1.0°

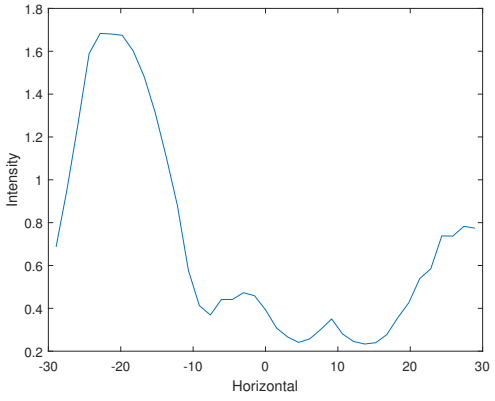

Figure 5.13: RSS over different scanning angles for three targets.

angle of the transmitted signal is $-20°$, the range and angle estimation result for the first target is shown in Fig. 5.14. The sum distance and the angle for the first target are estimated as 1.35 m and 105.7°, respectively. On the other side, when the scanning angle of the transmitted signal is 27°, the range and angle estimation results for the second target and the third target are shown in Fig. 5.15. The sum distance and the angle for the second target are estimated as 1.05 m and 40.2°, respectively. The sum distance and the angle for the third target are estimated as 2.55 m and 52.0°, respectively. The above results are summarized in Table. 5.5.

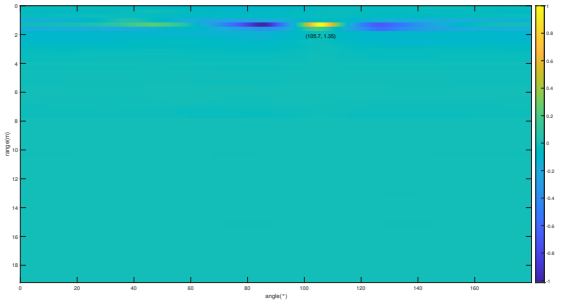

Figure 5.14: The range and angle estimations when the scanning angle is $-20°$.

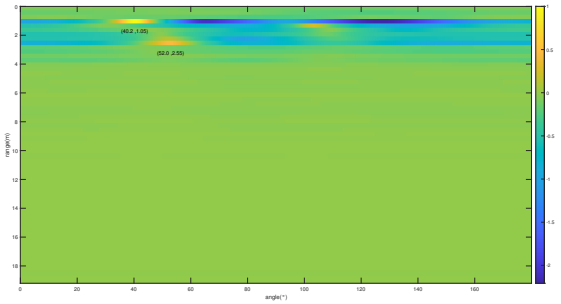

Figure 5.15: The range and angle estimations when the scanning angle is $27°$.

5.4 Conclusion

In this chapter, the development and evaluation of an ISAC prototype system designed for 6G technology was presented. In detail, the hardware architecture, frame structure, and experimental results of the prototype were shown. The system utilized components such as an AWG to generate OFDM signal in IF band, an mmWave phased array for transmitting signals and beam scanning, and a receiver with multiple RF chains for receiving signal echoes. Then, by performing standard OFDM channel estimation with signal echoes, the range and angle information about passive targets can be obtained. The experimental results showed the range and angle estimation error is small, which demonstrates the feasibility of ISAC for high data transmission and precise target sensing via mmWave OFDM communication signals.

Chapter 6

Conclusion

6.1 Conclusion

In this thesis, we proposed to realize device-free sensing functions via communication signals such that ubiquitous target sensing can be provided in the future 6G network. In Chapter 2, we considered device-free sensing in an OFDM cellular network for passive point target localization via communication signals. A novel two-phase sensing framework was adopted. In Phase I, we estimated the ranges between the BSs and the targets. In Phase II, we showed that the ghost target is not the bottleneck of device-free sensing in the case with perfect range estimation. Moreover, in the case of imperfect range estimation in Phase I, we proposed a maximum-likelihood (ML) based algorithm to match each range with the right target, and then estimated the location of each target based on its matched ranges to different BSs. As an extension of the case in Chapter 2, networked device-free sensing in an OFDM cellular system with multipath environment was investigated in Chapter 3. Similarly, a two-phase localization protocol was considered. In Phase I, we tackled the issue of synchronization among different BSs and estimated the ranges from one BS to the targets and to another BS (or the same BS). In Phase II, we jointly tackled the issues of NLOS mitigation, LOS identification, and data association. Specifically, an efficient algorithm was proposed to localize multiple passive targets by decoupling LOS identification from NLOS mitigation and data association. Chapter 4 studied multi-view based extended target three-dimensional (3D) reconstruction via communication signals. A mobile UE acquired the multiple single-view textureless images of the extended target by emitting OFDM communication signals to sense the target from different angles. Then, all single-view textureless images of the target were fused to reconstruct the target. In detail,

the measurement set obtained at each time slot was converted into a local probability density map of the target. Then, all the local probability density maps were added to form the global probability density map of the target, which is leveraged to represent the target reconstruction result. In Chapter 5, some practical experiments about communication signal based monostatic sensing were performed. The mmWave OFDM communication signals were leveraged by the transceiver to estimate the locations of the targets in the environment. The experimental results showed that the range and angle information about the targets can be extracted from the signal echoes. Through the simulation results, we can conclude that the communication signal based ISAC can achieve high performance of point target localization and extended target reconstruction in the 6G network. Thus, it is shown that the communication signal based target sensing is feasible in the future 6G network, which can provide a better quality of service to the user services.

6.2 Outlook

There are several interesting research directions for future ISAC-assisted device-free sensing. One particularly interesting direction is target recognition and tracking through communication signals, where the vital motion of the target needs to be captured and processed but requires a much higher range/angle/velocity resolution. Since the mapping between the target parameters and the channel in the environment is hard to model and quite complicated, artificial intelligence (AI) or machine learning (ML) appears as one promising solution, which is inherently model-free and has achieved good performance in some communication applications, such as channel estimation. Therefore, it motivates us to exploit ML-based methods for passive target sensing. Furthermore, reconfigurable intelligent surfaces (RIS) can control the propagation environment, which is also helpful for target sensing especially when the direct link between the target and the transmitter/receiver is blocked. Besides, RIS can help obtain better angle information of the target due to its large number of reflection elements, especially when the number of RF chains at the AP is not enough to acquire the angle information directly. Hence, it is desired to explore RIS-assisted target localization or target reconstruction.

Chapter 7

Appendix

7.1 Appendix A

Define $\mathcal{E}$ as the event that ghost target exists, i.e., there exists $\mathcal{X}^{\mathrm{G}} \neq \mathcal{X}$ satisfying (2.20) in Definition 2.1. Moreover, when event $\mathcal{E}$ occurs, define $\mathcal{E}_i$ as the event that $K-i$ true targets and $K-i$ ghost targets share the same coordinates, while the other i ghost targets and i true targets do not share any common coordinate, i.e., $|\mathcal{X}^{\mathrm{G}} \bigcap \mathcal{X}| = K-i$, $i = 2, \ldots, K$.[1] We then have $\mathcal{E} = \bigcup_{i=2}^{K} \mathcal{E}_i$. Next, when event $\mathcal{E}_i$ occurs, based on which i true targets possess different coordinates with the ghost targets, there are $\binom{K}{i}$ sub-events. Define $\mathcal{E}_i^{(r)}$ as the r-th sub-event, $r = 1, \ldots, \binom{K}{i}$. Then, it follows that $\mathcal{E}_i = \bigcup_{r=1}^{\binom{K}{i}} \mathcal{E}_i^{(r)}$, $i = 2, \ldots, K$. To summarize, we have

$$\Pr(\mathcal{E}) = \Pr\left(\bigcup_{i=2}^{K} \bigcup_{r=1}^{\binom{K}{i}} \mathcal{E}_i^{(r)} \right) \leq \sum_{i=2}^{K} \sum_{r=1}^{\binom{K}{i}} \Pr(\mathcal{E}_i^{(r)}), \tag{7.1}$$

where $\Pr(\mathcal{A})$ is the probability that event $\mathcal{A}$ happens.

Without loss of generality, let us define sub-event 1, i.e., $\mathcal{E}_i^{(1)}$, as the event that each of the coordinates of true targets $1, \ldots, i$ is not the coordinate of any ghost target, while each of the coordinates of true targets $i+1, \ldots, K$ is the coordinate of some ghost target. Note that error event $\mathcal{E}_i^{(1)}$ is equivalent to the event that in a system merely consisting of true target 1 to true target i (without the other $K-i$ true targets), there exist i ghost targets, whose coordinates are all different from the coordinates of the i true targets. In the following, we show that

[1] If $K-1$ true targets and $K-1$ ghost targets share the same coordinates, the remaining true target and ghost target will also have the same coordinate since three BSs can uniquely locate one target. As a result, under event $\mathcal{E}$, $i = 1$ will never happen.

$$\begin{aligned}\Pr(\mathcal{E}_i^{(1)}) &= \int_{\{x_1,y_1,\ldots,x_i,y_i\}\in\mathcal{B}_i^{(1)}} p(x_1,y_1,\ldots,x_i,y_i)dx_1dy_1\cdots dx_idy_i \\ &= \int_{\{x_1,y_1,\ldots,x_{i-1},y_{i-1}\}\in\tilde{\mathcal{B}}_i^{(1)}} \left(\int_{\{x_i,y_i\}\in\hat{\mathcal{B}}_i^{(1)}(x_1,y_1,\ldots,x_{i-1},y_{i-1})} p(x_i,y_i|x_1,y_1,\ldots,x_{i-1},y_{i-1})dx_idy_i\right) \\ &\qquad p(x_1,y_1,\ldots,x_{i-1},y_{i-1})dx_1dy_1\cdots dx_{i-1}dy_{i-1} \qquad (7.47) \\ &= \int_{\{x_1,y_1,\ldots,x_{i-1},y_{i-1}\}\in\tilde{\mathcal{B}}_i^{(1)}} \left(\int_{\{x_i,y_i\}\in\hat{\mathcal{B}}_i^{(1)}(x_1,y_1,\ldots,x_{i-1},y_{i-1})} p(x_i,y_i)dx_idy_i\right) \\ &\qquad p(x_1,y_1,\ldots,x_{i-1},y_{i-1})dx_1dy_1\cdots dx_{i-1}dy_{i-1}, \qquad (7.48)\end{aligned}$$

$\Pr(\mathcal{E}_i^{(1)}) = 0$, $i = 2,\ldots,K$. The similar approach can also be used to show that $\Pr(\mathcal{E}_i^{(r)}) = 0$, $\forall r \neq 1$.

Define $\mathcal{B}_i^{(1)}$ as the set of $(x_1,y_1,\ldots,x_i,y_i)$ such that if $(x_1,y_1,\ldots,x_i,y_i) \in \mathcal{B}_i^{(1)}$, the coordinates of the i true targets with coordinates $(x_1,y_1),\ldots,(x_i,y_i)$ can lead to i ghost targets with coordinates $(x_1^{\mathrm{G}},y_1^{\mathrm{G}}),\ldots,(x_i^{\mathrm{G}},y_i^{\mathrm{G}})$, where

$$(x_q^{\mathrm{G}},y_q^{\mathrm{G}}) \neq (x_k,y_k),\ k,q = 1,\ldots,i. \qquad (7.46)$$

Moreover, define $p(\cdot)$ as the probability density function (PDF). Then, we have (7.47) and (7.48), where $\tilde{\mathcal{B}}_i^{(1)}$ is the set of $(x_1,y_1,\ldots,x_{i-1},y_{i-1})$ such that if $(x_1,y_1,\ldots,x_{i-1},y_{i-1}) \in \tilde{\mathcal{B}}_i^{(1)}$, there exists some (x_i,y_i) to satisfy $(x_1,y_1,\ldots,x_i,y_i) \in \mathcal{B}_i^{(1)}$, and $\hat{\mathcal{B}}_i^{(1)}(x_1,y_1,\ldots,x_{i-1},y_{i-1})$ is the set of (x_i,y_i) such that given any $(x_1,y_1,\ldots,x_{i-1},y_{i-1}) \in \tilde{\mathcal{B}}_i^{(1)}$, if $(x_i,y_i) \in \hat{\mathcal{B}}_i^{(1)}(x_1,y_1,\ldots,x_{i-1},y_{i-1})$, then the coordinates of the i true targets $(x_1,y_1),\ldots,(x_i,y_i)$ can lead to i ghost targets with coordinates $(x_1^{\mathrm{G}},y_1^{\mathrm{G}}),\ldots,(x_i^{\mathrm{G}},y_i^{\mathrm{G}})$ satisfying (7.46). In the above, (7.48) holds because all the targets are independently located in the network.

In the following, we prove that given any $\{x_1,y_1,\ldots,x_{i-1},y_{i-1}\} \in \tilde{\mathcal{B}}_i^{(1)}$, there are a finite number of elements in the set $\hat{\mathcal{B}}_i^{(1)}(x_1,y_1,\ldots,x_{i-1},y_{i-1})$. If this is true, then when (x_i,y_i) is uniformly distributed in a continuous two-dimension region consisting of an infinite number of points, the probability that (x_i,y_i) falls on the finite number of points in $\hat{\mathcal{B}}_i^{(1)}(x_1,y_1,\ldots,x_{i-1},y_{i-1})$ is zero, i.e., $\int_{\{x_i,y_i\}\in\hat{\mathcal{B}}_i^{(1)}(x_1,y_1,\ldots,x_{i-1},y_{i-1})} p(x_i,y_i)dx_idy_i = 0$, $\forall\{x_1,y_1,\ldots,x_{i-1},y_{i-1}\} \in \tilde{\mathcal{B}}_i^{(1)}$. This will indicate that $\Pr(\mathcal{E}_i^{(1)}) = 0$ according to (7.48) because $\int_{\{x_1,y_1,\ldots,x_{i-1},y_{i-1}\}\in\tilde{\mathcal{B}}_i^{(1)}} p(x_1,y_1,\ldots,x_{i-1},y_{i-1})\,dx_1dy_1\cdots dx_{i-1}dy_{i-1}$ is finite when target 1 to target $i-1$ are located uniformly in the network.

Define

$$\mathcal{D}_m^{(i)} = \{d_{m,1}, \ldots, d_{m,i}\}, \quad \forall m, \tag{7.49}$$

as the set consisting of the values of distance between BS m and target 1 to target i, and $\mathcal{D}_m^{(i)}(g)$ as the g-th largest element in $\mathcal{D}_m^{(i)}$. Moreover, define $g_{m,k}^{(i)}$ such that $d_{m,k} = \mathcal{D}_m^{(i)}(g_{m,k}^{(i)})$, $k = 1, \ldots, i$, $m = 1, \ldots, M$. Given any $\{x_1, y_1, \ldots, x_{i-1}, y_{i-1}\} \in \tilde{\mathcal{B}}_i^{(1)}$, $i-1$ elements in $\mathcal{D}_m^{(i)}$ are fixed, $\forall m$. Define the range set to localize target i as

$$\mathcal{T}_i = \{\mathcal{D}_1^{(i)}(g_{1,i}^{(i)}), \ldots, \mathcal{D}_M^{(i)}(g_{M,i}^{(i)})\}, \tag{7.50}$$

which consists of the remaining one variable range of each BS. In the following, we study all the possibilities of $\mathcal{T}_i$ such that with (x_i, y_i) localized by $\mathcal{T}_i$ and the given $\{x_1, y_1, \ldots, x_{i-1}, y_{i-1}\} \in \tilde{\mathcal{B}}_i^{(1)}$, i ghost targets with coordinates $(x_1^{\mathrm{G}}, y_1^{\mathrm{G}}), \ldots, (x_i^{\mathrm{G}}, y_i^{\mathrm{G}})$ satisfying (7.46) exist.

Consider a matching solution $\{\bar{g}_{m,1}^{(i)}, \ldots, \bar{g}_{m,i}^{(i)}\}_{m=1}^M$ that is different from the correct matching solution $\{g_{m,1}^{(i)}, \ldots, g_{m,i}^{(i)}\}_{m=1}^M$ and satisfies $\{\bar{g}_{m,1}^{(i)}, \ldots, \bar{g}_{m,i}^{(i)}\} = \{1, \ldots, i\}$, $\forall m$. Note that there are $(i!)^M - 1$ matching solutions satisfying the above conditions. According to Definition 2.1, a matching solution can lead to i ghost targets if and only if for each $q \in \{1, \ldots, i\}$, there exists a solution $(x_q^{\mathrm{G}}, y_q^{\mathrm{G}})$ to the following M equations:

$$\sqrt{(a_m - x_q^{\mathrm{G}})^2 + (b_m - y_q^{\mathrm{G}})^2} = \mathcal{D}_m^{(i)}(\bar{g}_{m,q}^{(i)}), \ \forall m \in \mathcal{M}. \tag{7.51}$$

Note that if we can find a $q \in \{1, \ldots, i\}$ such that $\mathcal{D}_m^{(i)}(\bar{g}_{m,q}^{(i)}) = \mathcal{D}_m^{(i)}(g_{m,i}^{(i)})$ holds for at least three values of m, then it indicates that $(x_q^{\mathrm{G}}, y_q^{\mathrm{G}}) = (x_i, y_i)$, because true target i and ghost target q have the same distance values to three BSs, and three BSs not on the same line can localize a unique target. This violates the definition of $\mathcal{B}_i^{(1)}$ where all true targets and ghost targets have different coordinates, i.e., (7.46). As a result, for any $q \in \{1, \ldots, i\}$, $\mathcal{D}_m^{(i)}(\bar{g}_{m,q}^{(i)}) = \mathcal{D}_m^{(i)}(g_{m,i}^{(i)})$ holds for at most two values of m, denoted by $m_{q,1}$ and/or $m_{q,2}$, and if $m \in \mathcal{M}_q = \{m | m \in \mathcal{M}, m \neq m_{q,1}, m \neq m_{q,2}\}$, we have $\mathcal{D}_m^{(i)}(\bar{g}_{m,q}^{(i)}) = \mathcal{D}_m^{(i)}(g_{m,k}^{(i)})$ for some $k \in \{1, \ldots, i-1\}$, where $\mathcal{D}_m^{(i)}(g_{m,k}^{(i)})$'s are known given $\{x_1, y_1, \ldots, x_{i-1}, y_{i-1}\} \in \tilde{\mathcal{B}}_i^{(1)}$. Note that if $M \geq 4$, $|\mathcal{M}_q| \geq 2$, $\forall q$. As a result, for any q, the following $|\mathcal{M}_q| \geq 2$ equations with known $\mathcal{D}_m^{(i)}(\bar{g}_{m,q}^{(i)})$'s have at most two possible solutions for the coordinate of ghost target q:

$$\sqrt{(a_m - x_q^{\mathrm{G}})^2 + (b_m - y_q^{\mathrm{G}})^2} = \mathcal{D}_m^{(i)}(\bar{g}_{m,q}^{(i)}), \ \forall m \in \mathcal{M}_q. \tag{7.52}$$

Then, for any q, there are at most two possible values of $\mathcal{D}^{(i)}_{m_{q,1}}(g^{(i)}_{m_{q,1},i}) = \mathcal{D}^{(i)}_{m_{q,1}}(\bar{g}^{(i)}_{m_{q,1},q})$ and at most two possible values of $\mathcal{D}^{(i)}_{m_{q,2}}(g^{(i)}_{m_{q,2},i}) = \mathcal{D}^{(i)}_{m_{q,2}}(\bar{g}^{(i)}_{m_{q,2},q})$. Note that $\bigcup_{q=1}^{i}\{m_{q,1}, m_{q,2}\} = \mathcal{M}$, since if ghost target exists, for each m, there must exist some q such that $\mathcal{D}^{(i)}_{m}(\bar{g}^{(i)}_{m,q}) = \mathcal{D}^{(i)}_{m}(g^{(i)}_{m,i})$ according to Definition 2.1. As a result, given each matching solution $\{\bar{g}^{(i)}_{m,1}, \ldots, \bar{g}^{(i)}_{m,i}\}_{m=1}^{M}$, $\mathcal{D}^{(i)}_{m}(g^{(i)}_{m,i})$ has at most two possible values, $\forall m$, and there are thus at most 2^M possibilities for the set $\mathcal{T}_i$ defined in (7.50). Recall that there are $(i!)^M - 1$ feasible matching solutions of $\{\bar{g}^{(i)}_{m,1}, \ldots, \bar{g}^{(i)}_{m,i}\}_{m=1}^{M}$. Therefore, given any $\{x_1, y_1, \ldots, x_{i-1}, y_{i-1}\} \in \tilde{\mathcal{B}}^{(1)}_i$, we have

$$|\hat{\mathcal{B}}^{(1)}_i(x_1, y_1, \ldots, x_{i-1}, y_{i-1})| \leq ((i!)^M - 1)2^M. \tag{7.53}$$

To summarize, when $M \geq 4$, given any $\{x_1, y_1, \ldots, x_{i-1}, y_{i-1}\} \in \tilde{\mathcal{B}}^{(1)}_i$, the number of elements in the set $\hat{\mathcal{B}}^{(1)}_i(x_1, y_1, \ldots, x_{i-1}, y_{i-1})$ is finite. As stated in the above, this indicates that $\Pr(\mathcal{E}^{(1)}_i) = 0$ in (7.48). Similarly, we can prove that $\Pr(\mathcal{E}^{(r)}_i) = 0$, $\forall r \neq 1$. According to (7.1), it follows that $\Pr(\mathcal{E}) = 0$. Theorem 2.3 is thus proved.

7.2 Appendix B

First, we show that two necessary conditions for the existence of ghost targets are as follows

$$\bigcup_{q\in\mathcal{K}} \mathcal{S}_{k,q} = \mathcal{M}, \quad \forall k \in \mathcal{K}, \tag{7.54}$$

$$\bigcup_{k\in\mathcal{K}} \mathcal{S}_{k,q} = \mathcal{M}, \quad \forall q \in \mathcal{K}. \tag{7.55}$$

Specifically, given some $\mathcal{X}^{\mathrm{G}} \neq \mathcal{X}$, suppose that (7.54) does not hold. In this case, suppose that there exist $\bar{m} \in \mathcal{M}$ and $\bar{k} \in \mathcal{K}$ such that $\bar{m} \notin \bigcup_{q\in\mathcal{K}} \mathcal{S}_{\bar{k},q}$. This indicates that $d_{\bar{m},\bar{k}}$ is not in the set $\mathcal{D}^{\mathrm{G}}_{\bar{m}}$. In other words, $\mathcal{D}_{\bar{m}} \neq \mathcal{D}^{\mathrm{G}}_{\bar{m}}$. As a result, for any $\mathcal{X}^{\mathrm{G}} \neq \mathcal{X}$ such that (7.54) does not hold, it cannot be the set of coordinates of ghost targets according to Definition 2.1. Similarly, for any $\mathcal{X}^{\mathrm{G}} \neq \mathcal{X}$ such that (7.55) does not hold, it cannot be the set of coordinates of ghost targets. To summarize, if $\mathcal{X}^{\mathrm{G}} \neq \mathcal{X}$ is the set of coordinates of ghost targets, then (7.54) and (7.55) should hold.

In the following, we prove Lemma 2.4 with $M = 4$ and $K = 2$ based on the above two necessary conditions. First, consider the case when $\mathcal{X}^{\mathrm{G}} \neq \mathcal{X}$ satisfies that $\mathcal{X}^{\mathrm{C}}$ defined in (2.25)

is not an empty set, i.e., $(x_k, y_k) = (x_q^{\mathrm{G}}, y_q^{\mathrm{G}})$ for some $k, q \in \mathcal{K}$. We show by contradictory that in this case, $\mathcal{X}^{\mathrm{G}}$ cannot be the coordinates of ghost targets. Suppose that $\mathcal{X}^{\mathrm{G}}$ consists of the coordinates of ghost targets. Then, conditions (7.54) and (7.55) indicate that $d_{m,\bar{k}} = d_{m,\bar{q}}$, $m = 1,2,3,4$, where $\bar{k} \in \mathcal{K} \neq k$ and $\bar{q} \in \mathcal{K} \neq q$. Since any 3 BSs are not on the same line, $d_{m,\bar{k}} = d_{m,\bar{q}}$, $m = 1,2,3,4$, indicates that $(x_{\bar{k}}, y_{\bar{k}}) = (x_{\bar{q}}^{\mathrm{G}}, y_{\bar{q}}^{\mathrm{G}})$. Together with $(x_k, y_k) = (x_q^{\mathrm{G}}, y_q^{\mathrm{G}})$, this contradicts to the fact that $\mathcal{X}^{\mathrm{G}} \neq \mathcal{X}$. As a result, if $\mathcal{X}^{\mathrm{G}} \neq \mathcal{X}$ satisfies that $\mathcal{S}_{k,q} = \mathcal{M}$ for some k and q, then $\mathcal{X}^{\mathrm{G}}$ cannot be the coordinates of ghost targets.

Next, consider the case when $\mathcal{X}^{\mathrm{G}} \neq \mathcal{X}$ satisfies that $\mathcal{X}^{\mathrm{C}}$ defined in (2.25) is an empty set. In the following, we show the necessary conditions for the existence of ghost targets in this case. Suppose that $\mathcal{X}^{\mathrm{G}}$ consists of the coordinates of ghost targets. Then, conditions (7.54) and (7.55) indicate that

$$\sum_{q=1}^{2} |\mathcal{S}_{k,q}| = 4, \quad \forall k \in \mathcal{K}, \tag{7.56}$$

$$\sum_{k=1}^{2} |\mathcal{S}_{k,q}| = 4. \quad \forall q \in \mathcal{K}. \tag{7.57}$$

Because any 3 BSs are not on the same line and $\mathcal{X}^{\mathrm{C}}$ defined in (2.25) is an empty set, we have $|\mathcal{S}_{k,q}| \leq 2$, $\forall k, q$. To satisfy (7.56) and (7.57), we must have $|\mathcal{S}_{k,q}| = 2$, $\mathcal{S}_{k,1} \bigcap \mathcal{S}_{k,2} = \emptyset$, and $\mathcal{S}_{1,q} \bigcap \mathcal{S}_{2,q} = \emptyset$, $\forall k, q$. Then, it follows that $\mathcal{S}_{1,1} = \mathcal{S}_{2,2} = \{1,2,3,4\}/\mathcal{S}_{1,2}$ and $\mathcal{S}_{1,2} = \mathcal{S}_{2,1} = \{1,2,3,4\}/\mathcal{S}_{1,1}$. $\mathcal{S}_{1,1} = \mathcal{S}_{2,2}$ and $|\mathcal{S}_{1,1}| = |\mathcal{S}_{2,2}| = 2$ require that the line connecting the two BSs in $\mathcal{S}_{1,1} = \mathcal{S}_{2,2}$ is the perpendicular bisector of the line segment connecting (x_1, y_1) and $(x_1^{\mathrm{G}}, y_1^{\mathrm{G}})$ as well as the line segment connecting (x_2, y_2) and $(x_2^{\mathrm{G}}, y_2^{\mathrm{G}})$. Similarly, we can show based on $\mathcal{S}_{1,2} = \mathcal{S}_{2,1}$ and $|\mathcal{S}_{1,2}| = |\mathcal{S}_{2,1}| = 2$ that the line connecting the two BSs in $\mathcal{S}_{1,2} = \mathcal{S}_{2,1}$ is the perpendicular bisector of the line segment connecting (x_1, y_1) and $(x_2^{\mathrm{G}}, y_2^{\mathrm{G}})$ as well as the line segment connecting (x_2, y_2) and $(x_1^{\mathrm{G}}, y_1^{\mathrm{G}})$. The above shows that the necessary conditions for the existence of the ghost targets are as follows: 1. the line connecting the BSs in $\mathcal{S}_{1,1} = \mathcal{S}_{2,2}$ is perpendicular to that connecting the BSs in $\mathcal{S}_{1,2} = \mathcal{S}_{2,1}$; and 2. the line segment connecting (x_1, y_1) and $(x_1^{\mathrm{G}}, y_1^{\mathrm{G}})$, that connecting (x_2, y_2) and $(x_2^{\mathrm{G}}, y_2^{\mathrm{G}})$, that connecting (x_1, y_1) and $(x_2^{\mathrm{G}}, y_2^{\mathrm{G}})$, and that connecting (x_2, y_2) and $(x_1^{\mathrm{G}}, y_1^{\mathrm{G}})$ form a rectangle. As a result, if the first necessary condition does not hold, there never exist the ghost targets. On the other hand, if the first necessary condition holds, we show that the probability that the second necessary condition holds is zero when the two targets are located uniformly in the network. Let (x_0, y_0) denote the intersection point of the two perpendicular lines that connect the BSs in $\mathcal{S}_{1,1} = \mathcal{S}_{2,2}$ and connect the BSs in $\mathcal{S}_{1,2} = \mathcal{S}_{2,1}$. If the second necessary condition is true, then we have $x_1 + x_2 = 2x_0$ and

$y_1 + y_2 = 2y_0$, which define a two-dimension plane in the four-dimension space for x_1, x_2, y_2, y_2. If the two targets are located uniformly in the network, $x_1 + x_2 = 2x_0$ and $y_1 + y_2 = 2y_0$ occur with probability zero. As a result, if the first necessary condition is true, there exist no ghost targets almost surely if the targets are located uniformly in the network.

By combining the cases when $\mathcal{X}^{\mathrm{C}}$ is not an empty set and is an empty set, Lemma 2.4 is thus proved.

Reference

[1] H. Deng and B. Himed, "Interference mitigation processing for spectrum-sharing between radar and wireless communications systems," *IEEE Trans. Aerosp. Electron. Syst.*, vol. 49, no. 3, pp. 1911–1919, 2013.

[2] A. Aubry, A. De Maio, M. Piezzo, and A. Farina, "Radar waveform design in a spectrally crowded environment via nonconvex quadratic optimization," *IEEE Trans. Aerosp. Electron. Syst.*, vol. 50, no. 2, pp. 1138–1152, 2014.

[3] A. Aubry, A. De Maio, Y. Huang, M. Piezzo, and A. Farina, "A new radar waveform design algorithm with improved feasibility for spectral coexistence," *IEEE Trans. Aerosp. Electron. Syst.*, vol. 51, no. 2, pp. 1029–1038, 2015.

[4] L. Zheng, M. Lops, and X. Wang, "Adaptive interference removal for uncoordinated radar/communication coexistence," *IEEE J. Sel. Topics Siganl Process.*, vol. 12, no. 1, pp. 45–60, Feb. 2017.

[5] F. Liu, C. Masouros, A. Li, T. Ratnarajah, and J. Zhou, "Mimo radar and cellular coexistence: A power-efficient approach enabled by interference exploitation," *IEEE Trans. Signal Process.*, vol. 66, no. 14, pp. 3681–3695, 2018.

[6] N. Nartasilpa, A. Salim, D. Tuninetti, and N. Devroye, "Communications system performance and design in the presence of radar interference," *IEEE Trans. Commun.*, vol. 66, no. 9, pp. 4170–4185, 2018.

[7] B. Li, A. P. Petropulu, and W. Trappe, "Optimum co-design for spectrum sharing between matrix completion based mimo radars and a mimo communication system," *IEEE Trans. on Signal Process.*, vol. 64, no. 17, pp. 4562–4575, Sep. 2016.

[8] Y. Li, L. Zheng, M. Lops, and X. Wang, "Interference removal for radar/communication co-existence: The random scattering case," *IEEE Trans. Wireless Commun.*, vol. 18, no. 10, pp. 4831–4845, Oct. 2019.

[9] H. B. Jain, I. P. Roberts, and S. Vishwanath, "Enabling in-band coexistence of millimeter-wave communication and radar," in *2020 IEEE International Radar Conference (RADAR)*, 2020, pp. 772–777.

[10] Z. Wei, F. Liu, C. Masouros, N. Su, and A. P. Petropulu, "Toward multi-functional 6g wireless networks: Integrating sensing, communication, and security," *IEEE Commun. Mag.*,, vol. 60, no. 4, pp. 65–71, Apr. 2022.

[11] C.-H. Wang, C. D. Ozkaptan, E. Ekici, and O. Altintas, "Poster: Multi-carrier modulation on fmcw radar for joint automotive radar and communication," in *Proc. IEEE Veh. Netw. Conf. (VNC)*. IEEE, 2018, pp. 1–2.

[12] Z. Dou *et al.*, "Radar-communication integration based on msk-lfm spread spectrum signal," *Int. J. Commun. Netw. Syst. Sci.*, vol. 10, no. 08, p. 108, 2017.

[13] Y. Zhang, Q. Li, L. Huang, and J. Song, "Waveform design for joint radar-communication system with multi-user based on mimo radar," in *Proc. IEEE Radar Conf. (RadarConf)*. IEEE, 2017, pp. 0415–0418.

[14] Z. Lin and Z. Wang, "Interleaved OFDM signals for MIMO radar," *IEEE Sensors J.*,, vol. 15, no. 11, pp. 6294–6305, Nov. 2015.

[15] A. Hassanien, M. G. Amin, E. Aboutanios, and B. Himed, "Dual-function radar communication systems: A solution to the spectrum congestion problem," *IEEE Signal Process. Mag.*, vol. 36, no. 5, pp. 115–126, Sep. 2019.

[16] D. Ma, N. Shlezinger, T. Huang, Y. Liu, and Y. C. Eldar, "Joint radar-communication strategies for autonomous vehicles: Combining two key automotive technologies," *IEEE Signal Process. Mag.*, vol. 37, no. 4, pp. 85–97, Jul. 2020.

[17] R. C. Daniels, E. R. Yeh, and R. W. Heath, "Forward collision vehicular radar with ieee 802.11: Feasibility demonstration through measurements," *IEEE Trans. Veh. Technol.*,, vol. 67, no. 2, pp. 1404–1416, Feb. 2017.

[18] P. Kumari, J. Choi, N. González-Prelcic, and R. W. Heath, "IEEE 802.11 ad-based radar: An approach to joint vehicular communication-radar system," *IEEE Trans. Veh. Technol.*, vol. 67, no. 4, pp. 3012–3027, Apr. 2017.

[19] P. Kumari, N. J. Myers, and R. W. Heath, "Adaptive and fast combined waveform-beamforming design for mmwave automotive joint communication-radar," *IEEE J. Sel. Topics Sig. Process.*, vol. 15, no. 4, pp. 996–1012, June 2021.

[20] C. Sturm and W. Wiesbeck, "Waveform design and signal processing aspects for fusion of wireless communications and radar sensing," *Proc. IEEE*, vol. 99, no. 7, pp. 1236–1259, Jul. 2011.

[21] J. Johnston, L. Venturino, E. Grossi, M. Lops, and X. Wang, "Mimo ofdm dual-function radar-communication under error rate and beampattern constraints," *IEEE J. Sel. Areas Commun.*, vol. 40, no. 6, pp. 1951–1964, 2022.

[22] M. F. Keskin, H. Wymeersch, and V. Koivunen, "Mimo-ofdm joint radar-communications: Is ici friend or foe?" *IEEE J. Sel. Topics Signal Process.*, vol. 15, no. 6, pp. 1393–1408, Nov. 2021.

[23] G. Hakobyan and B. Yang, "A novel ofdm-mimo radar with non-equidistant dynamic subcarrier interleaving," in *Proc. European Radar Conf. (EuRAD).* IEEE, Oct. 2016, pp. 45–48.

[24] Y. Liu, G. Liao, J. Xu, Z. Yang, and Y. Zhang, "Adaptive ofdm integrated radar and communications waveform design based on information theory," *IEEE CCommun. Lett.*, vol. 21, no. 10, pp. 2174–2177, Oct. 2017.

[25] T. Huang and T. Zhao, "Low pmepr ofdm radar waveform design using the iterative least squares algorithm," *IEEE Signal Process. Lett.*, vol. 22, no. 11, pp. 1975–1979, Nov. 2015.

[26] L. Gaudio, M. Kobayashi, B. Bissinger, and G. Caire, "Performance analysis of joint radar and communication using ofdm and otfs," in *2Proc. IEEE Int. Conf. Commun. Workshops (ICC Workshops).* IEEE, 2019, pp. 1–6.

[27] L. Gaudio, M. Kobayashi, G. Caire, and G. Colavolpe, "On the effectiveness of otfs for joint radar parameter estimation and communication," *IEEE Trans. Wireless Commun.*, vol. 19, no. 9, pp. 5951–5965, Sep. 2020.

[28] M. F. Keskin, H. Wymeersch, and A. Alvarado, "Radar sensing with otfs: Embracing isi and ici to surpass the ambiguity barrier," in *Proc. IEEE Int. Conf. Commun. Workshops (ICC Workshops)*. IEEE, 2021, pp. 1–6.

[29] L. Zheng and X. Wang, "Super-resolution delay-doppler estimation for OFDM passive radar," *IEEE Trans. Signal Process.*, vol. 65, no. 9, pp. 2197–2210, May 2017.

[30] L. Liu and S. Zhang, "A two-stage radar sensing approach based on MIMO-OFDM technology," in *Proc. IEEE Globecom Workshops (GC) Wkshps.* IEEE, 2020, pp. 1–6.

[31] S. H. Dokhanchi, B. S. Mysore, K. V. Mishra, and B. Ottersten, "A mmWave automotive joint radar-communications system," *IEEE Trans. Aerosp. Electron. Syst.*, vol. 55, no. 3, pp. 1241–1260, Jun. 2019.

[32] C. B. Barneto, E. Rastorgueva-Foi, M. F. Keskin, T. Riihonen, M. Turunen, J. Talvitie, H. Wymeersch, and M. Valkama, "Millimeter-wave mobile sensing and environment mapping: Models, algorithms and validation," *IEEE Trans. Veh. Technol.*, vol. 71, no. 4, pp. 3900–3916, Apr. 2022.

[33] J. Yang, C.-K. Wen, and S. Jin, "Hybrid active and passive sensing for SLAM in wireless communication systems," *IEEE J. Sel. Areas Commun.*, Jul. 2022.

[34] B. Paul, A. R. Chiriyath, and D. W. Bliss, "Survey of RF communications and sensing convergence research," *IEEE Access*, vol. 5, pp. 252–270, 2016.

[35] L. Zheng, M. Lops, Y. C. Eldar, and X. Wang, "Radar and communication coexistence: An overview: A review of recent methods," *IEEE Signal Process. Mag.*, vol. 36, no. 5, pp. 85–99, Sep. 2019.

[36] K. V. Mishra, M. R. B. Shankar, V. Koivunen, B. Ottersten, and S. A. Vorobyov, "Toward millimeter-wave joint radar communications: A signal processing perspective," *IEEE Signal Process. Mag.*, vol. 36, no. 5, pp. 100–114, Sep. 2019.

[37] A. Hassanien, M. G. Amin, E. Aboutanios, and B. Himed, "Dual-function radar communication systems: A solution to the spectrum congestion problem," *IEEE Signal Process. Mag.*, vol. 36, no. 5, pp. 115–126, Sep. 2019.

[38] F. Liu, C. Masouros, A. Petropulu, H. Griffiths, and L. Hanzo, "Joint radar and communication design: Applications, state-of-the-art, and the road ahead," *IEEE Trans. Commun.*, vol. 68, no. 6, pp. 3834–3862, Jun. 2020.

[39] D. K. P. Tan, J. He, Y. Li, A. Bayesteh, Y. Chen, P. Zhu, and W. Tong, "Integrated sensing and communication in 6G: Motivations, use cases, requirements, challenges and future directions," in *Proc. 2021 1st IEEE Int. Online Symp. on Joint Commun. & Sens. (JC&S)*, Feb. 2021.

[40] J. A. Zhang, M. L. Rahman, K. Wu, X. Huang, Y. J. Guo, S. Chen, and J. Yuan, "Enabling joint communication and radar sensing in mobile networks - A survey," [Online] Available: https://arxiv.org/abs/2006.07559.

[41] G. R. Muns, K. V. Mishra, C. B. Guerra, Y. C. Eldar, and K. R. Chowdhury, "Beam alignment and tracking for autonomous vehicular communication using IEEE 802.11 ad-based radar," in *Proc. IEEE Conf. Comput. Commun. (Infocom) Wkshps.*, Apr. 2019, pp. 535–540.

[42] A. Hassanien, M. G. Amin, Y. D. Zhang, and F. Ahmad, "Dual-function radar-communications: Information embedding using sidelobe control and waveform diversity," *IEEE Trans. Signal Process.*, vol. 64, no. 8, pp. 2168–2181, Apr. 2015.

[43] C. Sahin, J. Jakabosky, P. M. McCormick, J. G. Metcalf, and S. D. Blunt, "A novel approach for embedding communication symbols into physical radar waveforms," in *Proc. IEEE Radar Conf. (RadarConf)*, May 2017, pp. 1498–1503.

[44] G. Mao, B. Fidan, and B. D. O. Anderson, "Wireless sensor network localization techniques," *Comput. Netw.*, vol. 51, no. 10, pp. 2529–2553, Jul. 2007.

[45] J. A. del Peral-Rosado, R. Raulefs, J. A. Lopez-Salcedo, and G. Seco-Granados, "Survey of cellular mobile radio localization methods: From 1G to 5G," *IEEE Commun. Surveys Tuts.*, vol. 20, no. 2, pp. 1124–1148, 2nd Quart. 2017.

[46] A. Liu *et al.*, "A survey on fundamental limits of integrated sensing and communication," [Online] Available: https://arxiv.org/abs/2104.09954.

[47] M. Kobayashi, H. Hamad, G. Kramer, and G. Caire, "Joint state sensing and communication over memoryless multiple access channels," in *Proc. IEEE Int. Symp. Inf. Theory (ISIT)*, Jul. 2019, pp. 270–274.

[48] W. Zhang, S. Vedantam, and U. Mitra, "Joint transmission and state estimation: A constrained channel coding approach," *IEEE Trans. Inf. Theory*, vol. 57, no. 10, pp. 7084–7095, Oct. 2011.

[49] A. R. Chiriyath, B. Paul, G. M. Jacyna, and D. W. Bliss, "Inner bounds on performance of radar and communications co-existence," *IEEE Trans. Signal Process.*, vol. 64, no. 2, pp. 464–474, Jan. 2016.

[50] F. Liu, C. Masouros, A. Li, H. Sun, and L. Hanzo, "MU-MIMO communications with MIMO radar: From co-existence to joint transmission," *IEEE Trans. Wireless Commun.*, vol. 17, no. 4, pp. 2755–2770, Apr. 2018.

[51] F. Liu, L. Zhou, C. Masouros, A. Li, W. Luo, and A. Petropulu, "Toward dual functional radar-communication systems: Optimal waveform design," *IEEE Trans. Signal Process.*, vol. 66, no. 16, pp. 4264–4279, Aug. 2018.

[52] M. L. Rahman, J. A. Zhang, X. Huang, Y. J. Guo, and R. W. Heath, "Framework for a perceptive mobile network using joint communication and radar sensing," *IEEE Trans. Aerosp. Electron. Syst.*, vol. 56, no. 3, pp. 1926–1941, Jun. 2020.

[53] A. Shahmansoori, G. E. Garcia, G. Destino, G. Seco-Granados, and H. Wymeersch, "Position and orientation estimation through millimeter-wave MIMO in 5G systems," *IEEE Trans. Wireless Commun.*, vol. 17, no. 3, pp. 1822–1835, Mar. 2018.

[54] S. Buzzi, C. D'Andrea, and M. Lops, "Using massive MIMO arrays for joint communication and sensing," in *Proc. 53rd Asilomar Conf. Signals Syst. Comput.,*, Nov. 2019, pp. 5–9.

[55] L. Liu and S. Zhang, "A two-stage radar sensing approach based on MIMO-OFDM technology," in *Proc. IEEE Global Commun. Conf. (Globecom) Wkshps.*, Dec. 2020.

[56] T. Hwang, C. Yang, G. Wu, S. Li, and G. Y. Li, "OFDM and its wireless applications: A survey," *IEEE Trans. Veh. Technol.*, vol. 58, no. 4, pp. 1673–1694, May 2009.

[57] 3GPP, "Summary of Release 15 Work Items," 3rd Generation Partnership Project (3GPP), TR 21.915 Version 1.1.0 Release 15, 2018.

[58] R. Mahler, "Statistical multisource-multitarget information fusion," 2007.

[59] S. Aditya, A. F. Molisch, N. Rabeah, and H. M. Behairy, "Localization of multiple targets with identical radar signatures in multipath environments with correlated blocking," *IEEE Trans. Wireless Commun.*, vol. 17, no. 1, pp. 606–618, Jan. 2017.

[60] E. Everett, A. Sahai, and A. Sabharwal, "Passive self-interference suppression for full-duplex infrastructure nodes," *IEEE Trans. Wireless Commun.*, vol. 13, no. 2, pp. 680–694, Feb. 2014.

[61] M. Yuan and Y. Lin, "Model selection and estimation in regression with grouped variables," *J. R. Stat. Soc. Ser. B, Stat. Methodol.*, vol. 68, no. 1, pp. 49–67, Feb. 2006.

[62] A. Zaidi *et al.*, "Designing for the future: the 5G NR physical layer," *Ericsson Technol. Rev.*, 2017.

[63] D. J. Torrieri, "Statistical theory of passive location systems," *IEEE Trans. Aerosp. Electron. Syst.*, no. 2, pp. 183–198, Mar. 1984.

[64] M. Gavish and A. J. Weiss, "Performance analysis of bearing-only target location algorithms," *IEEE Trans. Aerosp. Electron. Syst.*, vol. 28, no. 3, pp. 817–828, Jul. 1992.

[65] H. W. Kuhn, "The hungarian method for the assignment problem," *Nav. Res. Logist. Quart.*, vol. 2, no. 1, pp. 83–97, 1955.

[66] ITU-R, "M.2160 : Framework and overall objectives of the future development of imt for 2030 and beyond," *[Online]. Available: https://www.itu.int/rec/R-REC-M.2160/en*, 2023.

[67] X. Mu, Y. Liu, L. Guo, J. Lin, and L. Hanzo, "NOMA-aided joint radar and multicast-unicast communication systems," *IEEE J. Sel. Areas Commun.*, vol. 40, no. 6, pp. 1978–1992, Jun. 2022.

[68] C. G. Tsinos, A. Arora, S. Chatzinotas, and B. Ottersten, "Joint transmit waveform and receive filter design for dual-function radar-communication systems," *IEEE J. Sel. Topics Signal Process.*, vol. 15, no. 6, pp. 1378–1392, Nov. 2021.

[69] L. Liu, S. Bi, and R. Zhang, "Joint power control and fronthaul rate allocation for throughput maximization in ofdma-based cloud radio access network," *IEEE Trans. Commun.*, vol. 63, no. 11, pp. 4097–4110, Nov. 2015.

[70] D. Gesbert, S. Hanly, H. Huang, S. S. Shitz, O. Simeone, and W. Yu, "Multi-cell mimo cooperative networks: A new look at interference," *IEEE J. Sel. Areas Commun.*, vol. 28, no. 9, pp. 1380–1408, Dec. 2010.

[71] A. Checko, H. L. Christiansen, Y. Yan, L. Scolari, G. Kardaras, M. S. Berger, and L. Dittmann, "Cloud ran for mobile networks—a technology overview," *IEEE Commun. Surveys Tuts.*, vol. 17, no. 1, pp. 405–426, Firstquarter 2014.

[72] A. Liu, Z. Huang, M. Li, Y. Wan, W. Li, T. X. Han, C. Liu, R. Du, D. K. P. Tan, J. Lu *et al.*, "A survey on fundamental limits of integrated sensing and communication," *IEEE Commun. Surveys Tuts.*, vol. 24, no. 2, pp. 994–1034, Feb. 2022.

[73] L. Xie, S. Song, Y. C. Eldar, and K. B. Letaief, "Collaborative sensing in perceptive mobile networks: Opportunities and challenges," *IEEE Wireless Commun.*, vol. 30, no. 1, pp. 16–23, Feb. 2023.

[74] A. Zhang, M. L. Rahman, X. Huang, Y. J. Guo, S. Chen, and R. W. Heath, "Perceptive mobile networks: Cellular networks with radio vision via joint communication and radar sensing," *IEEE Veh. Technol. Mag.*, vol. 16, no. 2, pp. 20–30, Jun. 2020.

[75] G. Mao, B. Fidan, and B. D. Anderson, "Wireless sensor network localization techniques," *Comput. Netw.*, vol. 51, no. 10, pp. 2529–2553, Jan. 2007.

[76] S. Aditya, A. F. Molisch, and H. M. Behairy, "A survey on the impact of multipath on wideband time-of-arrival based localization," *Proc. IEEE*, vol. 106, no. 7, pp. 1183–1203, Jul. 2018.

[77] I. Guvenc and C.-C. Chong, "A survey on TOA based wireless localization and NLOS mitigation techniques," *IEEE Commun. Surveys Tuts.*, vol. 11, no. 3, pp. 107–124, Aug. 2009.

[78] X. Chen, F. Dovis, S. Peng, and Y. Morton, "Comparative studies of GPS multipath mitigation methods performance," *IEEE Trans. on Aerosp. Electron. Syst.*, vol. 49, no. 3, pp. 1555–1568, Jul. 2013.

[79] M. Kotaru, K. Joshi, D. Bharadia, and S. Katti, "Spotfi: Decimeter level localization using wifi," in *Proc. ACM SIGCOMM Comput. Commun. Rev.*, vol. 45, 2015, pp. 269–282.

[80] P.-C. Chen, "A non-line-of-sight error mitigation algorithm in location estimation," in *Proc. IEEE Int. Conf. Wireless Commun. Networking (WCNC)*, vol. 1, Sep. 1999, pp. 316–320.

[81] S. Venkatesh and R. M. Buehrer, "A linear programming approach to NLOS error mitigation in sensor networks," in *Proc. IEEE Int. Symp. Inf. Processing Sensor Netw. (IPSN)*, Apr. 2006, pp. 301–308.

[82] N. Decarli, D. Dardari, S. Gezici, and A. A. D'Amico, "LOS/NLOS detection for UWB signals: A comparative study using experimental data," in *Proc. 5th IEEE Int. Symp. Wireless Pervasive Comput.*, May. 2010, pp. 169–173.

[83] Q. Shi, L. Liu, S. Zhang, and S. Cui, "Device-free sensing in OFDM cellular network," *IEEE J. Sel. Areas Commun.*, vol. 40, no. 6, pp. 1838–1853, Jan. 2022.

[84] A. B. Poore, "Multidimensional assignment formulation of data association problems arising from multitarget and multisensor tracking," *Computational Optimization and Applications*, vol. 3, no. 1, pp. 27–57, Mar. 1994.

[85] A. P. Poore and N. Rijavec, "A Lagrangian relaxation algorithm for multidimensional assignment problems arising from multitarget tracking," *SIAM J. Optim.*, vol. 3, no. 3, pp. 544–563, 1993.

[86] Y. Bar-Shalom and E. Tse, "Tracking in a cluttered environment with probabilistic data association," *Automatica*, vol. 11, no. 5, pp. 451–460, Jan. 1975.

[87] T. Fortmann, Y. Bar-Shalom, and M. Scheffe, "Sonar tracking of multiple targets using joint probabilistic data association," *IEEE J. Ocean. Eng.*, vol. 8, no. 3, pp. 173–184, Jul. 1983.

[88] D. Reid, "An algorithm for tracking multiple targets," *IEEE Trans. Automat. Contr.*, vol. 24, no. 6, pp. 843–854, Dec. 1979.

[89] J. Shen and A. F. Molisch, "Estimating multiple target locations in multi-path environments," *IEEE Trans. Wireless Commun.*, vol. 13, no. 8, pp. 4547–4559, Aug. 2014.

[90] T. M. Schmidl and D. C. Cox, "Robust frequency and timing synchronization for OFDM," *IEEE Trans. Commun.*, vol. 45, no. 12, pp. 1613–1621, Dec. 1997.

[91] M. Morelli, C.-C. J. Kuo, and M.-O. Pun, "Synchronization techniques for orthogonal frequency division multiple access (OFDMA): A tutorial review," *Proc. of IEEE*, vol. 95, no. 7, pp. 1394–1427, July 2007.

[92] H. Li, L. Han, R. Duan, and G. M. Garner, "Analysis of the synchronization requirements of 5G and corresponding solutions," *IEEE Commun. Stand. Mag.*, vol. 1, no. 1, pp. 52–58, Mar. 2017.

[93] T. Hwang, C. Yang, G. Wu, S. Li, and G. Y. Li, "OFDM and its wireless applications: A survey," *IEEE Trans. Veh. Technol.*, vol. 58, no. 4, pp. 1673–1694, May 2008.

[94] L. Liu, Y.-F. Liu, P. Patil, and W. Yu, "Uplink-downlink duality between multiple-access and broadcast channels with compressing relays," *IEEE Trans. Inf. Theory*, vol. 67, no. 11, pp. 7304–7337, Nov. 2021.

[95] M. Grant, S. Boyd, and Y. Ye, "Cvx: Matlab software for disciplined convex programming," *http://cvxr.com/cvx*, Mar. 2009.

[96] J. Neira and J. D. Tardós, "Data association in stochastic mapping using the joint compatibility test," *IEEE Trans. Robot. Autom.*, vol. 17, no. 6, pp. 890–897, Dec. 2001.

[97] T. Bailey, E. M. Nebot, J. Rosenblatt, and H. F. Durrant-Whyte, "Data association for mobile robot navigation: A graph theoretic approach," in *IEEE Int. Conf. Robot. Automat.*, vol. 3, 2000, pp. 2512–2517.

[98] W. E. L. Grimson, *Object recognition by computer: the role of geometric constraints.* Mit Press, 1991.

[99] Z. Ma and S. Liu, "A review of 3D reconstruction techniques in civil engineering and their applications," *Adv. Eng. Informat.*, vol. 37, pp. 163–174, Aug. 2018.

[100] M. Zollhöfer, P. Stotko, A. Görlitz, C. Theobalt, M. Nießner, R. Klein, and A. Kolb, "State of the art on 3D reconstruction with RGB-D cameras," *Comput. Graph. Forum.*, vol. 37, no. 2, pp. 625–652, May 2018.

[101] X.-F. Han, H. Laga, and M. Bennamoun, "Image-based 3D object reconstruction: State-of-the-art and trends in the deep learning era," *IEEE Trans. Pattern Anal. Mach. Intell.*, vol. 43, no. 5, pp. 1578–1604, Nov. 2019.

[102] R. Shahbazian and I. Trubitsyna, "Human sensing by using radio frequency signals: A survey on occupancy and activity detection," *IEEE Access*, vol. 11, pp. 40 878–40 904, 2023.

[103] F. Liu, C. Masouros, A. Petropulu, H. Griffiths, and L. Hanzo, "Joint radar and communication design: Applications, state-of-the-art, and the road ahead," *IEEE Trans. Commun.*, vol. 68, no. 6, pp. 3834–3862, Jun. 2020.

[104] J. A. Zhang, M. L. Rahman, K. Wu, X. Huang, Y. J. Guo, S. Chen, and J. Yuan, "Enabling joint communication and radar sensing in mobile networks—A survey," *IEEE Commun. Surveys Tuts.*, vol. 24, no. 1, pp. 306–345, 1st Quart. 2022.

[105] F. Liu, Y. Cui, C. Masouros, J. Xu, T. X. Han, Y. C. Eldar, and S. Buzzi, "Integrated sensing and communications: Towards dual-functional wireless networks for 6G and beyond," *IEEE J. Sel. Areas Commun.*, vol. 40, no. 6, pp. 1728–1767, Jun. 2022.

[106] F. Zhang, C. Wu, B. Wang, and K. R. Liu, "mmEye: Super-resolution millimeter wave imaging," *IEEE Internet Things J.*, vol. 8, no. 8, pp. 6995–7008, Apr. 2020.

[107] D. Wang, X. Cui, X. Chen, Z. Zou, T. Shi, S. Salcudean, Z. J. Wang, and R. Ward, "Multi-view 3D reconstruction with transformers," in *Proc. IEEE/CVF Int. Conf. Comput. Vision (ICCV)*, 2021, pp. 5722–5731.

[108] Y. M. Kim, C. Theobalt, J. Diebel, J. Kosecka, B. Miscusik, and S. Thrun, "Multi-view image and ToF sensor fusion for dense 3D reconstruction," in *Proc. IEEE/CVF Int. Conf. Comput. Vision (ICCV)*, 2009, pp. 1542–1549.

[109] S. Khan, O. Javed, Z. Rasheed, and M. Shah, "Human tracking in multiple cameras," in *Proc. IEEE/CVF Int. Conf. Comput. Vision (ICCV)*, vol. 1, 2001, pp. 331–336.

[110] H. Rhodin, J. Spörri, I. Katircioglu, V. Constantin, F. Meyer, E. Müller, M. Salzmann, and P. Fua, "Learning monocular 3D human pose estimation from multi-view images," in *Proc. IEEE/CVF Comput. Vis. Pattern Recognit. (CVPR)*, 2018, pp. 8437–8446.

[111] H. Xie, H. Yao, X. Sun, S. Zhou, and S. Zhang, "Pix2vox: Context-aware 3D reconstruction from single and multi-view images," in *Proc. IEEE/CVF Int. Conf. Comput. Vision (ICCV)*, 2019, pp. 2690–2698.

[112] R. Schmidt, "Multiple emitter location and signal parameter estimation," *IEEE Trans. Antennas Propag.*, vol. 34, no. 3, pp. 276–280, Mar. 1986.

[113] A. P. Liavas and P. A. Regalia, "On the behavior of information theoretic criteria for model order selection," *IEEE Trans. Signal Process.*, vol. 49, no. 8, pp. 1689–1695, Aug. 2001.

[114] F. Guidi, A. Guerra, and D. Dardari, "Personal mobile radars with millimeter-wave massive arrays for indoor mapping," *IEEE Trans. Mobile Comput.*, vol. 15, no. 6, pp. 1471–1484, Jun. 2015.

[115] C. B. Barneto, T. Riihonen, M. Turunen, M. Koivisto, J. Talvitie, and M. Valkama, "Radio-based sensing and indoor mapping with millimeter-wave 5G NR signals," in *Proc. IEEE Int. Conf. Localization GNSS (ICLGNSS)*, Jun. 2020, pp. 1–5.